SU-SEL-68-037

Locating Refractive Index Variations With Bistatic-Radar

by

Edwin C. Thiede

May 1968

SCIENTIFIC REPORT NO. 27

Prepared under
National Aeronautics and
Space Administration
Grant NsG 377

RADIOSCIENCE LABORATORY

STANFORD ELECTRONICS LABORATORIES

STANFORD UNIVERSITY • STANFORD, CALIFORNIA

SEL-68-037

LOCATING REFRACTIVE INDEX VARIATIONS WITH BISTATIC-RADAR

by

Edwin C. Thiede

May 1968

Scientific Report No. 27

Prepared under

National Aeronautics and Space Administration
Grant NsG 377

Radioscience Laboratory
Stanford Electronics Laboratories
Stanford University Stanford California

ABSTRACT

A randomly varying medium causes both amplitude and phase fluctuations on a wave propagating through it. The time variations of the medium are shown to provide a mechanism for viewing isolated regions along the propagation path. A general technique for locating these fluctuation regions is introduced by this research. This allows one to measure the distribution of refractive index variations versus distance along the propagation path. The unusual feature of the new technique is that this distribution is obtained by using only one antenna at each end of the propagation path.

The technique is mechanized for space applications by using a transmitter and receiver both in the spacecraft and on the ground. The spacecraft receiver and transmitter are connected in a manner which enables the integrated uplink phase modulation to be relayed back down to the ground receiver on a slightly different carrier frequency. This bistatic-radar technique provides two copies of the modulation waveform from each source region. The two copies are separated with a time delay which corresponds to the range of the source. Autocorrelating the ground receiver signal gives a positive correlation only when the time delay of each source region is matched.

In developing the description of the technique, several extensions to the theory of wave propagation in a random medium are made. A nonlinear wave equation is derived to include the time variations in addition to the usual spatial variations. This equation leads to the retarded potential solution which is then applied to the bistatic-radar mechanization. The wave theory solution is extended to point out the Fresnel zone weighting effect which varies with the distance along the propagation path.

The resolution of a source distribution in the medium is shown to be limited by the larger of either the spatial scale size or the time scale size. Some effects on the resolution cell due to the radar motion are also discussed.

The signal autocorrelation function is estimated by integrating or time averaging the receiver output lag-product over the total length of the observation time. It is shown how the signal-to-noise ratio may be improved by processing the time averaged autocorrelation through a matched filter.

An experiment at S-band is proposed to measure the electron density variations in the solar wind over a path length on the order of one AU. Processing ten hours of data will give a unity signal-to-noise ratio for forty-two resolution cells in a four-tenths of an AU path length or fifteen resolution cells in one AU path length.

CONTENTS

SYMBOLS

A	Magnitude of $R_s(\tau)$ for τ at source center
$A(\bar{r},t)$	Amplitude of the em wave
a	Spatial scale size
a', b'	Generalized scale sizes
$\bar{B}$	Magnetic field density vector
B	Log amplitude-fluctuation ratio
b	Local source distribution scale size
c	Speed of light in a vacuum
$\bar{D}$	Electric field density vector
D	Wave parameter, squared ratio of the first Fresnel zone radius over the scale size
D_F	Diameter of the first Fresnel zone
d_R	Minimum resolution distance
$\bar{E}$	Electric field intensity vector
E	Electric field intensity scalar
e_o	Permittivity of free space
$F(z,\tau)$	Local, normalized, refractive index correlation
f	Frequency
G_k	Shape factor in the eigenvalue u_k
$\bar{H}$	Magnetic field intensity vector
$H(jf)$	Filter transfer function
$h(t)$	Filter impulse function
i	$\sqrt{-1}$
$\bar{J}$	Current density vector
$\bar{k}$	Direction of wave propagation vector

k	Wave number for free space, $k = \lvert\bar{k}\rvert$
L	Likelihood ratio
ℓ	Raypath separation
$M(z,f)$	Refractive index power spectrum
M	Number of resolution cells along the propagation
N	Number of independent observation samples
$N(\bar{r},t)$	Electron number density function
$\bar{N}$	Mean electron number density
N_o	Thermal noise spectral density
N_w	Whitened noise spectral density
$n(\bar{r},t)$	Refractive index function
n_o	Mean refractive index value
p_i	Range to source, i = blank,1,2,...
$Q_s(f)$	Power spectrum of the received phase signal
$R_s(\tau)$	Autocorrelation of the received phase signal
R	Propagation path length
$\bar{r}$	Position vector
r	Magnitude of $\bar{r}$
Δr	Magnitude of $(\bar{r}' - \bar{r})$
$S(t)$, $S(\bar{r},t)$	Phase fluctuation of the em wave
T	Observation time duration
T_R	Time ambiguity associated with d_r
t	Time
$u(\bar{r},t)$	Refractive index variable quantity
$V_{za,b}$	Radar-site velocities along the path
$V_{na,b}$	Radar-site velocities perpendicular to the path

$V(\bar{r},t)$	Complex phase of the em wave
v	Propagation velocity
W	Equivalent bandwidth of the medium
W_r	Receiver bandwidth
$\hat{x}$, $\hat{y}$, $\hat{z}$	Unit vectors
$x(t)$	Whitened received signal plus noise
$y(t)$	Received signal plus noise
z_1, z_2	Propagation path coordinates
z	$z_2 - z_1$, difference coordinate
z_0	$(z_2 + z_1)/2$, sum coordinate
α	RMS magnitude of the refractive index variations
α_N	RMS magnitude of the electron density variations
γ	Mismatched filter performance coefficient
$\delta(\tau)$, δ_j	Dirac delta functions
λ_k	$y(t) = m(t) + n(t)$ eigenvalue
$\Lambda(t/T)$	Triangle function
μ_k	$m(t)$ eigenvalue
ν_k	$n(t)$ eigenvalue
$\xi(\tau)$	Signal correlation shape function
μ_o	Permeability of free space
π	Pi
ρ	Volume charge density
$\sigma(z_1)$	Refractive index distribution function
τ	Time lag
Φ_s, Φ_c	Functions related to the Fresnel zone

$\phi_k(t)$	Eigenfunction
ω	Radian frequency
∇^2	Vector Laplacian
$\bar{\nabla}$	$\hat{x}\partial/\partial x + \hat{y}\partial/\partial y + \hat{z}\partial/\partial z$
$\bar{\Box}$	$\bar{\nabla} + (n/\omega)\ \bar{k}\partial/\partial t$

ACKNOWLEDGMENTS

I wish to express special thanks to Professor Bruce B. Lusignan for his suggestions and many discussions during the course of this research. I also thank Professors A. M. Peterson and V. R. Eshleman for their guidance, encouragement, and support. The discussions and help from the other members of the staff at the Center for Radar Astronomy is remembered too.

Financial support for this research was provided by the National Aeronautics and Space Administration through Grant NsG 377.

I. INTRODUCTION

A. Background

This research introduces a new use for bistatic* radar--a technique for obtaining spatial resolution of the refractive index variations along the line of propagation in a random time varying media. The advantages of bistatic radar for the study of the solar system have been utilized by several authors. Eshleman in 1960, introduced the idea at several meetings and wrote a summary [1] in 1964 of the theoretical and experimental aspects of bistatic radar measurements of the solar system. Lusignan [2] in 1963, proposed the use of bistatic radar to detect a polarization effect on em waves traveling through relativistic-solar particle streams. Fjeldbo [3] in 1964, demonstrated that bistatic radar could be used to study planet surfaces, atmospheres and ionospheres. Fjeldbo, et al [4] successfully used this technique to study the Martian atmosphere and ionosphere. Gee [5] in 1965, investigated the detection and measuring of shock waves propagating outward from the sun with a bistatic radar. Tyler [6] in 1967, developed a bistatic radar imaging technique for the mapping of planetary surfaces. He has successfully used his technique to study the surface of the Moon.

Before going into the specific details of this research, a broad view of the objective is presented. Figure 1 shows the essential elements of the bistatic radar equipment and the resulting processed data. As in the usual bistatic mode, there are two well separated sites which we have labeled as the spacecraft and the ground station. Both sites have a receiver and transmitter such that transmitter_1 on the ground sends to receiver_1 at the spacecraft and transmitter_2 at the spacecraft sends to receiver_2 on the ground. The phase coherent transponder causes the spacecraft receiver and the transmitter which operate on two different frequencies to act like a mirror to the uplink carrier phase modulation. It does this by stripping the phase from the uplink carrier and immediately phase-modulating it onto the downlink carrier.

*In a bistatic-radar the receiver and transmitter are well separated.

The solar wind shown in Fig. 1 is basically an electron-proton plasma in which the refractive index variations are due to electron density variations. Regions of variation cause both phase and amplitude modulation on the em carriers which pass through them. From Fig. 1 it is apparent that both an uplink transmitter wave and a downlink transmitter wave are traveling in each region along the path. In any single region the electron density variations cause the same random waveform to be modulated onto

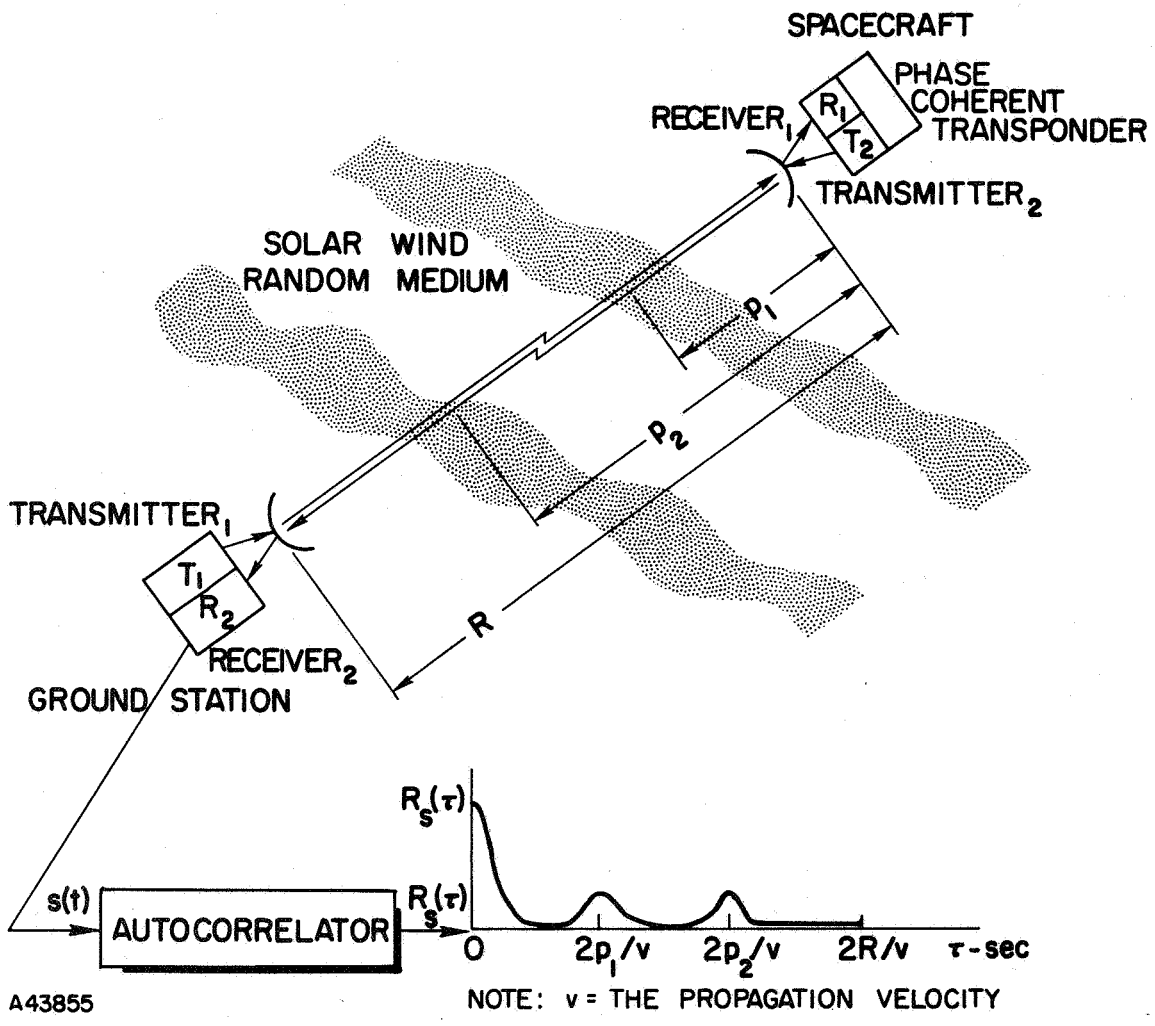

Fig. 1. DUAL BISTATIC RADAR SYSTEM.

both transmitter waves. The modulated downlink transmitter wave reaches the ground receiver first and is immediately demodulated to yield the random waveform corresponding to the source variations. The modulation on the uplink wave arrives at the ground receiver somewhat later because it must first travel to the spacecraft and then be retransmitted back to the ground receiver. Upon receiving the ground receiver it is demodulated to yield a delayed copy of the random waveform corresponding to the source variations. The time delay between the two modulation waveforms is determined by the time it takes the uplink phase modulation to be reflected back to the source region. This delay τ_1 is proportional to twice the range p_1 of the source from the spacecraft; $\tau_1 = 2p_1/v$. Additional source regions at other ranges also contribute random modulation waveforms on top of the waveforms from region p_1; however, they have correspondingly different time delays. The lag-product of the phase modulation from the ground receiver is formed with a lag of τ_1. Time averaging this lag-product will cause the correlated waveform from the source region p_1 to yield a positive mean value which corresponds to the mean square magnitude of the source electron density variations. The random waveforms from the other sources will average to zero because they are uncorrelated at a lag of τ_1.

B. Description of Present Work

To determine what properties of the refractive index variations can be measured, the effect of the medium on the transmitted em carrier wave is derived. A fairly standard nonmagnetic medium is defined by a list of assumptions. Notably, the random medium is assumed to be statistically nice: statistically homogeneous (locally), statistically isotropic, and stationary. From the appropriate constitutive relations and Maxwell's equations, a general wave equation is derived. It is a nonlinear and inhomogeneous differential equation. We neglect the inhomogeneous terms by constraining the rate of change of the refractive index relative to both the carrier wavelength and period. Finally, using the Rytov [9] approach, with an incident plane wave, the general equation is transformed into a complex-phase wave equation.

$$|\overline{\nabla V}|^2 + i\nabla^2 V - (n/c)^2 [(\omega - \dot{V})^2 + i\ddot{V}] = 0$$

This equation is an extension of the wave equation used by Chernov [7] and Tatarski [8] because it includes the time varying terms $\dot{V}$ and $\ddot{V}$. The above equation leads to the retarded potential form of solution which is essential to this research.

The real part of V is proportional to the wavenumber k. By letting k get large in the complex-phase wave equation and considering only zeroth and first order terms in k^{-1} we get the ray theory version of the differential equation. In addition, the above step neatly separates the real (actual phase) and the imaginary (log-amplitude ratio) parts into two separate equations. Solving the equations by the Greens function/Fourier transform method we get the phase and amplitude fluctuation expressions as a function of time. At this point the dual bistatic radar setup of Fig. 1 is incorporated into the solution to yield the coherent two way phase and amplitude fluctuations as seen by the ground station. The two way amplitude fluctuation is not actually available unless one uses an amplitude coherent transponder. The phase and amplitude time autocorrelations are now a straightforward calculation.. The new form of these correlations is a direct result from using the coherent bistatic radar and the retarded potential wave equation solution. The phase correlation is

$$R_s(\tau) = k^2 \iint_0^R dz_1\, dz_2\, \sigma(z_1)\sigma(z_2)[F(z, \tau - z/v) + F(z, \tau + z/v)$$

$$+ F(z, \tau - 2z_0/v) + F(z, \tau + 2z_0/v)] \quad ,$$

$$z = z_2 - z_1; \; 2z_0 = z_2 + z_1 \; .$$

The complete derivation of this equation in Chapter II and the study of its properties in Chapter III are a major result of this research.

The $\sigma(\ )$ function gives the magnitude and distribution of each source as a function of its position along the path. $\sigma(\ )$ is the quantity we wish to measure. $F(z,\tau)$ is the normalized correlation function of the refractive index. It has a value of one for $z = \tau = 0$; and, experimental evidence [22] indicates that it is nearly zero when either z exceeds some spatial scale size 'a' or τ exceeds some time scale size $1/W$. R is the total path length as shown in Fig. 1.

The two receiver self-correlation terms $F(z, \tau \pm z/v)$ act as an all pass weighting function to enable $R_s(\tau)$ to sum all values of the product $\sigma(z_1)\ \sigma(z_2)$ for $|z| \leq a$ and $|\tau| \leq 1/W + a/v$. They cause the large peak at the origin of $R_s(\tau)$ as shown in Fig. 1. The two receiver cross-correlation terms $F(z, \tau \pm 2z_o/v)$ will cause $R_s(\tau)$ to selectively view a small range of $\sigma(z_1)\ \sigma(z_2)$ at each nonzero value of τ when $|z| \leq a$ and $|\tau \pm 2z_o/v| \leq 1/W$. For example when τ takes on values around $2p_1/v$ in Fig. 1, $R_s(\tau)$ will correspond to the mean square magnitude of the source distribution centered at p_1. It will be slightly smeared due to the nonzero values of a and $1/W$.

Returning to the complex-phase wave equation, it may be linearized by the difference equation approach. Again the Greens function/Fourier transform method of solution yields the wave theory version for the phase and amplitude fluctuation expressions. Again the bistatic radar is incorporated to calculate the two way phase and amplitude correlations. In contrast to the ray case, the Fresnel zone now enters into the correlation integrands with a multiplier for each of the four $F(,)$ terms. The multiplier weights the fluctuation source magnitude as a function of its location Λ and spatial scale size a. As the traveling wave accumulates the fluctuations, the sources near the path center are always weighted the heaviest in the two cross-correlation $F(,)$ terms as shown in Fig. 2. The wave parameter D is the squared ratio of the first Fresnel zone over the scale size. When $D \ll 1$ the multiplier has a constant value of two over the entire path.

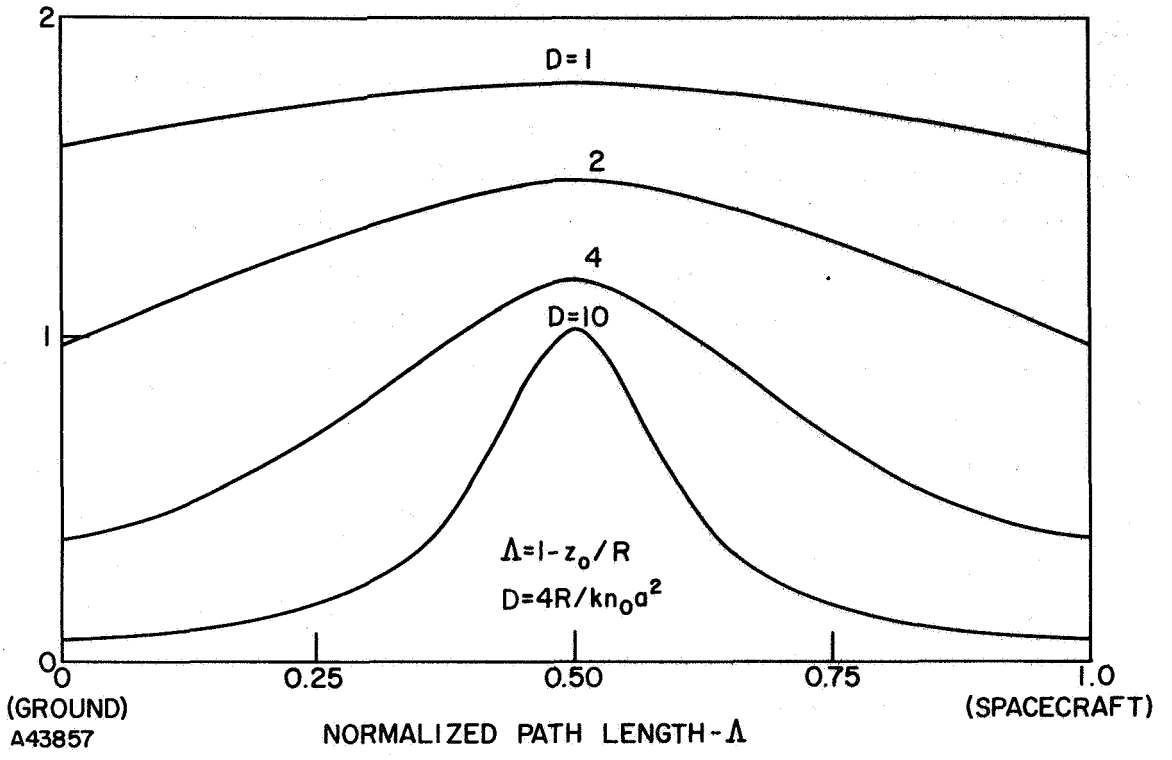

Fig. 2. WEIGHTING FUNCTION FOR CROSS-CORRELATION TERMS.

Equivalent power spectrum expressions are easily obtained for the fluctuating signals, also. The power spectrum for the phase correlation $R_s(\tau)$ is,

$$Q_s(f) = 4k^2 \int_0^R\int dz_1\ dz_2\ \sigma(z_1)\ \sigma(z_2)\ M(z,f)\ \cos\ (\omega z_1/v)\ \cos\ (\omega z_2/v) \quad .$$

$M(z,f)$ is the Fourier transform of $F(z,\tau)$. The equivalent bandwidth W of the medium is now defined in the usual manner as the square root of the second moment of the spectrum $M(o,f)$. W is the inverse of the time scale. The bandwidth parameter and the spectral representation are used in later resolution and filter discussions.

There are three parameters related to the refractive index variation source which may be measured from the autocorrelation function. They are

the location, magnitude, and scale size shown in Fig. 3 for a single source region. The general scale a' from the receiver self-correlation terms is used to classify the medium into a narrow or wide band category. Under gaussian assumptions,

$$a' = \left(\frac{1}{W}2 + \frac{a^2}{v^2}\right)^{1/2} .$$

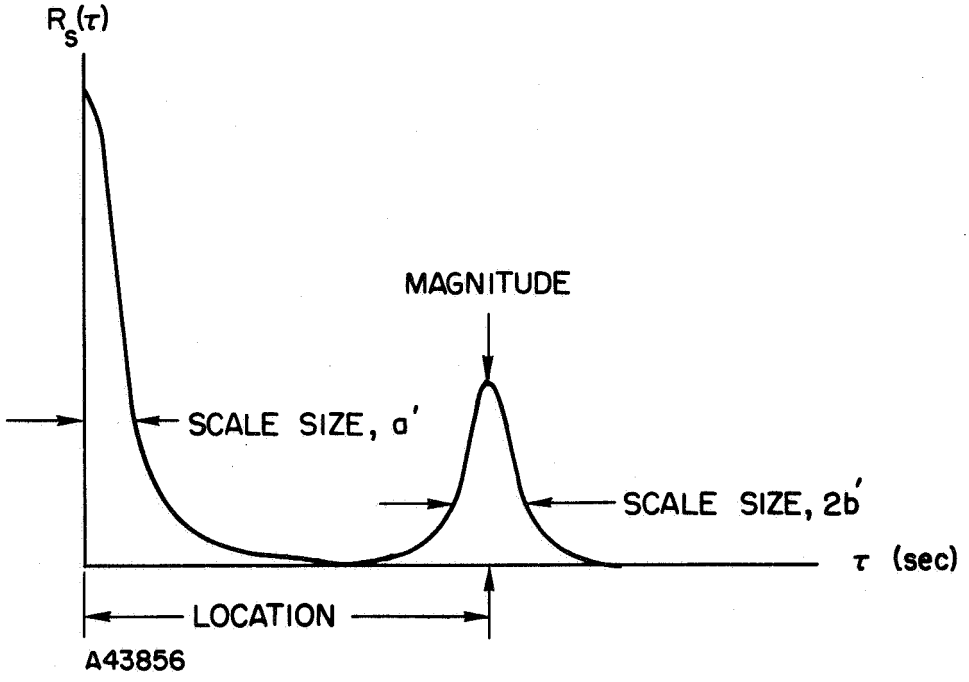

Fig. 3. MEASURABLE CROSS-CORRELATION PARAMETERS.

Most real mediums appear to be in the narrow band category where $(1/W^2) \gg (a^2/v^2)$. Another general scale size b' appears in the receiver cross-correlation terms shown in Fig. 3. It combines the time scale and the source distribution scale b,

$$b' = \left(\frac{1}{W}2 + \frac{4b^2}{v^2}\right)^{1/2} .$$

The resolution of sources in the correlation function is first approached by considering the minimum distance between two equal, independent point sources. A second approach treats the square of the source

correlation function as a signal ambiguity function. Both approaches give approximately the same value, $T_R = 1.26/W$ (gaussian case), for the correlation time ambiguity T_R. This means the resolution distance is $d_R = vT_R/2 = 0.63\ v/W$. d_R sets a practical lower limit on the propagation path length such that $R > d_R$. Finally, the sample interval is related to the ambiguity as $\nabla\tau \leq 1/2W = 2d_R/v = T_R/2.52$ (gaussian case).

It is an advantage to filter out the very low frequency effects which cause the large spreading seen in the autocorrelation function. Additionally one may wish to use bandpass filtering to select a desired section of the spectrum for closer scrutiny. The price one pays for this is first a reduction in the number of independent samples which reduces the signal to noise ratio. Secondly, there is a smoothing (spreading) of the remaining correlation peaks with a resulting loss in resolution.

The relative motion between the sources and the radar sites causes both cumulative and relativistic aberrations. Both depend upon the ratio of "spacecraft velocity/propagation velocity", hence, they will generally be negligible. However, the cumulative aberration also depends on the observation time such that long records may need correcting. The cumulative aberration for a source-spacecraft relative velocity v_{za} along the path is,

$$\Delta\tau = 2t(v_{za}/c)/(1-v_{za}/c) \qquad 0 \leq t \leq T \quad .$$

Time averaging the received signal lag-product $y(t)\ y(t+\tau)$ is the most natural way to estimate the correlation function. For a stationary random process this procedure is a minimum mean square error (MMSE) estimator of the correlation function.

The quality of the estimate is expressed in terms of the estimator signal-to-noise ratio (SNR). By assuming a gaussian signal collected from all of the sources and a large, additive, white, gaussian noise of bandwidth W; an explicit form of the SNR is obtained. If A is the magnitude of $R_s(\tau)$ for a typical source located at $\tau = 2p/v$ and M

is the number of resolution calls along the propagation path, the SNR is approximately,

$$SNR_{TA} = 2WTA^2/(WN_0 + 2AM)^2 \quad .$$

Maximum likelihood (ML) estimation enables one to estimate the magnitude and location of a single, independent, refractive-index variation source. This estimator is the familiar matched filter. Ideally it requires a priori knowledge of the location and scale size or shape of the source autocorrelation function. The structure of the dual bistatic radar autocorrelation function causes the matched filter to be sensitive to the source location but not the source shape. By sweeping a reasonable shape function through values of τ corresponding to the propagation path, the source locations and magnitudes can be measured from the noisy data. This is, in fact, how a trained investigator examines the time-averaged correlation data. The matched filter is obviously a better estimator than the time average because it weighs the data relative to the signal source. If T_s is the signal time resolution constant, the SNR of the matched filter is,

$$SNR_{ML} = 2TA^2T_s/N_o^2 \quad .$$

In the worst case ($WN_o > 2AM$), the SNR_{ML} is larger than the SNR_{TA} by the factor WT_s which is usually larger than one.

Radar astronomy is the primary motivation for this research. The results of this research may be applied to the study of the solar wind. The basic model of the solar wind assumes that electron-proton plasma clouds are flowing more or less radially outward from the Sun. An important effect of this plasma medium is that the magnitude of the received signal correlations are inversely proportional to the carrier frequency. Thus the lowest carrier frequency consistent with other assumptions is desired for maximum sensitivity. Several spacecraft out in the solar wind operating at VHF-band and S-band frequencies already carry a coherent transponder. They could be used to apply this new technique as shown in Fig. 1.

II. THE SIGNAL AND THE MEDIUM

All real propagation media have inhomogeneities which are random in size as well as being randomly distributed through the medium. Most of these media also have time variations which are due to the inhomogeneities having a drift velocity, turbulence, heat conduction, diffusion, etc. If we transmit an em wave through such media, the radiation will be scattered by the random inhomogeneities and it will arrive at the receiver with amplitude and phase fluctuations.

The problem of characterizing these fluctuations has been studied by many investigators throughout the world. The most complete treatments appear in books written by Chernov [7] and Tatarski [8]. Both books also contain lengthy lists of references to most of the other authors. Chernov uses a method attributed to Rytov to calculate the fluctuations of acoustical waves. The advantage of Rytov's method over the small perturbation method is that the fluctuations calculated are not restricted to be small. In Chapter II we use the Rytov approach in our derivation of the amplitude and phase fluctuations of em waves for the dual bistatic radar system.

A. Quasi-Homogeneous Wave Equation

The necessary wave equation is derived from Maxwell's equations and to the constitutive relations. A linearized form of the wave equation is solved by the method of Greens function and Fourier transforms.

The following assumptions are made to define the medium:

1. Non-conducting
2. Infinite in extent
3. Isotropic
4. Slowly varying

$$|\nabla n/n| \ll |kn|^2 \quad ,$$

and,

$$|\dot{n}/n| \ll \omega \quad .$$

n is the refractive index, k is the wave number, and ω is the frequency.

5. Weakly inhomogeneous

$$n(\bar{r},t) = n_o + u(\bar{r},t) , \qquad |u| \ll n_o .$$

6. Statistically homogeneous and isotropic

$$\langle u(\bar{r}_1)\ u(\bar{r}_2)\rangle = \sigma(\bar{r}_1)\ \sigma(\bar{r}_2)\ F(|\bar{r}_2 - \bar{r}_1|) .$$

This defines the spatial randomness. Statistically homogeneous means the correlation depends on the coordinate difference while statistically isotropic means the correlation has the same scale size in all three directions.

F() describes the properties local to an arbitrary point.

7. Wide sense stationary

$$\langle u(t)\rangle = \text{constant} ,$$

$$\langle u(t_1)\ u(t_2)\rangle = F(t_2 - t_1) .$$

This defines the time randomness to be a function of the coordinate difference, also.

8. Large scale size 'a'

$$kn_o a \gg 1 .$$

This condition means the scattering is directed into a narrow cone centered on the line of propagation.

The following Maxwell equations are used.

$$\bar{\nabla} \times \bar{E} = -\dot{\bar{B}} ,$$

$$\bar{\nabla} \times \bar{H} = J + \dot{\bar{D}} ,$$

$$\bar{\nabla} \cdot \bar{D} = \rho . \qquad (2.1)$$

The constitutive relations are required, also.

$$\bar{B} = \mu_o \bar{H} ,$$

$$\bar{D} = e_o n^2 \bar{E} . \qquad (2.2)$$

The list of assumptions implies that $\rho = \bar{J} = 0$; that is, there are no sources in the medium.

Observe from (2.2) that $\bar{\nabla} \cdot \bar{D} = 0$ but,

$$\bar{\nabla} \cdot \bar{E} = \bar{E} \cdot \overline{\nabla n^2}/n^2 \ . \tag{2.3}$$

Using (2.3) and the vector identity,

$$\bar{\nabla} \times \bar{\nabla} \times \bar{E} = \bar{\nabla}(\bar{\nabla} \cdot \bar{E}) - \nabla^2 \bar{E} \ ,$$

in (2.1) and (2.2) gives,

$$\nabla^2 E - \mu_o \ddot{\bar{D}} = \overline{-\nabla(\bar{E} \cdot \overline{\nabla \ln n^2})} \ .$$

Carry out the two time derivatives in $\ddot{\bar{D}}$ to get

$$\nabla^2 \bar{E} - (n/c)^2 \ddot{\bar{E}} = \overline{-\nabla(\bar{E} \cdot \overline{\nabla \ln n^2})} + (2\dot{n}^2 \dot{\bar{E}} + \ddot{n}^2 \bar{E})/c^2 \ . \tag{2.4}$$

By using the slowly varying assumption, No. 4, the two right-hand quantities in (2.4) can be neglected (Appendix A) to get,

$$\nabla^2 \bar{E} - (n/c)^2 \ddot{\bar{E}} = 0 \ . \tag{2.5}$$

The rectangular components of $\bar{E}$ may now be found from three similar scalar wave equations. Without loss of generality, we consider the equation for one of the components,

$$\nabla^2 E - (n/c)^2 \ddot{E} = 0 \ . \tag{2.6}$$

In general, we are looking for a solution $E(\bar{r}, t)$ of the form

$$E = Ae^{i(\omega t - S)} \tag{2.7}$$

where the amplitude and phase are real functions of $\bar{r}$ and t; $A = A(\bar{r}, t)$ and $S = S(\bar{r}, t)$. We use Rytov's [9] approach and define a complex-phase function $V = V(\bar{r}, t)$ such that,

$$E = A_o e^{i(\omega t - V)} , \tag{2.8}$$

where A_o is constant.

Comparing (2.7) and (2.8) gives,

$$V = S + i \ln (A/A_o) . \tag{2.9}$$

Observe that the $\text{Re } V = S$, the phase; and, the $\text{Im } V = \ln (A/A_o)$, the amplitude. Plugging (2.8) into (2.6) gives an equation for the complex phase V,

$$\left|\overline{\nabla V}\right|^2 + i\nabla^2 V - (n/c)^2 \left[(\omega - \dot{V})^2 + i\ddot{V}\right] = 0 . \tag{2.10}$$

This important equation for the complex phase is the starting point for both the ray theory and the wave theory characterizations in the next two sections.

The inclusion of the retarded potential argument in (2.10) represents a slight extension to the existing theory on propagation through a randomly inhomogeneous medium. This argument is neglected by most authors since there is no way to make use of it in the existing measurement apparatus. The proposed dual bistatic radar scheme motivates this extension since it relies on the retarded potential argument for its operation.

B. Ray Theory

We first solve (2.10) for the geometrical optics or ray theory approximation. The appropriate equation is found by letting the free space wave number k get very large ($k = \omega/c$). This is the same as assuming that a, the scale size of the inhomogeneities, is large compared to wavelength λ. A second condition required for the ray theory approximation (to be shown in Section II.C) is that $\sqrt{\lambda R} \ll a$. R is the length

of the propagation path. The physical meaning of the second condition is: the size of the first Fresnel zone must be small compared to the scale size of the inhomogeneities.

To demonstrate the k dependence in (2.10), we write S in an alternate form, $S = kS_2$ such that (2.9) is

$$V = kS_2 + i \ \ell n \ (A/A_o) \ . \tag{2.11}$$

By putting (2.11) into (2.10), dividing by k^2, and grouping terms according to k^{-n},

$$k^0: \ |\overline{\nabla S_2}|^2 - (n/c)^2 \ (c - \dot{S}_2)^2 = 0 \ . \tag{2.12}$$

$$k^{-1}: \ [\overline{2\nabla S_2} \cdot \overline{\nabla \ell n \ (A/A_o)} + \nabla^2 S_2] - (n/c)^2 \ [-2(c - \dot{S}_2) \ \ell n \dot{} (A/A_o) + \ddot{S}_2] = 0 . \tag{2.13}$$

k^{-2}: neglect.

This process conveniently separated (2.10) into real, (2.12), and imaginary, (2.13), parts.

Rewriting (2.12) and (2.13) in our S and V notation gives

$$|\nabla S|^2 = (n/c)^2 \ (\omega - \dot{S})^2 \ , \tag{2.14}$$

$$2\overline{\nabla S} \cdot \overline{\nabla \ \ell n \ A/A_o} + \overline{\nabla^2 S} = (n/c)^2 \ [-2(\omega - \dot{S}) \ \ell n \dot{} (A/A_o) + \ddot{S}] \ . \tag{2.15}$$

Define a vector $(n/k)\overline{k}$ to represent the index of refraction in the direction of the wave normal. Rewrite (2.14) as

$$\overline{\nabla S} = (n/\omega) \ (\omega - \dot{S})\overline{k} = - (n\dot{S}/\omega)\overline{k} + n\overline{k} . \tag{2.16}$$

We have chosen the same sign for both square roots in writing (2.16) because it leads to the retarded potential form of solution. Different signs for the square roots would give the advanced potential form.

To check the form of (2.15) and (2.16), define the following operator,

$$\bar{\square} \stackrel{df}{=} \bar{\nabla} + (n/\omega)\bar{k}\,\partial_t \quad . \tag{2.17}$$

This makes the phase equation (2.16),

$$\overline{\square S} = n\bar{k} \quad . \tag{2.18}$$

By substituting for $\overline{\nabla S}$ from (2.16) into (2.15) and using (2.17), the amplitude equation (2.15) is

$$2\bar{G} \cdot \overline{\square B} + \bar{\square} \cdot \bar{G} = 0 , \tag{2.19}$$

where

$$G \stackrel{df}{=} (\omega - \dot{S})\bar{k} ,$$

$$B \stackrel{df}{=} \ell n\, A/A_o . \tag{2.20}$$

Equations (2.18) and (2.19) are similar in form to those derived in Stratton [10], but significantly differ in that we have included the time variation in the refractive index. The importance of this time variation is that it leads to the retarded potential phase and amplitude solutions.

To solve (2.18) we first find the difference equation between the actual equation and the static homogeneous equation. This difference equation is solved by finding the Greens function through the method of Fourier transforms and countour integration. Using the Greens function, we write the final answer in integral form.

For the static homogeneous medium, the refractive index $n(\bar{r}, t) = n_o$, a constant, (2.18) or (2.16) gives

$$\overline{\nabla S_o} = n_o \bar{k} \quad . \tag{2.21}$$

Define the difference variable as $S_1 = S - S_o$ and the refractive index as $n(\bar{r}, t) = n_o + u(\bar{r}, t)$. n_o is the mean value of $n(r, t)$; and, $u(\bar{r}, t)$

is a random process such that $|u| \ll n_o$ by assumption No. 5 of Section IIA.

Substract (2.21) from (2.16) to get

$$\overline{\nabla S_1} + (n\dot{S}/\omega)\overline{k} = (n - n_o)\overline{k} \quad . \tag{2.22}$$

By assumption No. 5,

$$n\dot{S} = n\dot{S}_1 = (n_o + u)S_1 \cong n_o\dot{S}_1 \quad ,$$

such that,

$$\overline{\nabla S_1} + (n_o/\omega)\dot{S}_1\overline{k} = u\overline{k} \quad . \tag{2.23}$$

Without loss of generality, we may solve (2.23) by finding any one of the three typical components. After the manner in (2.17) we define the spatial derivative as $\partial_r \overset{df}{=} \partial/\partial r$ for $r = x,y,z$ and $S_{1r} = \partial S_1/\partial r$.
A typical component is

$$S_{1r} + (n_o/\omega)\dot{S}_1 k = uk \tag{2.24}$$

where we keep in mind that k is really $k^{(r)}$, that component of the wave normal in the r-th direction..

Define the following Fourier transform,

$$S(p,s) = \int_{-\infty}^{\infty} dr \int_{-\infty}^{\infty} dt S(r,t)\ e^{-i(st - pr)} \tag{2.25}$$

and,

$$S(r,t) = \int_{-\infty}^{\infty} (dp/2\pi) \int_{-\infty}^{\infty} (ds/2\pi)\ S(p,s)\ e^{i(st - pr)} \quad . \tag{2.26}$$

To find the Greens function, S_{1G}, replace uk in (2.24) by $k\delta(r - r')$ $\delta(t - t')$ and compute the Fourier transform of (2.24) with (2.25). Since

the solution depends upon the difference of $r-r'$ and $t-t'$, set $r' = t' = 0$. We get

$$-ipS_1 + is(1/v)S_1 = 1$$

where $v \overset{df}{=} c/n_o$. Therefore,

$$S_1(p,s) = -iv/(s - vp) \quad . \tag{2.27}$$

The inverse transform of (2.27) by the use of (2.26) gives S_{1G}.

$$S_{1G}(r,t) = -iv/(2\pi)^2 \int_{-\infty}^{\infty} dp\, e^{-ipr} \int_{-\infty}^{\infty} ds\, e^{ist}/(s - vp) \quad . \tag{2.28}$$

The s integral involves a choice in the path of integration. Make the assumption that $S_{1G} = 0$ for $t < 0$, that is, the process is causal. Then the contour must go under the pole as shown in Fig. 4.

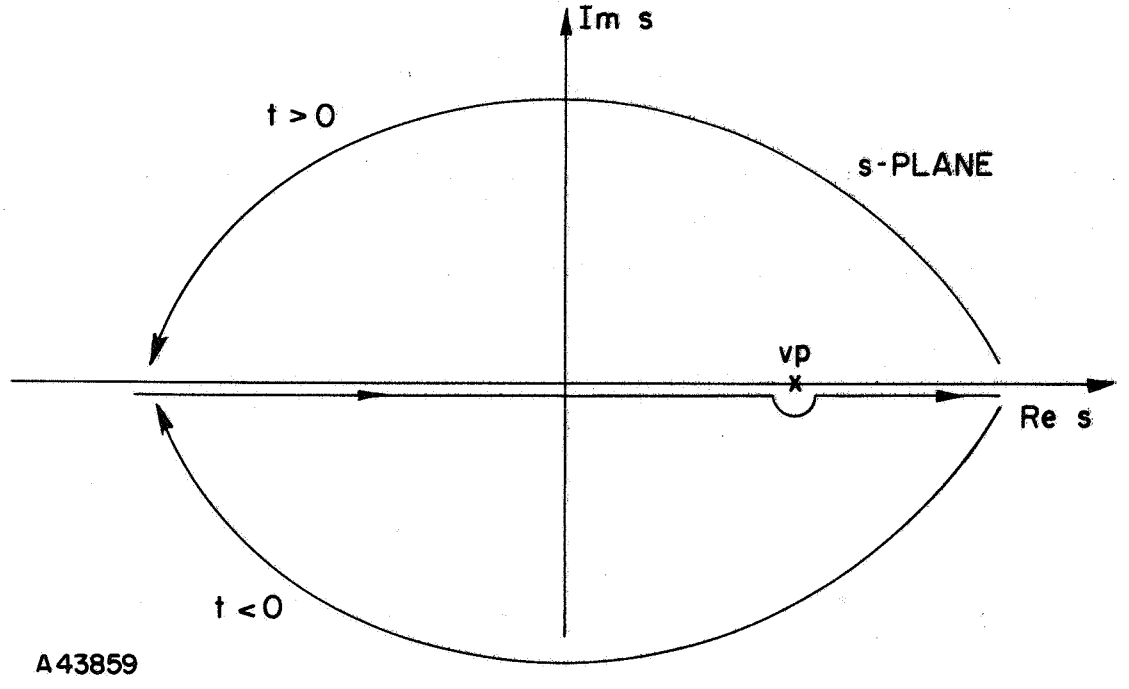

Fig. 4. CASUAL CONTOUR.

Using this contour (2.28) becomes

$$S_{1G}(r,t) = (v/2\pi) \int_{-\infty}^{\infty} dp\, e^{-i(r - vt)p} = v\delta(r - vt) \ . \qquad (2.29)$$

The solution of (2.24) is (recalling $r \to |r - r'|$ and $t \to t - t'$)

$$S_{1G}(r,t) = vk \int dr' \int dt'\ u(\bar{r}',t')\ \delta[|r - r'| - v(t - t')] \ .$$

Doing the t' integration,

$$S_1(r,t) = k \int dr'\ u(\bar{r}', t - |r - r'|/v); \qquad \begin{array}{l} r = x,y,z, \\ r' = x',y',z', \\ r' = (z',y',z'). \end{array} \qquad (2.30)$$

Equation (2.30) is a statement of Fermat's principle of least time. It states that an em ray between two points travels the path which it can traverse in the shortest time. $S_1(r,t)$ is called the retarded-potential phase because of the time argument in u. This argument, $t - |r - r'|/v$, says that the contribution to the phase at time t and position r must take into account the finite propagation velocity v for a disturbance which is a distance $|r - r'|$ away from r.

We want to compute the autocorrelation function of $S = S_o + S_1$. $S_o = n_o kr$ is a constant once the path length is fixed and would be subtracted out of the correlation. Therefore, the subscript 1 is dropped in (2.30). Furthermore, we choose the direction of propagation to be along the $+z$ axis such that the spacecraft is at $z = 0$ and the ground station is at $z = R$ as shown in Fig. 1. We update (2.30) for the one-way phase from the spacecraft to the ground station.

$$S(R, t_g) = k \int_o^R dz'\ u(x',y',z',\ t_g - (R - z')/v). \qquad (2.31)$$

t_g is time measured at the ground. We switch the time reference to the spacecraft by noting that $t_g = t_s + R/v$. Then

$$S(R, t_s) = k \int_o^R dz' \; u(x', y', z', \; t_s + z'/v) \; . \qquad (2.32)$$

The one-way phase going from the ground to the spacecraft is [by setting $r = 0$ in (2.30)]

$$S(o, t_s) = k \int_o^R dz' \; u(x', y', z', \; t_s - z'/v) \; . \qquad (2.33)$$

In the ray theory approximation the inclination of the ray is small so that $x \ll a$ and $y \ll a$. Therefore, we set $x' = y' \cong 0$ such that $r' \cong (0, 0, z') \equiv (z')$. The total phase at the ground, receiver_2, is the sum of (2.32) and (2.33). Dropping the "s" subscript and the prime notation,

$$S(t) = k \int_o^R dz[u(z, t - z/v) + u(z, t + z/v)] \; . \qquad (2.34)$$

The time autocorrelation is the expected value of the product $S(t_1) \; S(t_2)$ which is written as

$$R_S(t_1, t_2) = \langle S(t_1) \; S(t_2) \rangle \; .$$

Multiply $S(t_1)$ and $S(t_2)$ and take the expected value to get

$$R_s(t_1, t_2) = k^2 \int_o^R \int_o dz_1 \; dz_2 \; \langle [u(z_1, t_1 - z_1/v) + u(z_1, t_1 + z_1/v)]$$

$$\cdot \; [u(z_2, t_2 - z_2/v) + u(z_2, t_2 + z_2/v)] \rangle \; . \qquad (2.35)$$

At this point we use the two statistical assumptions of Section IIA:

6. The medium is locally statistically homogenous so that the correlation function depends only upon the spatial coordinate difference of $u(\bar{\alpha},\beta)$, namely $|\bar{\alpha}_2 - \bar{\alpha}_1|$.
7. The medium is statistically stationary so that the correlation function depends only upon the time coordinate difference of $u(\bar{\alpha},\beta)$, namely $|\beta_2 - \beta_1|$.

The expected value quantity in (2.35) gives four terms which are the refractive index correlations. We represent these four terms with new functions $\sigma()$ and $F(,)$.

$$\langle u(z_1, t_1 - z_1/v)\, u(z_2, t_2 - z_2/v)\rangle = \sigma(z_1)\,\sigma(z_2)\, F[z_2 - z_1, t_2 - t_1 - (z_2 - z_1)/v]$$

$$\langle u(z_1, t_1 + z_1/v)\, u(z_2, t_2 + z_2/v)\rangle = \sigma(z_1)\,\sigma(z_2)\, F[z_2 - z_1, t_2 - t_1 + (z_2 - z_1)/v]$$

$$\langle u(z_1, t_1 - z_1/v)\, u(z_2, t_2 + z_2/v)\rangle = \sigma(z_1)\,\sigma(z_2)\, F[z_2 - z_1, t_2 - t_1 + (z_2 + z_1)/v]$$

$$\langle u(z_1, t_1 + z_1/v)\, u(z_2, t_2 - z_2/v)\rangle = \sigma(z_1)\,\sigma(z_2)\, F[z_2 - z_1, t_2 - t_1 - (z_2 + z_1)/v] \qquad (2.36)$$

$\sigma()$ is a source distribution function which depends upon position. At a particular point its magnitude is the standard deviation of the source variation at this point. $F(,)$ is the normalized refractive index correlation function such that $|F(,)| \leq 1$ and $F(o,o) = 1$. Essentially the two arguments of F contain the space and time scale size information. F is implicitly a function of position through the scale size parameters, also.

The following change of variables is used to reduce (2.35) and (2.36).

$$z_o = (z_2 + z_1)/2$$
$$z = z_2 - z_1$$
$$\tau = t_2 - t_1 \,. \qquad (2.37)$$

Now (2.35) may be written as,

$$R_s(\tau) = k^2 \iint_o^R dz_1\, dz_2\, \sigma(z_1)\, \sigma(z_2)\, [F(z, \tau - z/v) + F(z, \tau + z/v)$$

$$+ F(z, \tau - 2z_o/v) + F(z, \tau + 2z_o/v)] \ . \qquad (2.38)$$

The two F functions $F(z, \tau \pm z/v)$ in (2.38) represent the one way self-correlation terms; and, their arguments depend only upon the coordinate differences. The last two F functions $F(z, \tau \pm 2z_o/v)$ in (2.38) represent the two way cross-correlation terms such that the sum of $(z_1 + z_2) = 2z_o$ appears in the time argument of F. The terms with the sum argument enable one to use $R_s(\tau)$ to isolate the local sources versus position along the path. Chapter III discusses these two terms in detail.

We return to (2.19) and solve for the amplitude fluctuations. This is done by fixing the $\bar{k}$ vector to lie along the +z axis such that $\bar{k} = k\hat{z}$. This reduces (2.19) to the following scalar equation.

$$B_z + (n/c)B_t = -1/2(\omega - \dot{S})[\partial_z(\omega - \dot{S}) + (n/c)\, \partial_t(\omega - \dot{S})] \ . \qquad (2.39)$$

We get for the solution,

$$B = -(1/2)\, \ell n\, (\omega - \dot{S}) + \text{constant} \ , \qquad (2.40)$$

where from (2.34),

$$\dot{S} = k \int_o^R dz\, [\dot{u}(z, t - z/v) + \dot{u}(z, t + z/v)] \ . \qquad (2.41)$$

The constant in (2.40) is found by observing that for zero path length ($R = 0$), $\dot{S} = 0$ such that,

$$B = \ell n\, [A(o, o, o)/A_o] = 0 = -(1/2)\, \ell n\, \omega + \text{constant} \ .$$

Plugging this into (2.40) gives

$$B = \ell n\ A/A_o = -(1/2)\ \ell n\ (1 - \dot{S}/\omega), \tag{2.42}$$

or

$$A = A_o/(1 - \dot{S}/\omega)^{1/2}\ . \tag{2.43}$$

Equation (2.43) is inconvenient for computing statistical averages so we use (2.42) to compute the log-amplitude autocorrelation.

$$R_B(t_1, t_2) = \langle B(t_1)\ B(t_2)\rangle = (1/4)\ \langle \ell n\ (1 - \dot{S}(t_1)/\omega)\ \ell n\ (1 - \dot{S}(t_2)/\omega)\rangle\ .$$

By the slowly varying assumption, $\dot{S}/\omega \ll 1$, we may use the power series expansion of ℓn to write,

$$R_B(t_1, t_2) = (1/4\omega^2)\ \langle \dot{S}(t_1)\ \dot{S}(t_2)\rangle + \ldots \tag{2.44}$$

and neglect all higher order terms. Using our previous assumptions of stationarity and statistical homogeneity, (2.44) becomes

$$R_B(\tau) = -(1/4\omega^2)\ d^2R_s(\tau)/d\tau^2 \tag{2.45}$$

In writing (2.45) we have made use of the autocorrelation derivative [11].

C. Wave Theory

Reconsider (2.10) for the more general wave theory case. Equation (2.10) may be written as

$$|\overline{\nabla V}|^2 + i\nabla^2 V - (n/c)^2\ (\dot{V}^2 - 2\omega\dot{V} + i\ddot{V}) = (kn)^2\ . \tag{2.46}$$

The difference equation approach, motivated by Chernov, is used to solve the complex-phase equation. Denote the solution for a static homogeneous medium to be V_o corresponding to a constant refractive index n_o,

$$|\overline{\nabla V}_o|^2 + i\nabla^2 V_o = (kn_o)^2 \ . \qquad (2.47)$$

Define the difference variable as $V_1 = V - V_o$ and the refractive index as $n = n_o + u(\vec{r}, t)$. Subtract (2.47) from (2.46) to get $(\dot{V}_1 = \dot{V})$

$$|\overline{\nabla V}_1|^2 + 2\overline{\nabla V}_o \cdot \overline{\nabla V}_1 + i\nabla^2 V_1 - [(n_o + u)/c]^2 [\dot{V}_1^2$$

$$- 2\omega\dot{V}_1 + i\ddot{V}_1] = k^2 u(2n_o + u) \ . \qquad (2.48)$$

For a weakly inhomogeneous medium, assumption No. 5 of Section IIA, $u \ll n_o$ such that (2.48) is,

$$\underline{|\overline{\nabla V}_1|^2 + 2\overline{\nabla V}_o \cdot \overline{\nabla V}_1} + i\nabla^2 V_1 - (1/v)^2 \underline{(\dot{V}_1^2 - 2\omega\dot{V}_1} + i\ddot{V}_1) = 2k^2 n_o u \ , \qquad (2.49)$$

where $v = c/n_o$. The two underlined terms in (2.49) are approximately,

$$\overline{\nabla V}_1 \cdot (\overline{\nabla V}_1 + 2\overline{\nabla V}_o) \cong 2\overline{\nabla V}_1 \cdot \overline{\nabla V}_o$$

$$\dot{V}_1(\dot{V}_1 - 2\omega) \approx -2\omega\dot{V}_1 \qquad (2.50)$$

by requiring that

$$|\overline{\nabla V}_1|/|\overline{\nabla V}_o| = |\overline{\nabla V}_1|/kn_o \ll 1 \qquad (2.51a)$$

$$|\dot{V}_1|/\omega \ll 1 \ . \qquad (2.51b)$$

The approximation (2.50) makes (2.49) a linear equation,

$$[2\overline{\nabla V}_1 \cdot \overline{\nabla V}_o + i\nabla^2 V_1] - (1/v)^2 [-2\omega\dot{V}_1 + i\ddot{V}_1] = 2k^2 n_o u \qquad (2.52)$$

The conditions in (2.51) are a definition of the "slowly varying" medium for the complex-phase function V. Since $V_1 = S_1 + i\,\ell n\,(A/A_o)$, (2.51) says that the relative phase change must be small in one RF wavelength and one RF period.

$$|\overline{\nabla S}_1|/kn_o \ll 1$$

and

$$|\dot{S}_1|/\omega \ll 1 \ . \qquad (2.53$$

Also, the relative amplitude change must be small in one RF wavelength and one RF period

$$|\overline{\nabla \ell n\ A/A_o}|/kn_o \ll 1$$

and

$$|\ell n\dot{}A/A_o|/\omega \ll 1 \ . \qquad (2.54)$$

The inequality (2.54) is true if the amount of scattering in going a cycle is small. The inequality (2.53) implies that the angle of inclination of the ray to the initial direction is small.

Observe that (2.54) is always true in a weakly inhomogeneous medium ($|u| \ll n_o$). For large scale fluctuations ($kn_o a \gg 1$), the scattered power is concentrated in a small solid angle $\theta \sim 1/kn_o a$ such that the angle of inclination of the ray is small, also. Small scale fluctuations ($kn_o a \ll 1$) cause isotropic scattering where it is not always true that the amplitude of the scattered waves is small compared to the amplitude of the incident waves. Therefore, the solution of (2.52) is generally restricted to the $kn_o a \gg 1$ case, assumption No. 8 of Section IIA.

We proceed to the solution of (2.52) by the Fourier transform and Greens function method. Motivated by Chernov [7] we define a function $W(\bar{r}, t)$ such that the static solution $E_o = \exp[i(\omega t - V_o)]$ factors out of V_1.

$$V_1 = W/E_o = W\ e^{-i(\omega t - V_o)} \ . \qquad (2.55)$$

This converts (2.52) to,

$$\nabla^2 W - (1/v)^2\ \ddot{W} = -2ik^2 n_o u\ E_o \ . \qquad (2.56)$$

To find the Greens function for (2.56) we consider,

$$\nabla^2 W - (1/v)^2 \ddot{W} = \delta(\bar{r} - \bar{r}')\ \delta(t - t') \ . \qquad (2.57)$$

Equation (2.57) is in a very standard form, more so than (2.24) of the ray theory section. We quote from [12] the Greens function as

$$W_G = -(v/4\pi|\bar{r} - \bar{r}'|).\ \delta[|\bar{r} - \bar{r}'| - v(t - t')], \qquad t > t' \ . \qquad (2.58)$$

This gives the solution of (2.56) as the volume and time integral

$$W(\bar{r}, t) = i\left(k^2 n_o v/2\pi\right) \int dv' \int dt'\ u(\bar{r}', t')\ E_o(r', t')$$

$$\cdot\ \delta[|\bar{r} - \bar{r}'| - v(t - t')]/|\bar{r} - \bar{r}'| \ .$$

Integrating out t' and letting $\Delta r \overset{df}{=} |\bar{r} - \bar{r}'|$,

$$W(\bar{r}, t) = i(k^2 n_o/2\pi) \int dv'\ u(\bar{r}', t - \Delta r/v)\ E_o(\bar{r}', t - \Delta r/v)/\Delta r \ . \qquad (2.59)$$

Putting (2.59) into (2.55) gives

$$V_1(\bar{r}, t) = i\left[k^2 n_o/2\pi\ E_o(\bar{r}, t)\right] \int dv'\ u(\bar{r}', t - \Delta r/v)\ E_o(\bar{r}', t - \Delta r/v)/\Delta r \ . \qquad (2.60)$$

By directing the k vector along the z direction, $V_o = kn_o z$ in E_o of (2.55). Replacing E_o in (2.60) gives,

$$V_1(\bar{r}, t) = i(k^2 n_o/2\pi) \int dv'\ u(\bar{r}', t - \Delta r/v)\ \frac{\exp}{\Delta r} \left\{-ikn_o[\Delta r - (z - z')]\right\}. \qquad (2.61)$$

For large scale inhomogeneities ($kn_o a \gg 1$), there is negligible reflection so that the region of integration is the infinite slab between $z' = 0$ and $z' = z$. In fact the region which contributes most to the signal at the receiver site is a cone whose apex is at the receiver and whose angle is $1/kn_o a$. This angle is usually much less than an antenna beamwidth so that we can neglect the antenna pattern transfer function in our derivations.

The real and imaginary parts of (2.61) are the one-way phase and amplitude fluctuations at $\bar{r} = (o, o, z)$.

$$S_1(z,t) = (k^2 n_o/2\pi) \int_0^z dz' \iint_{-\infty}^{\infty} dx'\ dy'$$

$$\cdot\ (\sin kn_o\ [\Delta r - (z - z')]/\Delta r)\ u(\bar{r}', t - \Delta r/v) \qquad (2.62)$$

$$B = \ell n\ [A(z,t)/A_o] = (k^2 n_o/2\pi) \int_0^z dz' \iint_{-\infty}^{\infty} dx'\ dy'$$

$$\cdot\ (\cos kn_o\ [\Delta r - (z - z')]/\Delta r)\ u(\bar{r}', t - \Delta r/v)\ . \qquad (2.63)$$

Equations (2.62) and (2.63) are identical to (90) and (91) derived by Chernov [13] with the exception that the retardation argument has been included here. This argument is necessary for our bistatic radar application. Before writing (2.62) and (2.63) in the bistatic form similar to (2.34) we form the Fresnel approximation with

$$\Delta r = \sqrt{(z - z')^2 + \rho^2}$$

where

$$\rho^2 = x'^2 + y'^2\ .$$

Because of the cone argument following (2.61), it is a good approximation to use $\rho^2 \ll (z - z')^2$. Since $z' \leq z$,

$$\Delta r \approx (z - z') + \rho^2/2(z - z') \tag{2.64}$$

and,

$$1/\Delta r \approx \frac{1}{(z - z')} \tag{2.65}$$

Using (2.64) and (2.65) in the sin and cos terms of (2.62) and (2.63) we define

$$\Phi_s(z - z', \rho) \stackrel{df}{=} [kn_o/2\pi(z - z')] \sin \left[kn_o\rho^2/2(z - z')\right]$$

$$\Phi_c(z - z', \rho) \stackrel{df}{=} [kn_o/2\pi(z - z')] \cos \left[kn_o\rho^2/2\pi(z - z')\right] . \tag{2.66}$$

Then (2.62) and (2.63) can be written in the Fresnel approximation form.

$$S_1(z, t) = k \int_o^z dz' \iint_{-\infty}^{\infty} dx'\, dy'\, \Phi_s\, u(\overline{r}', t - |z - z'|/v)$$

$$B(z, t) = k \int_o^z dz' \iint_{-\infty}^{\infty} dx'\, dy'\, \Phi_c\, u(\overline{r}', t - |z - z'|/v) . \tag{2.68}$$

Using the same argument leading up to (2.34), the phase from the spacecraft to the ground is,

$$S(R, t_s) = k \int_o^R dz' \iint_{-\infty}^{\infty} dx'\, dy'\, \Phi_s\, (R - z', \rho)\, u(\overline{r}', t_s + z'/v) . \tag{2.69}$$

The phase from the ground to the spacecraft is,

$$S(o,t_s) = k \int_o^R dz' \iint_{-\infty}^{\infty} dx'\ dy'\ \Phi_s\ (z',\rho)\ u(\bar{r}', t_s - z'/v)\ . \tag{2.70}$$

Sum (2.69) and (2.70) (dropping the "s" in t_s and the prime notation) to get the bistatic signal at the ground station, receiver$_2$.

$$S(t) = k \int_o^R dz \iint_{-\infty}^{\infty} dx\ dy \left\{ \Phi_s\ (z,\rho)\ u(\bar{r}, t - z/v) + \Phi_s\ (R - z,\rho) \right.$$

$$\left. \cdot\ u(\bar{r}, t + z/v) \right\}\ . \tag{2.71}$$

Similarly,

$$B(t) = k \int_o^R dz \iint_{-\infty}^{\infty} dx\ dy \left\{ \Phi_c\ (z,\rho)\ u(r, t - z/v) + \Phi_c\ (R - z,\rho) \right.$$

$$\left. \cdot\ u(r, t + z/v) \right\}\ . \tag{2.72}$$

We compute the time autocorrelation of the phase S as in (2.35),

$$R_s(t_1,t_2) = k^2 \iint_o^R dz_1\ dz_2 \iiiint_{-\infty}^{\infty} dx_1 dx_2 dy_1 dy_2 \left\langle \left\{ \Phi_s\ (z_1,\rho_1)\ u(\bar{r}_1, t_1 - z_1/v) \right.\right.$$

$$\left.\left. + \Phi_s\ (R - z_1,\rho_1)\ u(\bar{r}_1, t_1 + z_1/v) \right\} \left\{ \Phi_{2-} u_{2-} + \Phi_{2+} u_{2+} \right\} \right\rangle\ . \tag{2.73}$$

Again make the assumption of a statistically homogeneous and stationary medium so that the correlation function depends on the coordinate differences. We define the same $\sigma()$ and $F(,)$ functions as in (2.36) from the four product terms in (2.73).

For example,

$$\langle u(r_1, t_1 + z_1/v)\ u(r_2, t_2 - z_2/v)\rangle = \sigma(r_1)\ \sigma(r_2)$$

$$\cdot\ F(|r_2 - r_1|, \tau - (z_2 + z_1)/v)\ .$$

We make the assumption that the standard deviation distribution is independent of the x and y directions. That is,

$$\langle u_1 u_2\rangle = \sigma(z_1)\ \sigma(z_2)\ F(|r_2 - r_1|, \tau - (z_2 - z_1)/v)\ .$$

Physically this amounts to orienting the wave normal perpendicular to the homogeneous strata in the x and y directions. Even when there is no such strata the assumption is good because the x and y changes are masked by the scale size along the z-axis. Using (2.36), (2.73) becomes,

$$R_s(\tau) = k^2 \iint_0^R dz_1 dz_2\ \sigma(z_1)\sigma(z_2) \iiiint_{-\infty}^{\infty} dx\ dx_o\ dy\ dy_o \Big\{ \Phi_s(z_1,\rho_1)\ \Phi_s(z_2,\rho_2)\ F_1(\Delta r, \tau - z/v)$$

$$+ \Phi_s(z_1,\rho_1)\ \Phi_s(R - z_2,\rho_2)\ F_2(\Delta r, \tau + 2z_o/v) + \Phi_s(R - z_1,\rho_1)\ \Phi_s(z_2,\rho_2)\ F_3(\Delta r, \tau - 2z_o/v)$$

$$+ \Phi_s(R - z_1,\rho_1)\ \Phi_s(R - z_2,\rho_2)\ F_4(\Delta r, \tau + z/v)\Big\}. \qquad (2.74)$$

We have used the following center of mass and difference coordinates in (2.74):

$$z = z_2 - z_1, 2z_o = z_2 + z_1; \tau = t_2 - t_1; y = y_2 - y_1, 2y_o$$

$$= y_2 + y_1; \Delta r = |\overline{r}_2 - \overline{r}_1|; x = x_2 - x_1, 2x_o = x_2 + x_1\ .$$

Also, in (2.74) note the coding of the $F(,)$ function arguments by a subscript (i.e., $F(\Delta r, \tau - 2z_o/v) = F_3$). F_1 and F_4 are the self-correlation terms while F_2 and F_3 are the cross-correlation terms.

x_o and y_o can be integrated because they appear only in Φ_s through the ρ variable. For example, the first term in (2.74) contains the integral,

$$I = \iint_{-\infty}^{\infty} dx_o\, dy_o\, \Phi_s\left(z_1, \left[(x_o - x/2)^2 + (y_o - y/2)^2\right]^{1/2}\right) \Phi_s\left(z_2, \left[(x_o + x/2)^2 + (y_o + y/2)^2\right]^{1/2}\right) .$$

Using the identity in Appendix B this integral is

$$I = \tfrac{1}{2}[\Phi_s(z,\rho) + \Phi_s(2z_o,\rho)] , \tag{2.75}$$

where

$$\rho = (x^2 + y^2)^{1/2} .$$

Integrating the remaining three terms in a similar manner (2.74) becomes,

$$R_s(\tau) = (k^2/2) \iint_o^R dz_1\, dz_2\, \sigma(z_1)\, \sigma(z_2) \iint_{-\infty}^{\infty} dx\, dy \left[\Phi_s(z,\rho)(F_1 + F_4) + \Phi_s(2z_o,\rho)\, F_1 + \Phi_s(2[R - z_o],\rho)\, F_4 + \Phi_s(R - 2z_o,\rho)(F_2 + F_3) + \Phi_s(R - z,\rho)\, F_2 + \Phi_s(R + z,\rho)\, F_3\right] . \tag{2.76}$$

Starting with (2.72) we go through a similar exercise for the amplitude to get,

$$R_B(\tau) = (k^2/2) \iint_0^R dz_1\, dz_2\, \sigma(z_1)\, \sigma(z_2) \iint_{-\infty}^{\infty} dx\, dy \Big[\Phi_s(z,\rho)(F_1 + F_4)$$

$$- \Phi_s(2z_o,\rho)\, F_1 - \Phi_s(2[R - z_o],\rho)\, F_4 + \Phi_s(R - 2z_o,\rho)(F_2 + F_3)$$

$$- \Phi_s(R - z,\rho)\, F_2 - \Phi_s(R + z,\rho)\, F_3\Big] . \qquad (2.77)$$

The six terms in the integrands of (2.76) and (2.77) are identical. It is the + and - operations which cause the difference between R_s and R_B.

Further simplification of R_s and R_B is obtained by introducing polar coordinates (ρ,ϕ) in the (x,y) plane,

$$\iint_{-\infty}^{\infty} dx\, dy = \int_0^{\infty} \rho d\rho \int_0^{2\pi} d\phi . \qquad (2.78)$$

By assuming the scale size is the same in both x and y, all of the terms in (2.76) are independent of ϕ. Doing the ϕ integral gives,

$$R_s(\tau) = \pi k^2 \iint_0^R dz_1\, dz_2\, \sigma(z_1)\, \sigma(z_2) \int_0^{\infty} \rho d\rho \Big[\Phi_s(z,\rho)(F_1 + F_4)$$

$$+ \Phi_s(2z_o,\rho)\, F_1 + \Phi_s(2[R - z_o],\rho)\, F_4 + \Phi_s(R - 2z_o,\rho)(F_2 + F_3)$$

$$+ \Phi_s(R - z,\rho)\, F_2 + \Phi_s(R + z,\rho)\, F_3\Big] . \qquad (2.79)$$

All six of the ρ integrals in (2.79) may be written as,

$$I = 2\pi \int_0^{\infty} \rho d\rho\, \Phi_s(\beta,\rho)\, F_i(\rho, z, \tau_i) \qquad i = 1,2,3,4 .$$

$$\beta = z/kn_o,\ 2z_o/kn_o,\ 2[R - z_o]/kn_o,\ \ldots,\ [R + z]/kn_o .$$

$$\Phi_s(\beta,\rho) = (1/2\pi\beta) \sin(\rho^2/2\beta) . \qquad (2.80)$$

Make the change of variable $q = \rho^2/2$ such that (2.80) becomes,

$$I = (1/\beta) \int_0^\infty dq \, \sin(q/\beta) \, F_i(q, z, \tau_i) \ . \tag{2.81}$$

Successive integration of (2.81) by parts gives,

$$I = F_i(0, z, \tau_i) - \beta^2 F_{i(2q)}(0, z, \tau_i) + \beta^4 F_{i(4q)}(0, z, \tau_i) - \ldots . \tag{2.82}$$

where

$$F_{i(nq)} \overset{df}{=} \partial^n F_i(q, z, \tau_i)/\partial q^n \qquad n = 1, 2, 3, \ldots .$$

Further study of (2.82) requires a function F_i whose q derivatives are well behaved at the origin. The gaussian function in ρ is the classical choice; but, it probably is also realistic--at least near the origin. Lastly, a great deal of insight is gained using the gaussian function. Therefore, we let

$$F_i(\rho, z, \tau_i) = g_i(z, \tau_i) \, e^{-\rho^2/a^2} \ , \tag{2.83}$$

which is,

$$F_i(q, z, \tau_i) = g_i(z, \tau_i) \, e^{-2q/a^2} \ .$$

Plugging (2.83) into (2.82) gives the desired solution.

$$I = g_i(z, \tau_i)/[1 + (2\beta/a^2)^2] = F_i(0, z, \tau_i)/[1 + (2\beta/a^2)^2] \ . \tag{2.84}$$

Putting (2.84) back into (2.79) we can write $R_s(\tau)$ subject to the regular assumptions of Section A and the assumption that F_i is gaussian for ρ near zero.

$$R_s(\tau) = (k^2/2) \iint_o^R dz_1 dz_2 \; \sigma(z_1) \; \sigma(z_2) \left\{ (F_1 + F_4) \Big/ \left[1 + (2z/kn_o a^2) \right]^2 \right.$$

$$+ F_1 \Big/ \left[1 + (4z_o/kn_o a^2) \right]^2 + F_4 \Big/ \left[1 + (4[R - z_o]/kn_o a^2) \right]^2$$

$$+ (F_2 + F_3) \Big/ \left[1 + (2[R - 2z_o]/kn_o a^2) \right]^2$$

$$\left. F_2 \Big/ \left[1 + (2[R - z]/kn_o a^2) \right]^2 + F_3 \Big/ \left[1 + (2[R + z]/kn_o a^2) \right]^2 \right\} \quad (2.85)$$

In the above,

$$F_i = F_i(0, z, \tau_i) \equiv F_i(z, \tau_i) \quad \text{and} \quad z = z_2 - z_1, \; 2z_o = z_2 + z_1.$$

The maximum value of the $2\beta/a^2$ term in (2.84) is $D \overset{df}{=} 4R/kn_o a^2$; D is called the wave parameter. By introducing in (2.85) a normalized distance $\Lambda = 1 - z_o/R$ and using the wave parameter D, (2.85) can be made a little more readable.

$$R_s(\tau) = (k^2/2) \iint_o^R dz_1 dz_2 \; \sigma(z_1) \; \sigma(z_2) \left\{ \right.$$

$$F_1(z, \tau - z/v) \left[\frac{1}{1 + D^2 (z/2R)^2} + \frac{1}{1 + D^2 \Lambda^2} \right]$$

$$+ F_4(z, \tau + z/v) \left[\frac{1}{1 + D^2 (z/2R)^2} + \frac{1}{1 + D^2 (1 - \Lambda)^2} \right]$$

$$+ F_2(z, \tau + 2z_o/v) \left[\frac{1}{1 + (D^2/4)(1 - 2\Lambda)^2} + \frac{1}{1 + (D^2/4)(1 - z/R)^2} \right]$$

$$\left. + F_3(z, \tau - 2z_o/v) \left[\frac{1}{1 + (D^2/4)(1 - 2\Lambda)^2} + \frac{1}{1 + (D^2/4)(1 + z/R)^2} \right] \right\}. \quad (2.86)$$

The amplitude correlation R_B is easily found by comparing (2.76) and (2.77) and changing four of the + signs to - signs in (2.85) or (2.86).

For the small wave parameter case $D \ll 1$, the denominators in (2.86) approach unity. This reduces (2.86) to

$$R_s(\tau) = k^2 \iint_0^R dz_1 dz_2 \; \sigma(z_1) \; \sigma(z_2) \; [F_1 + F_4 + F_2 + F_3] \; , \qquad (2.87)$$

which is the ray theory expression (2.38). Physically a small wave parameter means that the radius of the first Fresnel zone is small compared to the inhomogeneity scale size as shown in Fig. 5a.

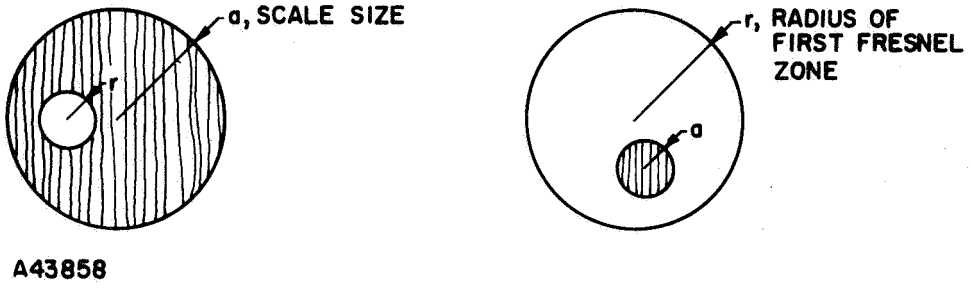

a. Small D, ray case b. Large D

Fig. 5. WAVE PARAMETER.

The physical meaning of the large $D \gg 1$ wave parameter case is shown in Fig. 5b. The large wave parameter case gives complicated expressions for the multipliers in the square brackets of (2.86). In general, $a \ll R$ such that the z/R terms may be neglected. Then the multipliers for the cross-correlated F functions (F_2 and F_3) are as illustrated in Fig. 6.

Figure 7 shows the multiplier for the F_1 or ground receiver self-correlation term. The F_4 or spacecraft self-correlation term is identical in shape but has its maximum value in the phase correlation (minimum in the amplitude correlation) at the spacecraft. For $D \ll 1$ in both Figs. 6 and 7, the multiplier value is a constant; it is very near two in the phase integrand and very near zero in the amplitude integrand.

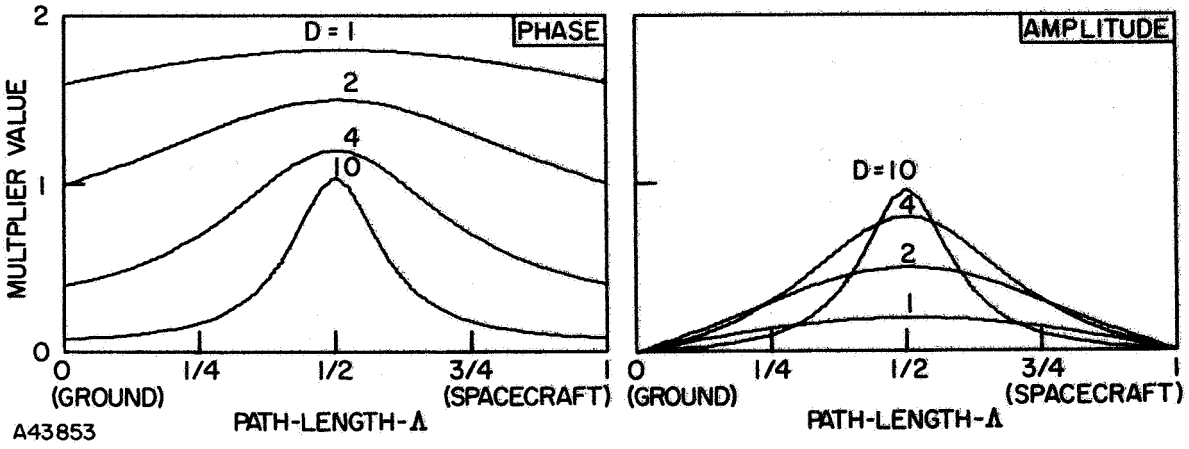

Fig. 6. CROSS-CORRELATION WEIGHTING MULTIPLIERS.

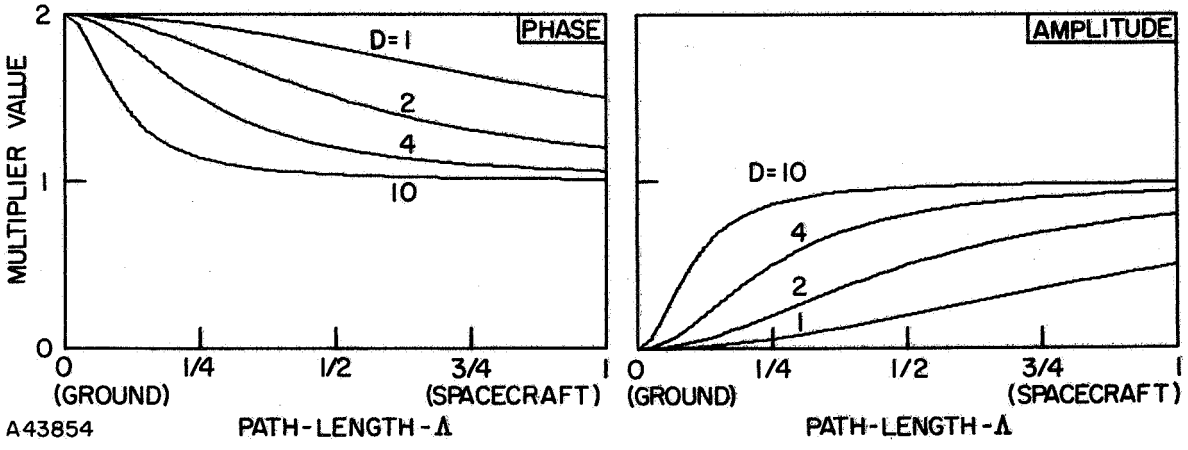

Fig. 7. SELF-CORRELATION WEIGHTING MULTIPLIERS.

Several conclusions may be drawn from these figures for the medium and large wave parameter case. First, the cross-correlation terms always weight the refractive index variations near the path center the heaviest. Thus R_s and R_B will "view" the path center best. Second, amplitude fluctuations are much stronger for large wave parameter conditions, that is, when several blobs can fit inside the first Fresnel zone. Three, the self-correlation terms will dominate in the R_s integrals near the ends of the path while they dominate in the R_B integrals near the path center.

We conclude this section with a brief look at the spherical wave approach to computing the amplitude and phase correlations. The fluctuations resulting from an incident spherical wave may be calculated from (2.60) by substituting,

$$E_o = (1/r)\ e^{i(\omega t - kn_o r)}\ , \qquad r = |\bar{r}|\ . \tag{2.88}$$

Thus,

$$V_1(r,t) = i(k^2 n_o r/2\pi)\int dv'\ u(\bar{r}', t - \Delta r/v)\ \frac{\exp\left\{-ikn[\Delta r - (r - r')]\right\}}{r'\Delta r} \tag{2.89}$$

where $\Delta r\ |\bar{r} - \bar{r}'|$. Equation (2.89) is equivalent to (2.61) for the plane wave case. By following the development from (2.61) to (2.88) it is apparent that the $\sigma(\ )$ and $F(,)$ functions and their arguments will remain the same and only the magnitude of the fluctuations may change. In fact for the large wave parameter case $D \gg 1$ the correlation expressions R_s and R_B are exactly the same [14]. Thus a spherical wave analysis does not change the basic results of this section.

D. Bandwidth

We finish the discussion of the signal and the medium by defining the equivalent bandwidth W of the medium. $1/W$ is the time scale of the medium. This is most easily done from a spectral analysis approach. The Fourier-Stieljes integral expansions for both the refractive index variation $u(z,t)$ and the received signal $S(t)$ are formed in (2.90),

$$S(t) = \int_{-\infty}^{\infty} dS(f)\ e^{i2\pi ft},$$

$$u(z,t) = \int_{-\infty}^{\infty} dU(z,f)\ e^{i2\pi ft}\ . \tag{2.90}$$

Taking the expected value of the quantities in (2.90) gives,

$$R_s(\tau) = \langle S(t_1)S^*(t_2)\rangle = \iint_{-\infty}^{\infty} \langle dS(f_1)\ dS^*(f_2)\rangle\ e^{i2\pi(f_1t_1 - f_2t_2)}$$

$$\sigma(z_1)\ \sigma(z_2)\ F(z,\tau) = \iint_{-\infty}^{\infty} \langle dU(z_1,f_1)\ dU^*(z_2,f_2)\rangle\ e^{i2\pi(f_1t_1 - f_2t_2)}\ . \tag{2.91}$$

But stationarity implies,

$$\langle dS(f_1)\ dS^*(f_2)\rangle = \delta(f_1 - f_2)\ Q_s(f_1)\ df_1df_2$$

$$\langle dU(z_1,f_1)\ dU^*(z_2,f_2)\rangle = \delta(f_1 - f_2)\ \sigma(z_1)\ \sigma(z_2)\ M(z,f_1)\ df_1df_2 \tag{2.92}$$

where $Q_s(f) \geq 0$ and $M(z,f) \geq 0$.
Therefore,

$$R_s(\tau) = \int_{-\infty}^{\infty} df\ Q_s(f)\ e^{i2\pi f\tau} \tag{2.93}$$

$$F(z,\tau) = \int_{-\infty}^{\infty} df\ M(z,f)\ e^{i2\pi f\tau} \tag{2.94}$$

The power spectral density for $F(z,\tau)$ is defined by (2.94) as $M(z,f)$. Using $M(f) = M(o,f)$, the one sided equivalent bandwidth W, termed the "medium bandwidth", is defined by the following three formulas:

$$\int_o^{\infty} df\ M(f) = E_s;\ (1/E_s)\int_o^{\infty} df\ f\ M(f) = f_o;$$

$$W \overset{df}{=} \left[(1/E_s)\int_o^{\infty} df(f - f_o)^2\ M(f)\right]^{1/2} \tag{2.95}$$

Equation (2.93) defines the power spectral density of $R_s(\ )$. By inverting (2.93) and substituting for R_s from (2.38) we get,

$$Q_s(f) = k^2 \iint_o^R dz_1 dz_2 \ \sigma(z_1)\ \sigma(z_2)\ M(z,f)\ [\cos\ (\omega z/v) + \cos\ (\omega 2z_o/v)]\ . \tag{2.96}$$

With a trigonometric change, (2.96) may be written as,

$$Q_s(f) = 4k^2 \iint_o^R dz_1 dz_2 \ \sigma(z_1)\ \sigma(z_2)\ M(z,f)\ [\cos\ (\omega z_1/v)\ \cos\ (\omega z_2/v)]\ . \tag{2.97}$$

where $z = z_2 - z_1$. Either (2.96) or (2.97) gives the equivalent frequency domain formula corresponding to the time domain formula (2.38).

Figure 8 illustrates the autocorrelation $R_s(\tau)$ and its power spectrum $Q_s(f)$ for a point source located at $z_o = p$. For the point source case, the correlation shape is $F(z,\tau)$; and, its Fourier transform $M(z,f)$ is the envelope of the power spectral density. The effect of the two cross-correlation terms located at $\tau = \pm\ 2p/v$ causes a sinusoidal oscillation in the envelope of the power spectrum with a distance between peaks of $\triangle f = v/2p$. This envelope oscillation results because the dual bistatic-radar of Fig. 1 provides two copies of the source waveform at the ground receiver; these two copies are separated by the delay $\tau = 2p/v$. Sources at different locations may have identical power spectrums $M(z,f)$ and still be separated in $R_s(\tau)$ because the envelope oscillation is different for each location. An exponential shape is arbitrarily chosen for the power spectrum envelope.

A similar pair of curves is shown in Fig. 9 for two identical point sources of the same magnitude and shape. Again the overall shape of the spectrum is determined by the shape of the two sources. However, the spectral oscillation which contains the location information does not give a direct readout of the source locations. This illustrates why the

autocorrelation function has been emphasized in the previous sections; it readily aids the eye in locating the signal sources.

In summary, Chapter II has developed from first principles the retarded-potential fluctuation signal for the dual bistatic-radar at the ground receiver. Two useful statistical characterizations R_S and R_B have been derived for this signal. Section IIa also lists the properties which define the propagation medium. Through the wave parameter D and

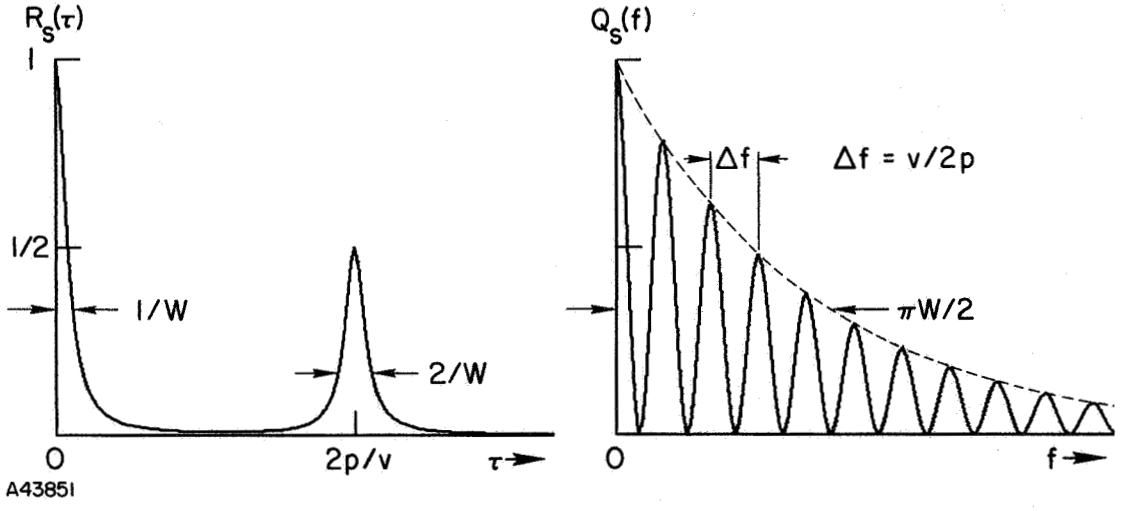

Fig. 8. SINGLE POINT SOURCE REPRESENTATION.

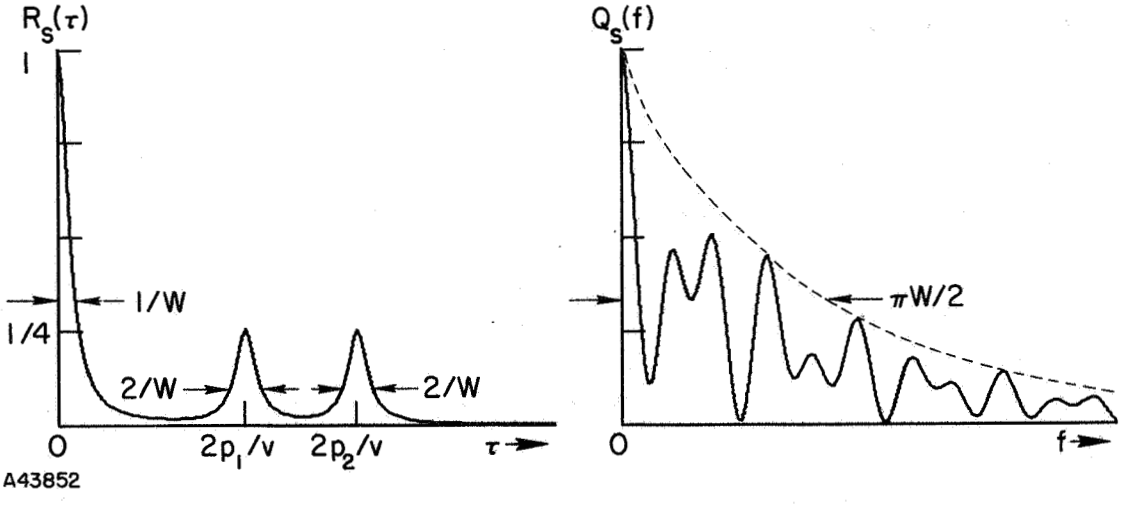

Fig. 9. DOUBLE POINT SOURCE REPRESENTATION.

Figs. 5, 6, and 7 some insight into the construction of the time correlation versus path length and scale size has been gained. Figures 8 and 9 illustrate the basic nature of the important cross-correlation terms in R_S and R_B. They are also useful for understanding the effects of filtering on the resolution as discussed in Chapter III.

III. CORRELATION FUNCTION INFORMATION

We will concern ourselves with the phase autocorrelation function (2.38) in the remaining chapters. It is the simplest expression with which to work; and, the results which we derive are applicable (with more complexity) to the amplitude correlation (2.45) and the wave theory correlation expressions derived in Chapter II, Section C. The discussion emphasizes the two cross-correlation terms of R_s and the propagation-medium information which may be obtained through these two terms.

A. Measurable Parameters

Upon reception of the carrier signal at the ground station, the carrier signal is demodulated by a phase lock loop demodulator. The output voltage waveform from the demodulator is the superposition of the modulation waveforms from each source region along the path.

The output voltage is proportional to $S(t)$ given by (2.34). We defer the consideration of the output noise from the demodulator until Chapter IV. Letting the gain of the receiver and processor be unity, the autocorrelation of the output voltage is given by (2.38). Both (2.34) and (2.38) are repeated below.

$$S(t_1) = k \int_o^R dz_1 \, [u(z_1, t_1 - z_1/v) + u(z_1, t_1 + z_1/v)]. \qquad (3.1)$$

$$R_s(\tau) = k^2 \int_0^R dz_1 dz_2 \; \sigma(z_1) \; \sigma(z_2) \; [F(z, \tau - 2z/v) + F(z, \tau + 2z/v)$$

$$+ F(z, \tau - 2z_o/v) + F(z, \tau + 2z_o/v)] \; , \qquad (3.2)$$

where $z = z_2 - z_1$, $2z_o = z_2 + z_1$, $\tau = t_2 - t_1$.

The source distribution function $\sigma(\,)$ is the quantity which is actually desired. The two functions $F(z, \tau \pm 2z_o/v)$ act as weighting function windows to enable one to measure $\sigma(\,)$ through $R_s(\tau)$. The

first example to illustrate this measuring ability is the point source of refractive index variations,

$$u(z_1, t) = \alpha\delta(z_1 - p)\ f(t) \ . \tag{3.3}$$

Let,

$$\langle f(t_1)\ f(t_2)\rangle = F(\tau) \neq 0 \qquad \text{for} \qquad |\tau| \leq 1/W \ .$$

$$= 0 \qquad \text{for} \qquad |\tau| \gg 1/W \ .$$

and $F(o) = 1$. Then,

$$S(t) = \alpha k \int_o^R dz_1[\delta(z_1 - p)\ f(t - z_1/v) + \delta(z_1 - p)\ f(t + z_1/v)]$$

$$= \alpha k[f(t - p/v) + f(t + p/v)] \ .$$

The correlation function is,

$$R_s(\tau) = \langle S(t_1)\ S(t_2)\rangle = \alpha^2 k^2[2F(\tau) + F(\tau + 2p/v) + F(\tau - 2p/v)] \ .$$

If $F(\tau)$ is a gaussian function,

$$F(\tau) = e^{-W^2\tau^2} \ , \tag{3.4}$$

Then,

$$R_s(\tau) = \alpha^2 k^2\left[2\ \exp\ (-W^2\tau^2) + \exp\ [-W^2(\tau + 2p/v)^2] + \exp\ [-W^2(\tau - 2p)\,v)^2]\right]. \tag{3.5}$$

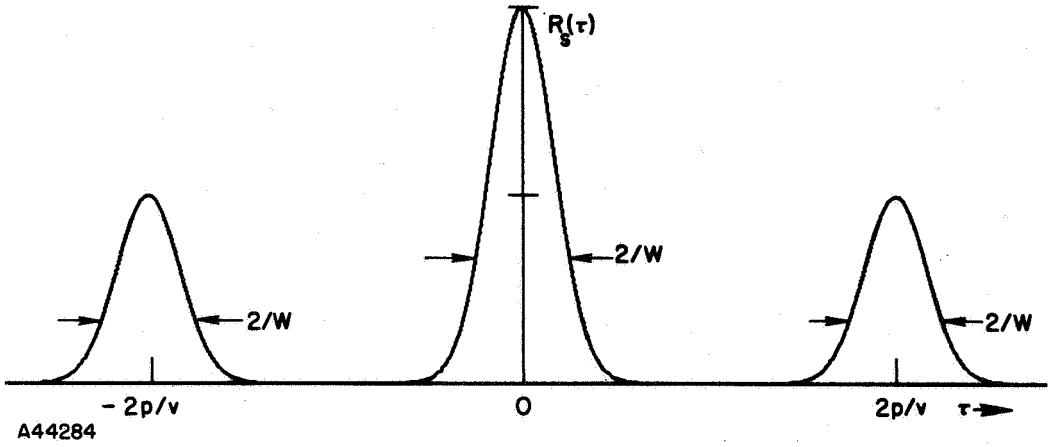

Fig. 10. AN AUTOCORRELATION FUNCTION EXAMPLE.

Figure 10 demonstrates three parameters which can be measured from the autocorrelation function.

Range: The peaks for $\tau \neq 0$ occur at $\tau = \pm 2p/v$. Therefore,

$$p = v\tau/2 \tag{3.6}$$

is the range in meters to the source from the spacecraft.

Magnitude: The magnitude of the variance of $u(,)$ at $z_1 = p$ is found from the magnitude of $R_s(\tau)$ at $\tau = \pm 2p/v$. For our point source (3.3), the variance is a constant $\sigma^2(p) = \alpha^2$. From (3.5) we get

$$\sigma^2(p) = R_s(\tau = 2p/v)/k^2 = \alpha^2 \ . \tag{3.7}$$

Scale Size: The time scale size $1/W$ is obtained by halving the width of the sub-peak which occurs at $\tau = \pm 2p/v$. In general a combination of spatial and time scale size appears in the correlation function $R_s(\tau)$. This will be shown in the next example.

From Fig. 10 and (3.5) it is apparent that the point source is smeared out by the weighting function $F(\tau)$ of (3.4). Since the time scale $1/W$ is the width of the viewing window, one cannot expect to

resolve any source narrower than 1/W. Although the shape is not recoverable, the source magnitude and location are preserved in $R_s(\tau)$. The local scale size 1/W of the source while not a parameter of $\sigma(\ )$ is still a valuable piece of information about the medium.

A second example is given to show the effect of spatial scale size and source distribution on $R_s(\tau)$. Let the source have a gaussian distribution with the scale b,

$$u(z_1, t) = \alpha \exp\left[-(z_1 - p)^2/b^2\right] f(z_1, t) \ . \tag{3.8}$$

$F(z_1, t)$ is a random function such that,

$$\langle u(z_1, t)\ u(z_2, t)\rangle = \alpha^2 \exp\left[-(z_1 - p)^2/b^2 - (z_2 - p)^2/b^2\right] F(z, \tau) \ .$$

Let the local refractive index correlation also be gaussian with spatial scale a and time scale 1/W.

$$F(z, \tau) = \exp\left(-z^2/a^2 - W^2\tau^2\right) \tag{3.9}$$

Now the phase demodulated signal is found from (3.1) and (3.8),

$$S(t) = \alpha k \int_o^R dz_1 \Big\{ \exp\left[-(z_1 - p)^2/b^2\right] f(z_1, t - z_1/v) + \exp\left[-(z_1 - p)^2/b^2\right] f(z_1, t + z_1/v) \Big\} \ .$$

Computing the autocorrelation of S(t) we get [after (3.2)],

$$R_s(\ ) = \langle S(t_1)\ S(t_2)\rangle = \alpha^2 k^2 \int_o^R dz_o \int_{-\infty}^{\infty} dz \exp\left[-2(z_o - p)^2/b^2 - z^2/2b^2\right] \cdot \left[F(z, \tau - z/v) + F(z, \tau + z/v) + F(z, \tau + 2z_o/v) + F(z, \tau - 2z_o/v)\right] \ . \tag{3.10}$$

To convert $dz_1 dz_2$ to $dz_o dz$ with $-\infty < z < \infty$, one must assume that $a \ll R$, that is, the spatial scale is much less than the total path length. . Using (3.9) we get,

$$R_s(\tau) = \alpha^2 k^2 \int_o^R dz_o \int_{-\infty}^{\infty} dz \exp\left[-2(z_o - p)^2/b^2 - z^2/q^2\right]$$

$$\cdot \Big\{ \exp\left[-W^2(\tau - z/v)^2\right] + \exp\left[-W^2(\tau + z/v)^2\right]$$

$$+ \exp\left[-W^2(\tau + 2z_o/v)^2\right] + \exp\left[-W^2(\tau - 2z_o/v)^2\right] \Big\}, \qquad (3.11)$$

where,

$$q^2 = 2a^2b^2/(a^2 + 2b^2) \; . \qquad (3.12)$$

Doing the integrals in (3.11) we get,

$$R_s(\tau) = (\pi\alpha^2 k^2 qb/W) \left[\frac{2 \exp\left\{-(\tau/a')^2\right\}}{a'} + \frac{\exp\left\{-[(\tau - 2p/v)/b']^2\right\}}{b'} \right.$$

$$\left. + \frac{\exp\left\{-[(\tau + 2p/v)/b']^2\right\}}{b'} \right] . \qquad (3.13)$$

In (3.13),

$$a' = \left(\frac{1}{W^2} + \frac{q^2}{v^2} \right)^{1/2}$$

$$b' = \left(\frac{1}{W^2} + \frac{4b^2}{v^2} \right)^{1/2} \; . \qquad (3.14)$$

Equation (3.13) is similar to (3.5), and, a plot of it would look much like Fig. 10. The difference is that the central peak has its magnitude changed by $\pi qb/Wa'$ and its scale is now a'. The side peaks have their magnitudes changed by $\pi qb/Wb'$ and their scale is now b'. From (3.14)

one concludes that the source location is undistorted in the general case; although, a broad correlation peak makes it difficult to measure precisely. However, the source magnitude generally is distorted by a combination of all the statistical scale sizes in the source region.

The three quantities q, a', and b' are given above for the gaussian case. However, modified forms of the quantities will appear for any choice of shape function so that they are fundamental factors. For example, b' demonstrates that the source distribution b is not measurable unless the transformation of b into the time domain is greater than the time scale, $2b/v \gg 1/W$. That is, the equivalent time distribution $2b/v$ must be larger than the weighting function window-width $1/W$.

The quantity q in (3.12) is approximately $q^2 \cong 2b^2$ when the spatial scale is larger than the distribution scale, $a \gg b$. For a real medium one expects $a \ll b$ which gives $q \cong a$. Using the expression for a' in (3.13) and $q \cong a$, the medium is separated into two categories.

Case 1. Wideband Medium. This case corresponds to $W \gg v/a$. This changes only the central peak term at $\tau = 0$ in (3.13). It becomes,

$$(2\pi\alpha^2 k^2 b\ v/W)\ \exp\ [-(\tau v/a)^2] \ .$$

Case 2. Narrowband Medium. In this case $W \ll v/a$. The central peak term of (3.13) now changes to,

$$2\pi\ ^2 k^2 ab\ \exp\ (-W^2\tau^2) \ .$$

In a propagation medium with a steady drift velocity such as the solar wind, the drift velocity is the dominant cause of the time fluctuations. For this case W is proportional to V_{drift}/a. When considering electromagnetic propagation $v_d \ll v = c$ so that the medium is always in the narrowband category.

B. Resolution Cell

The resolution of the correlation function is a measure of the smallest meaningful detail that can be distinguished. This statement is made precise by giving a mathematical definition of resolution based on the minimum distinguishable distance between two point sources. Two approaches will be taken: first, the minimum distance between two gaussian point sources will be calculated directly; and, second, a time resolution constant as defined by Woodward [15] will be calculated. Both approaches give approximately the same answer with the latter being more general.

Consider two point sources of refractive index variation at p_1 and p_2 similar to the one in Example 1 of Section IIIA,

$$u_1(z_1, t) = \alpha\delta(z_1 - p_1)\ f_1(t)$$

$$u_2(z_1, t) = \alpha\delta(z_1 - p_2)\ f_2(t)\ . \qquad (3.15)$$

f_1 and f_2 are random functions of time such that the expected values are,

$$\langle f_1(t_1)\ f_1(t_2)\rangle = F_1(\tau) = \exp(-W^2\tau^2)$$

$$\langle f_2(t_1)\ f_2(t_2)\rangle = F_2(\tau) = \exp(-W^2\tau^2) \qquad (3.16)$$

$$\langle f_1(t_1)\ f_2(t_2)\rangle = 0 \qquad \text{for all} \qquad \tau\ .$$

As in Section IIIA the received signal is of the form,

$$S(t) = \alpha k \int_o^R dz_1\{\delta(z_1 - p_1)[f_1(t - z_1/v) + f_1(t + z_1/v)]$$

$$+ \delta(z_1 - p_2)\ [f_2(t - z_1/v) + f_2(t + z_1/v)]\}$$

$$= \alpha k[f_1(t - p_1/v) + f_1(t + p_1/v) + f_2(t - p_2/v) + f_2(t + p_2/v)] \qquad (3.17)$$

$$R_s(\tau) = \langle S(t_1)\ S(t_2)\rangle = \alpha^2 k^2 [2F_1(\tau) + F_1(\tau + 2p_1/v) + F_1(\tau - 2p_1/v)$$

$$+ 2F_2(\tau) + F_2(\tau + 2p_2/v) + F_2(\tau - 2p_2/v)] \ . \qquad (3.18)$$

Using (3.16) in (3.18),

$$R_s(\tau) = \alpha^2 k^2 \Big\{ 4 \exp(-W^2\tau^2) + \exp[-W^2(\tau + 2p_1/v)^2]$$

$$+ \exp[-W^2(\tau - 2p_1/v)^2] + \exp[-W^2(\tau + 2p_2/v)^2] \qquad (3.19)$$

$$+ \exp[-W^2(\tau - 2p_2/v)^2] \Big\} \ .$$

Figure 11 is a sketch of (3.19).

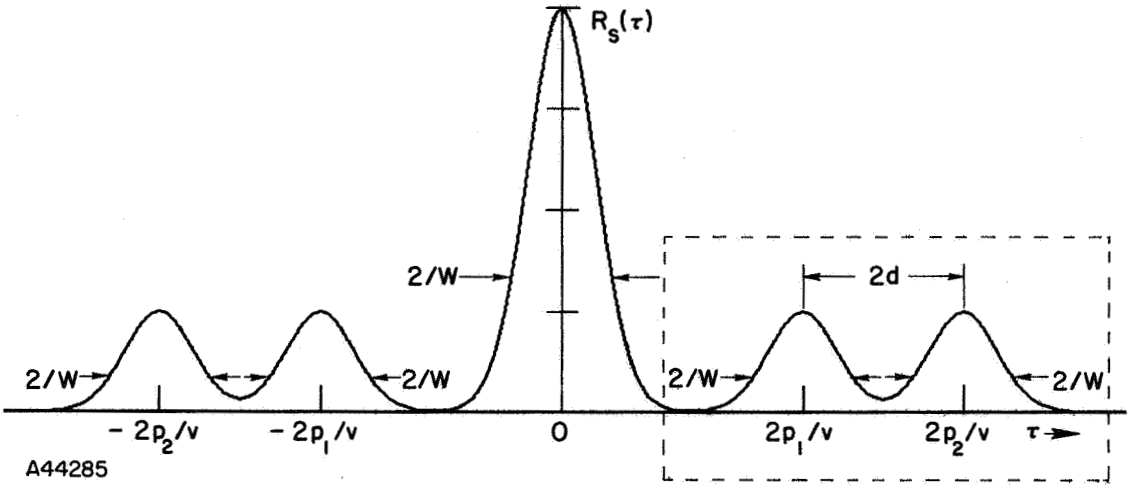

Fig. 11. RESPONSE WITH TWO POINT SOURCES.

We focus our attention on the response within the dotted rectangle of Fig. 11 and shift the τ origin midway between p_1 and p_2. With $d \overset{df}{=} p_2 - p_1$, the two terms within the rectangle are described by

$$R(\tau) = \exp[-W^2(\tau + d/v)^2] + \exp[-W^2(\tau - d/v)^2] \ . \qquad (3.20)$$

The approximate minimum value of d corresponds to equating $R(0)$ to $R(\pm d/v)$. Thus,

$$2 \exp[-(Wd/v)^2] = 1 + \exp[-4(Wd/v)^2] \ . \qquad (3.21)$$

Equation (3.21) gives a slightly large value for d_r since the actual peak has shifted off of d toward the origin (see Fig. 12).

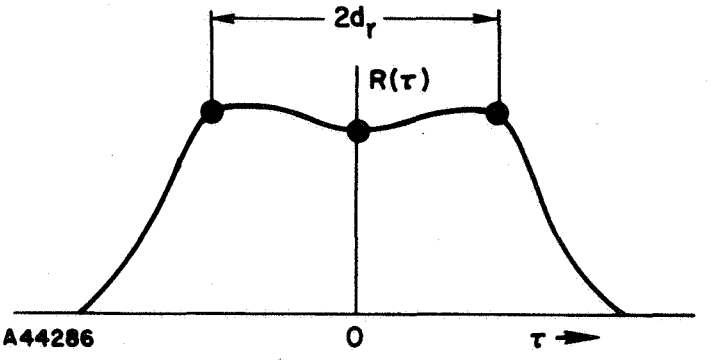

Fig. 12. APPROXIMATE SOLUTION FOR d_r.

The solution of (3.21) is,

$$(Wd_r/v)^2 \cong 0.61 \ . \tag{3.22}$$

Define a time resolution constant in seconds as,

$$T_R \stackrel{df}{=} 2d_r/v \ . \tag{3.23}$$

T_R is a measure of the amount of ambiguity the signal $u(z_1,t)$ produces in τ. Using (3.22) in (3.23) we get,

$$T_R = 1.562/W \ . \tag{3.24}$$

Let us think of the problem in a communication sense. We transmit a carrier waveform which of itself contains no information. Information about the medium is modulated on the carrier with a code over which we have no control. This code gives range information based on the time delay between the uplink and downlink waveforms. A measure of the ambiguity which the code produces in τ is given by Woodward [15]. We interpret his formula to apply to the local correlation function (τ

around $2p_1/v$, say) of a single point source. We write the local $R(\tau)$ as

$$R(\tau) = \exp\left[-W^2(\tau - 2p_1/v)^2\right] . \tag{3.25}$$

Then from Woodward,

$$T_R = \int_{\substack{\text{region}\\ \text{around}\\ 2p_1/v}} d\tau \; |R(\tau)|^2 / R^2(2p_1/v)$$

$$\cong \int_{-\infty}^{\infty} d\tau \exp\left[-2W^2(\tau - 2p_1/v)^2\right]$$

$$= \sqrt{\pi/2}/W \tag{3.26}$$

or

$$T_R = 1.26/W . \tag{3.27}$$

Equations (3.27) and (3.24) are in reasonable agreement and we shall consider (3.26) as a better definition of T_R. Then it is not necessary to assume an analytical form for $R(\tau)$ in order to calculate T_R.

It should be noted that our use of W in terms of the time ambiguity implies that W is the frequency span or the range of occupied frequencies of the signal. If the medium were acting as a pulse modulator the frequency span would not be equal to W. For the continuous type of media, with which we are concerned, W is equal to the frequency span. We use (3.27) in (3.23) to get the resolution distance,

$$d_r = 0.63 \; v/W . \tag{3.28}$$

Referring back to (3.19) and Fig. 11 we observe that the large central peak at $\tau = 0$ can also be used in (3.26) to find the average T_R.

In fact, this is a preferable method since the local peaks for $\tau \neq 0$ are likely to be dominated by the source distribution scale size b rather than by $1/W$.

One final observation concerning T_R is its connection to the Wide-band Medium, Case 1, Section IIIA. In this case we note that W is replaced by v/a. Therefore, [from (3.23) and (3.27)] for the gaussian case,

$$T_R = 1.26\ a/v$$

or

$$d_R = vT_R/2 = 0.63a\ . \qquad (3.29)$$

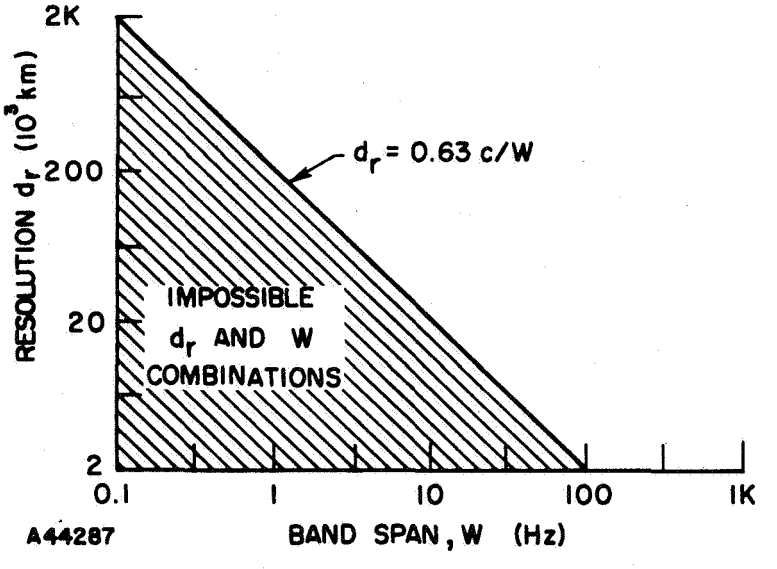

Fig. 13. RESOLUTION.

Figure 13 is based on (3.28) with $v \cong c$. The physically possible combinations of W and d_r are in the unshaded region above the line $d_r = 0.63c/W$. For example, a bandwidth of 10 Hz would enable one to resolve inhomogeneities of size 20,000 km and larger.

For useful results the propagation path length R must be longer than 0.63a in the wideband medium and longer than 0.63 v/W in the narrowband medium. For electromagnetic waves a real medium is narrowband so that,

$$R > 0.63v/W \ . \tag{3.30}$$

Up to this point the discussion has considered only the resolution cell length d_r. The effective cross-sectional diameter of the cell may be computed in terms of Fresnel zones; the number of zones depends in a complicated way on "a". But, the first zone is always the most significant. Thus, the effective diameter of the cylindrical resolution volume is,

$$\text{Diameter}_R = 2[\lambda z_1(1 - z_1/R)]^{1/2} \ , \qquad 0 \leq z_1 \leq R \ . \tag{3.31}$$

The resolution volume has the same significance in three dimensions as the resolution length has in one dimension: The detail of inhomogeneities smaller than the resolution volume is averaged together by the propagating wave and lost.

C. Filtering and Resolution

The fundamental tie between filtering and resolution is the frequency span of the signal. That is, an increase in the frequency span increases the resolution while the converse is true for a decrease in the frequency span. Equations (3.26) and (3.27) state this fact which is illustrated by the figure of this section.

Assume the ground and spacecraft receivers have a bandwidth large enough to capture the entire signal spectrum. There are three general reasons for filtering the signal further. First, to remove the very low signal frequencies which cause the wide skirts on the correlation peaks. Because the low frequencies usually contain the most energy they basically determine the frequency span of the unfiltered signal. By removing the high energy, low frequency spectra the energy at higher frequencies

enters into the frequency span calculation; and, the resulting frequency span is often larger. This increase in the frequency span causes an increase in resolution which means smaller detail is now more visible. Second, one may wish to select a particular frequency band for study (e.g., to look at some particular resonance in the spectrum). A loss in resolution is usually experienced because the frequency span is reduced. For a fixed observation length, a narrower band reduces the number of independent samples; and, this reduces the statistical signal to noise ratio.

Third, and sometimes most important, unwanted interference noise can be removed with a filter. This usually means removing all portions of the spectrum which do not contribute significant signal energy. However, large interference spikes in the signal spectrum are often removed, also. This third type of filtering does not affect the resolution when it is accomplished with a minimum effect on the signal energy spectrum.

Let $h(t)$ or $H(jf)$ represent the filter.

$$H(jf) = \int_{-\infty}^{\infty} dt\ h(t)\ \exp(-i2\pi ft) \tag{3.32}$$

The received signal may be directly filtered. It is expressed in the convolution form below.

$$S_f(t) = h(t) * S(t)\ . \tag{3.33}$$

The signal also may be filtered in the autocorrelation/power spectrum space as shown in Eq. (3.34).

$$\begin{aligned} R_{sf}(\tau) &= h(\tau) * h^*(-\tau) * R_s(\tau) \\ Q_{sf}(f) &= |H(jf)|^2\ Q_s(f) \end{aligned} \tag{3.34}$$

$Q_s(f)$ is defined at the end of Chapter II to be the Fourier transform of $R_s(\tau)$.

The series of drawings in Fig. 14 illustrate the before and after filtering effect on a signal with very low frequency components (all coordinates use linear scales in the figure). An RC high pass filter is used to remove the near-dc signals. The effective bandspan is seen to increase from 2.03 Hz in Part b to 3.14 Hz in Part d. The net effect, as shown in Part c, is the removal of the wide skirts around the correlation peak. Thus, our ability to distinguish the peak when it is among other sources is better.

Figure 15 illustrates the same effect except that the source is much closer to the origin. Now the negative correlation values in Part c begin to reduce the relative height of the correlation peak at $2p/v$. The negative correlation results from the removal of the near-dc energy; and, it causes some distortion of the correlation near the τ origin. However, one still improves the resolution of the peak at $2p/v$.

In Fig. 16 the above filter processing is applied to a correlation signal with three closely spaced correlation peaks. Again the improvement in resolution is apparent in Part c over the unfiltered data in Part a. The narrowest correlation peak on the left is distinguished better than the other two because its wider power spectrum is least affected by the removal of the very low frequency energy.

D. Moving Radar Sites

An aberration error in the range value may result from the relative motion between the radar sites and the refractive index source. At the outset we note that this aberration is usually negligible because it depends on the ratio of the "radar site velocity over the propagation velocity." The propagation velocity is approximately c, the speed of light. However, there is a cumulative effect associated with the aberration which may be important for long observation times T.

Relative motion along the propagation path is considered first. Suppose both the ground station and spacecraft have velocities relative to a fixed source as shown in Fig. 17a. The spacecraft motion tends to lengthen the path and the time delay between the uplink and downlink modulation waveforms. But the motion of the ground station acts to

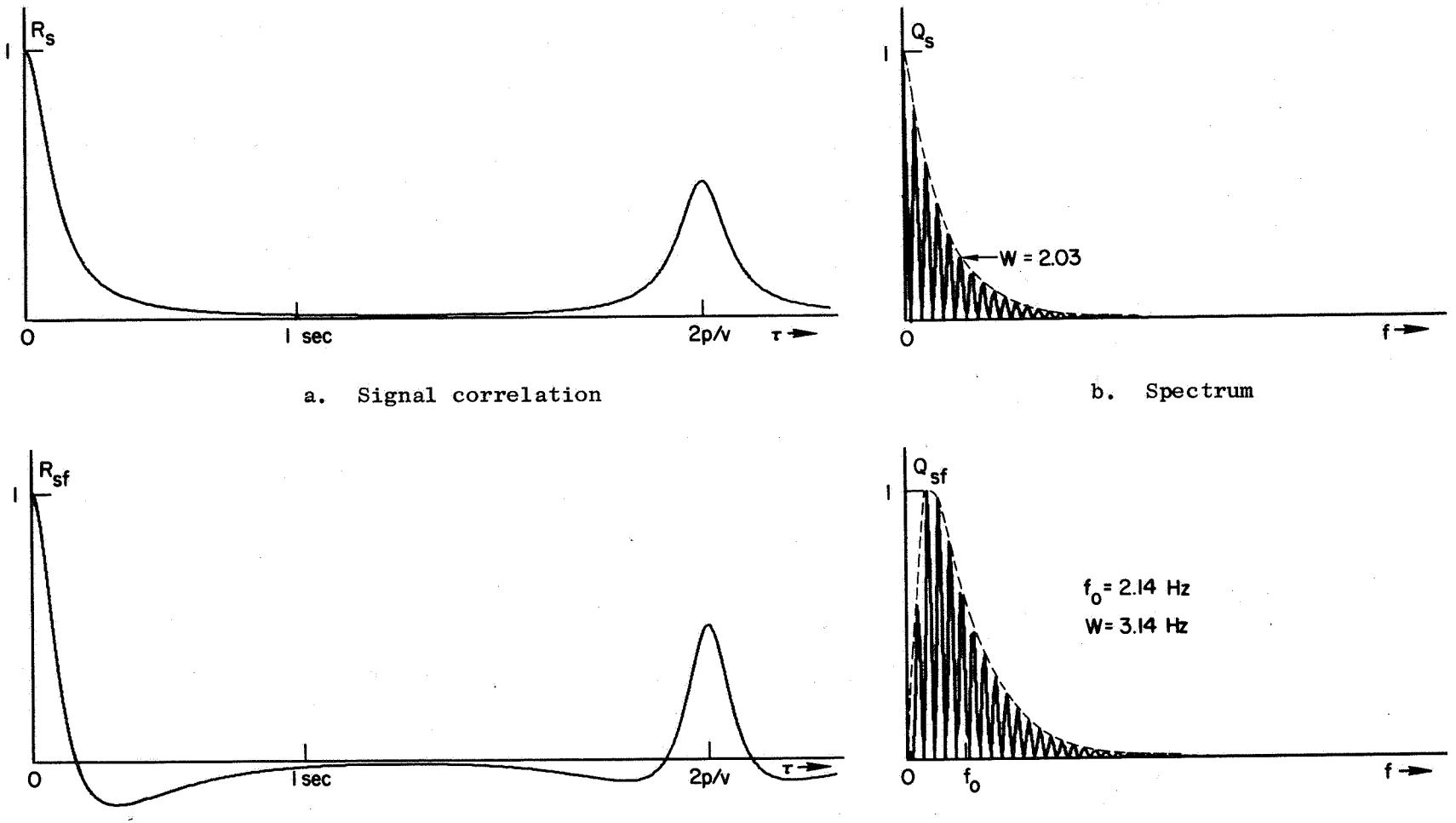

Fig. 14. IMPROVING RESOLUTION BY FILTERING OUT NEAR-DC SPECTRA.

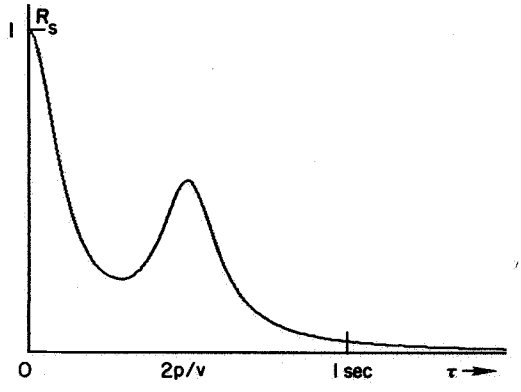

a. Signal correlation

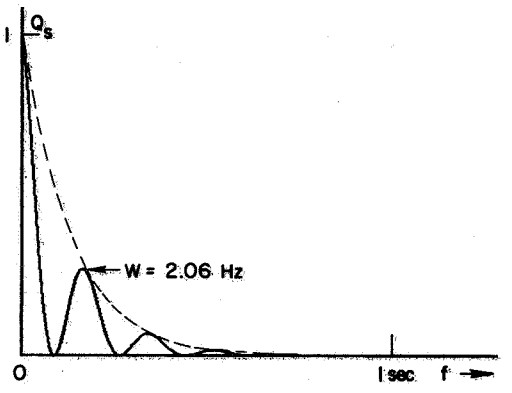

b. Spectrum

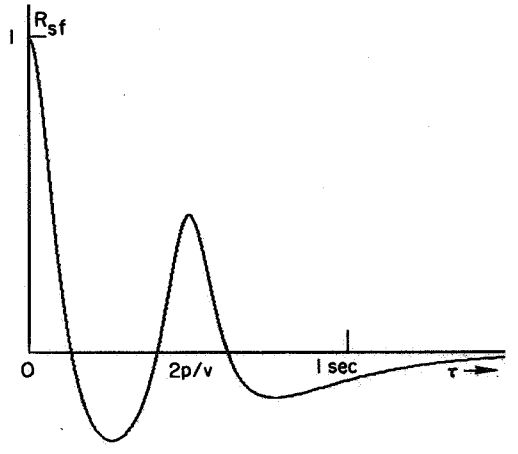

c. Filtered correlation

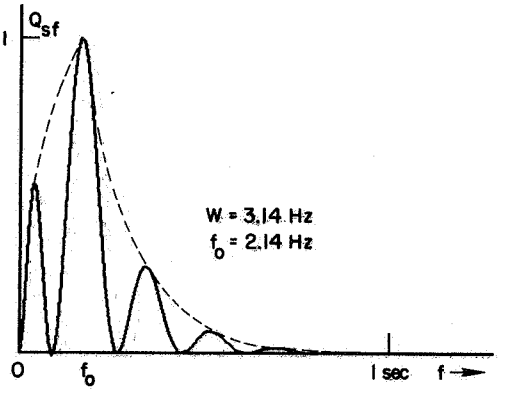

d. Filtered spectrum

Fig. 15. FILTERING DISTORTION NEAR τ ORIGIN.

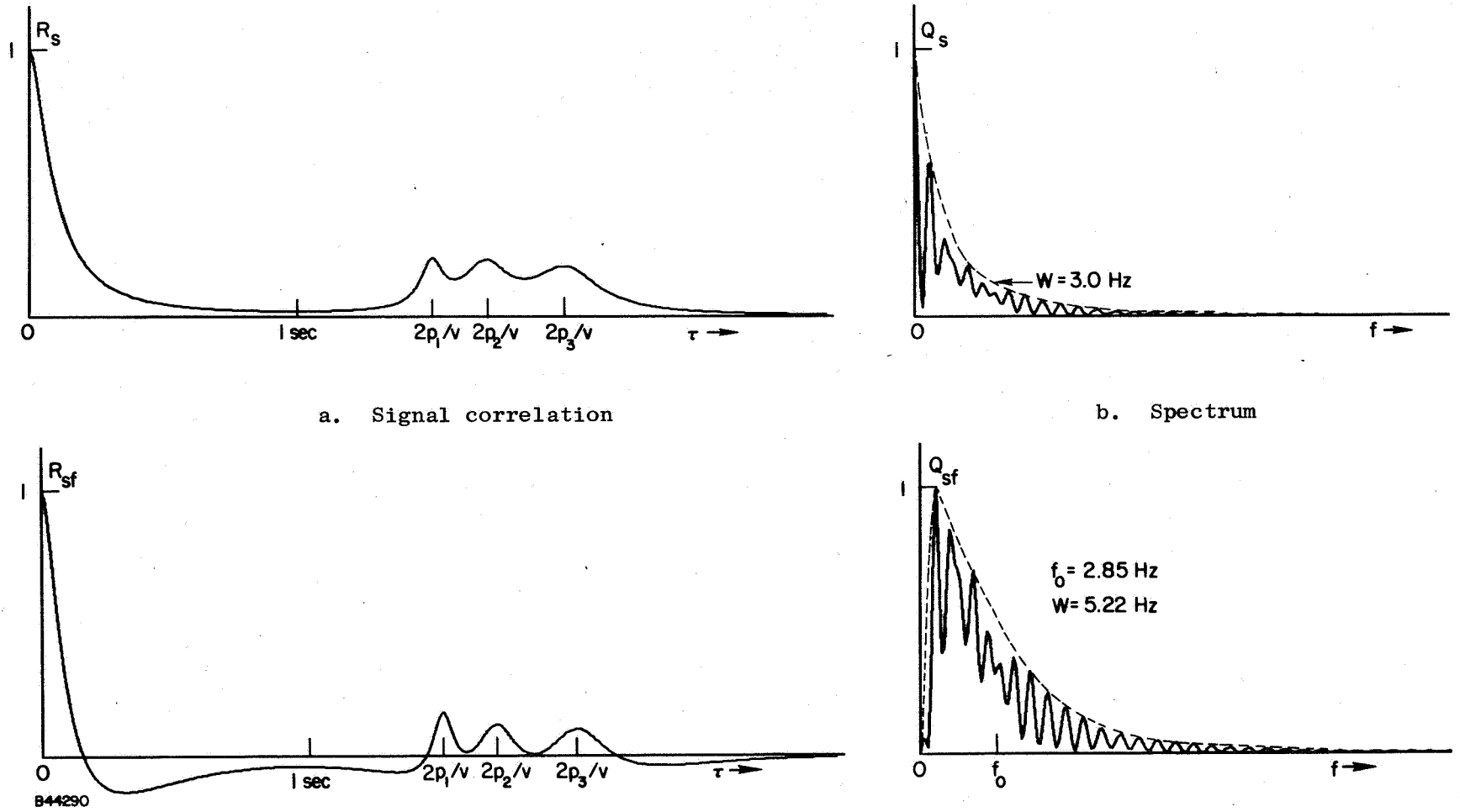

a. Signal correlation

b. Spectrum

c. Filtered correlation

d. Filtered spectrum

Fig. 16. MULTIPLE SOURCE FILTERING EXAMPLE.

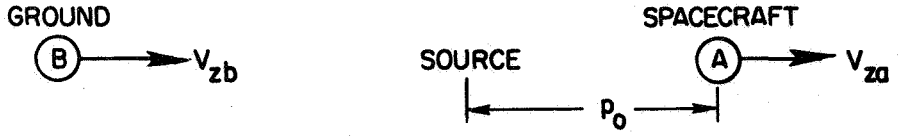

a. Radial motion

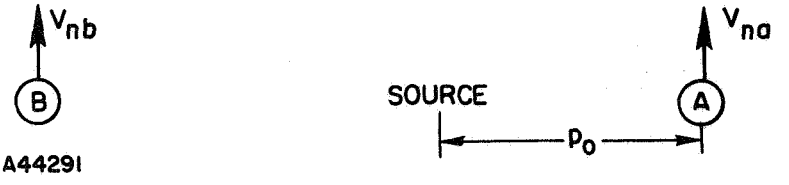

b. Perpendicular motion

Fig. 17. RELATIVE SOURCE/RADAR-SITE MOTION.

shorten the time delay. Thus the static time delay $\tau_o = 2p_o/c$ becomes,

$$\tau_o' = \frac{\tau_o}{(1 + V_{zb}/c)(1 - V_{za}/c)} , \qquad (3.35)$$

where the denominator product accounts for the fixed aberration effect.

For a fixed τ it is clear that the resolution volume moves with the coherent spacecraft. Therefore, the common resolution volume shortens as the observation time increases. This effect is the cumulative aberration associated with the radial motion. We calculate it by noting that p_o increases with time as $V_{za}t$. Using this fact in Eq. (3.35),

$$\tau_o' = \frac{2(p_o + V_{za}t)/c}{(1 + V_{zb}/c)(1 - V_{za}/c)} \cong 2(p_o + V_{za}t)/c , \quad 0 \leq t \leq T . \qquad (3.36)$$

The quantity $(V_{za}T/p_o)$ is the quantity which must be small. Since $0 \leq p_o \leq R$, this quantity may be significant. If important, this cumulative effect can be eliminated by tracking the relative source motion with τ_o' of Eq. (3.36) during the data averaging. This is done

by averaging the lag-product with τ_o',

$$(1/T)\int_o^T dt\ y(t)y(t+\tau_o') = (1/T)\int_o^T dt\ y(t)y[t(1+2V_{za}/c) + 2p_o/c] .$$

Thus, the resolution cell remains fixed at the point source as the spacecraft continues to move away.

There is no range aberration associated with purely perpendicular motion as shown in Fig. 17b. Figure 18a is an exaggerated sketch of the spatial position at regular time intervals when $V_{na} = V_{nb} = V_n$. It is possible for the uplink and downlink carrier waves to be in the same spatial volume at the same time. They simply start out at the appropriate time from their respective transmitters as shown in the figure. Since both the uplink and the downlink rays see a common volume at the proper range p, there is no range aberration. One can also see this by Lorentz transforming into the moving coordinate system of the radar-sites. Then, both sites are fixed such that the rays travel the same path between the spacecraft and the ground. Note that R and p are not changed because they are perpendicular to the direction of motion. Since p is unchanged by the transformation, there is no range aberration.

For the case when $V_{na} \neq V_{nb}$, the uplink and downlink rays never see exactly the same volume. We Lorentz transform into the moving spacecraft coordinate system to get Fig. 18b. The ground station relative change of position is due to V_{nb} being larger than V_{na}.

The ray path separation ℓ at range p increases until $p = R/2$; and then it decreases as shown in Fig. 18b. In the derivation of ℓ let $\Delta V = V_{nb} - V_{na}$ and $2X$ be the base of the triangle formed by the two rays in Fig. 18b. The time for the ray to travel from the ground station up to position p is

$$\Delta t = (x^2 + R^2)^{1/2}(R - p)/Rc . \qquad (3.37)$$

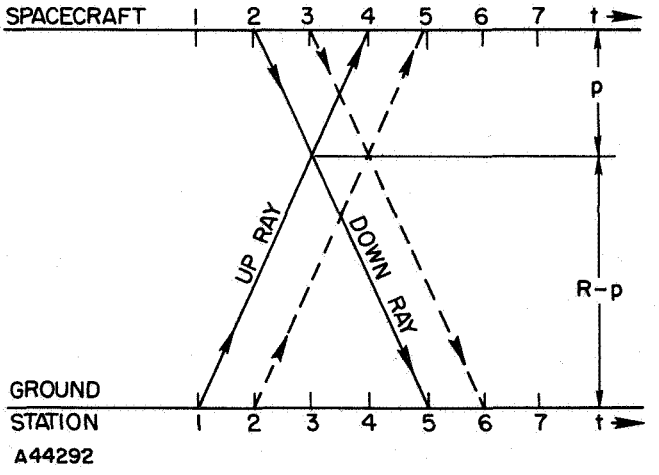

a. Equal velocity case

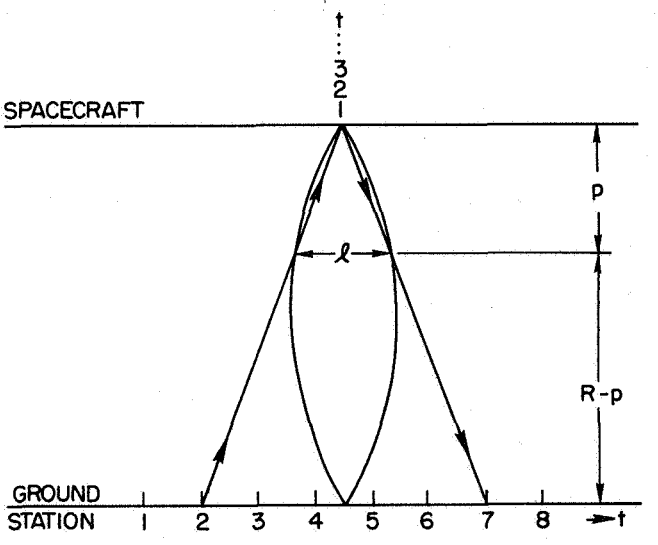

b. Unequal velocity case, $V_{nb} > V_{na}$

Fig. 18. RAY PATH SEPARATION EFFECT.

The value for X is $\Delta V \Delta t$ or,

$$\Delta t = X/\Delta V \ .$$

Putting Δt into (3.37) and solving for X gives

$$X = R(1 - p/R)(\Delta V/c)[1 - (1 - p/R)^2 V^2/c^2]^{-1/2} .$$

From similar triangles $\ell = 2pX/R$. Therefore

$$\ell = 2p(1 - p/R)(\Delta V/c)\gamma_p , \qquad (3.38)$$

where

$$\gamma p = [1 - (1 - p/R)^2 V^2/c^2]^{-1/2} .$$

For any practical radar system $\gamma_p \approx 1$ in (3.38).

ℓ is maximum when $p = R/2$; $\ell_M = (\Delta V)\ R/2c$. ℓ_M is significant when it is on the order of the effective resolution volume diameter D_F. Normally D_F is the diameter of the local first Fresnel zone associated with the range p and given by (3.31). Putting $Z_1 = p$ in (3.31) gives, $\ell/D_F = (\Delta V/c)[p(1 - p/R)/\lambda]^{1/2}$. Figure 19 is a plot of the percent common volume loss versus ℓ/D_F. The curve is based on the common area of two equal circles which are separated as shown.

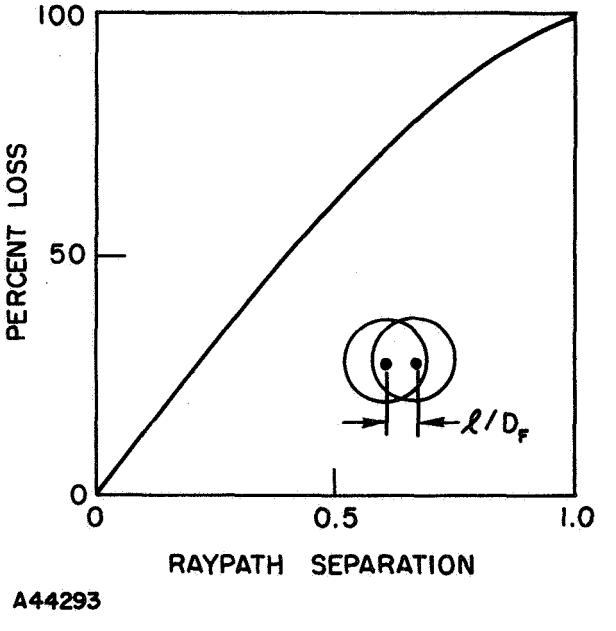

Fig. 19. LOSS OF COMMON RESOLUTION VOLUME.

The percent loss of common volume between the uplink and downlink rays reduces the signal correlation. The total phase fluctuation is unaffected by the size of ℓ; but, the amount of common signal from a given region is reduced according to Fig. 19. That is,

$$S_2(t) = (1 - \text{percent loss})S(t) .$$

The noise is increased by the amount (percent loss)S(t); but this is probably insignificant compared to the uncorrelated signal from other regions. Thus, correlation values will be reduced by

$$R_{s2}(\tau) = (1 - \text{percent loss})^2 R_s(\tau) . \qquad (3.39)$$

Equation (3.39) applies only when the relative motion between the resolution cell and the medium is zero. When the relative motion is not zero, both the up and the down rays eventually see nearly the same fluctuation phenomena. However, there is an additional time delay τ_ℓ given by the time required for the phenomena to move across the fixed ray path separation distance ℓ. In this case, the signal correlation is reduced only by the amount of decorrelation of the phenomena in time τ_ℓ.

The final effect associated with the perpendicular motion of the source and/or radar-sites is the change in the fluctuation spectral width W. This is a desirable effect when the width increases because the resolution increases. Consider the case of $V_{na} = V_{nb} = V_n$ as shown in Fig. 18a where the resolution cells move with the velocity V_n. Let V_m be the drift velocity of a medium in which the irregularities are frozen with respect to each other. The spectral broadening is largest when $|V_n - V_m|$ is largest. Thus, the best resolution of source regions within the medium occurs when the resolution cell and the medium are moving in opposite directions. In the case of a static medium one can make it visible by putting the radar sites in motion. Also, the turbulent, nondrift type of medium is more visible when the bandwidth is increased by the resolution cell motion.

IV. ESTIMATING THE CORRELATION FUNCTION

A. Time Average Estimator

We seek an accurate estimate of the autocorrelation function $R_s(\tau)$, $\tau \leq 2R/V$, based on the data obtained in an observation of length T. The data is the phase demodulated carrier wave which is corrupted by additive thermal noise. In this chapter we assume the carrier powers are fixed and large enough to lock up the spacecraft and ground receivers. The receiver output data is,

$$y(t) = s(t) + n(t) \tag{4.1}$$

$n(t)$ is the noise referred to the output of the phase detector. It is assumed to be gaussian, zero mean, stationary, and to have a constant spectral density $N_o/2$ in the frequency band $-W_r$ to W_r.

$$\langle n(t)n(t+\tau)\rangle = N_o W_r \operatorname{sinc}(2W_r\tau) \tag{4.2}$$

$n(t)$ is also uncorrelated with $s(t)$,

$$\langle n(t)s(t)\rangle = 0 \ . \tag{4.3}$$

The random process $s(t)$ is also assumed to be gaussian, zero mean, and stationary in the interval $0 \leq t \leq T$.

$$\langle s(t)s(t+\tau)\rangle = R_s(\tau) \ , \tag{4.4}$$

$R_s(\tau)$ is given by (2.38) or (2.86).

Consider the lag-product random variable $y(t)y(t+\tau)$ for a fixed τ. The time average of this random variable is,

$$\hat{R}_y(\tau) = (1/T)\int_o^T dt\ y(t)y(t+\tau) \ . \tag{4.5}$$

The expected value of $\hat{R}_y(\tau)$ is,

$$\langle \hat{R}_y(\tau) \rangle = (1/T) \int_o^T dt \, \langle y(t)y(t + \tau) \rangle \, .$$

From (4.1) to (4.4),

$$\langle y(t)y(t + \tau) \rangle = R_s(\tau) + N_o W_r \text{ sinc } (2W_r\tau) \, .$$

Therefore,

$$\langle \hat{R}_y(\tau) \rangle = R_s(\tau) + N_o W_r \text{ sinc } (2W_r\tau) \, . \tag{4.6}$$

By restricting τ away from the origin, $|\tau| > 1/2 \, W_r$,

$$\langle \hat{R}_y(\tau) \rangle = R_s(\tau) \tag{4.7}$$

Therefore, the time average $\hat{R}_y$ is an unbiased estimator of R_s for $1/2W_r < |\tau|$.

In Section IV.B we show that the variance of $\hat{R}_y \to 0$ as $\tau \to \infty$. This is another measure of the estimator quality which is stated mathematically as,

$$P_r[\hat{R}_y \to R_s; \quad |\tau| > 1/2W_r] \to 1 \quad \text{as} \quad T \to \infty \, . \tag{4.8}$$

This means the estimator is consistent in statistical terminology. Equation (4.8) merely states that the estimate $\hat{R}_y$ becomes near the true correlation R_s with probability approaching one as the observation length increases.

Just as we arbitrarily chose to time average the lag-product random variable in (4.5), we now choose to find the minimum average mean-square error (MMSE) estimate of $y(t)y(t + \tau)$ by a constant A. The average mean square error of the estimate is,

$$\epsilon \underline{\text{df}} \; (1/T) \int_0^T dt \, [y(t)y(t + \tau) - A]^2 \, .$$

The minimum of ϵ is found by setting $\partial\epsilon/\partial A = 0$. This gives,

$$A = (1/T)\int_0^T dt\ y(t)y(t+\tau)\ . \tag{4.9}$$

Since $A = \hat{R}_y$ we say $\hat{R}_y$ is a MMSE estimator of R_s. The MMSE criteria is another measure of the quality of the time average estimator. Therefore, three reasons for using $\hat{R}_y$ are: (1) it is unbiased, (2) it is consistent, and (3) it is a MMSE estimator.

B. Signal-to-Noise Ratio and Variability

The estimator signal-to-noise ratio is defined as

$$\text{SNR}(\tau) \overset{\text{df}}{=} \langle \hat{R}_y \rangle^2 / \text{Var}\ \hat{R}_y\ . \tag{4.10}$$

As a measure of how close the estimated value $\hat{R}_y$ is to its mean R_s, $1/2W_r \leq |\tau| \leq 2R/V$, we use the relative deviation [16],

$$|\hat{R}_y - R_s|/|R_s|\ ,$$

assuming R_s is not zero.

Using Chebyshev's inequality we get the result in probability that,

$$\Pr\ [|(\hat{R}_y - R_s)/R_s| \leq \delta] \geq 1 - 1/\delta^2\text{SNR}\ ,\quad \delta > 0\ . \tag{4.11}$$

Equations (4.10) and (4.11) establish the significance between SNR and the estimator $\hat{R}_y$. Sepcifically (4.11) is used to establish the length of the observation T such that our error in estimating R_s most likely does not exceed δ.

1. Continuous Data SNR

A more explicit form of (4.10) is developed using the results of Section IV.A. The variance is,

$$\text{Var } \hat{R}_y = \langle \hat{R}_y^2 \rangle - \langle \hat{R}_y \rangle^2 \tag{4.12}$$

From (4.5)

$$\langle \hat{R}_y^2 \rangle = (1/T^2) \iint_0^T dt_1\, dt_2 \langle y(t_1)\, y(t_1 + \tau)\, y(t_2) y(t_2 + \tau) \rangle \tag{4.13}$$

Since $y(t)$ is a zero mean gaussian variable we can use the product rule,

$$\langle y_1 y_2 y_3 y_4 \rangle = \langle y_1 y_2 \rangle \langle y_3 y_4 \rangle + \langle y_1 y_3 \rangle \langle y_2 y_4 \rangle + \langle y_1 y_4 \rangle \langle y_2 y_3 \rangle \ . \tag{4.14}$$

The terms in (4.14) have a direct correspondence to those in (4.13). Combining (4.12) to (4.14) gives

$$\text{Var } \hat{R}_y = (1/T^2) \iint_0^T dt_1\, dt_2 [\langle y(t_1)\, y(t_2) \rangle \langle y(t_1 + \tau)\, y(t_2 + \tau) \rangle$$

$$+ \langle y(t_1)\, y(t_2 + \tau) \rangle \langle y(t_1 + \tau)\, y(t_2) \rangle] \tag{4.15}$$

From (4.6)

$$\langle y(\alpha) y(\beta) \rangle = N_o W_r \text{ sinc } [2W_r(\beta - \alpha)] + R_s(\beta - \alpha) \tag{4.16}$$

Use the form of (4.16) in (4.15) and a change of variables, $t = t_2 - t_1$, to get

$$\text{Var } \hat{R}_y = (1/T) \int_{-T}^{T} dt\, \Lambda\,(t/T) \left\{ N_o^2 W_r^2 \text{ sinc}^2 (2W_r t) + 2N_o W_r\, R_s(t) \text{ sinc } (2W_r t) \right.$$

$$\left. + R_s^2(t) + N_o^2 W_r^2 \text{ sinc } [2W_r(t + \tau)] \text{ sinc } [2W_r(t - \tau)] \right]$$

$$+ R_s(t+\tau)\, R_s(t-\tau) + N_o W_r \operatorname{sinc}\,[2W_r(t+\tau)]\, R_s(t-\tau)$$

$$+ N_o W_r \operatorname{sinc}\,[2W_r(t-\tau)]\, R_s(t+\tau) \quad . \tag{4.17}$$

These terms can be integrated by a straight forward process.

The required integrals are listed below.

$$\Lambda(t/T) = \begin{cases} (1 - |t|/T) & \text{for } t \le T \\ 0 & \text{otherwise} \end{cases}$$

$$\int_{-T}^{T} dt\, \Lambda\,(t/T)\, \operatorname{sinc}^2\,(2W_r t) \cong 1/2W_r \quad .$$

$$\int_{-T}^{T} dt\, \Lambda\,(t/T)\, \operatorname{sinc}\,[2W_r(t-\tau)]\, R_s(t+\tau) \cong R_s(2\tau)/2W_r \quad .$$

$$\int_{-T}^{T} dt\, \Lambda\,(t/T)\, \operatorname{sinc}\,[2W_r(t-\tau)]\, \operatorname{sinc}\,[2W_r(t+\tau)] \cong \operatorname{sinc}\,(4W_r\tau)/2W_r \quad . \tag{4.18}$$

Using the evenness of $R_s(\tau)$ and (4.18) the reduced variance is,

$$\operatorname{Var} \hat{R}_y = (1/T)\left\{(W_r N_o^2/2)\left[1 + \operatorname{sinc}\,(4\,W_r\tau)\right] + N_o\left[R_s(0) + \Lambda(\tau/T)R_s(2\tau)\right]\right.$$

$$\left. + \int_{-T}^{T} dt\, \Lambda\,(t/T)\left[R_s^2(t) + R_s(t-\tau)R_s(t+\tau)\right]\right\} \quad . \tag{4.19}$$

Expressions (4.6) and (4.19) when substituted in (4.10) give the $\mathrm{SNR}(\tau)$ in terms of N_o, $R_s(\tau)$, and T. Note in (4.20) that the $\mathrm{SNR}(\tau)$ is directly proportional to T, the observation length. For $|\tau| > 1/2\ W_r$ and T large,

$$SNR(\tau) = \frac{T\,R_s^2(\tau)}{W_r N_o^2/2 + N_o[R_s(0) + R_s(2\tau)] + \int_{-T}^{T} dt[R_s^2(t) + R_s(t-\tau)R_s(t+\tau)]} \tag{4.20}$$

For the case of no additive noise, $n(t) = 0$, there still exists cross noise which causes variability in the measurement. In this case the $SNR(\tau)$ is found by setting $N_o = 0$ in (4.12) and (4.19). Then,

$$SNR(\tau) = TR_s^2(\tau) \Big/ \int_{-T}^{T} dt \left[R_s^2(t) + R_s(t-\tau)R_s(t+\tau)\right] . \tag{4.21}$$

It is useful to evaluate the SNR for M independent, identical point sources along the propagation path. The distribution and correlation weighting functions are,

$$\sigma(z_1) = \alpha \sum_{j=1}^{M} \delta(z_1 - jc/2W), \quad 0 \le z_1 \le R .$$
$$F(z,\tau) = \text{sinc}\,(2z/a)\ \text{sinc}\,(2W\tau) . \tag{4.22}$$

The source magnitudes are all α and the sources are separated by $c/2W$. From $F(z,\tau)$ we see that $c/2W$ is the sinc function resolution distance. Thus, M is also the number of resolution cells along the path. Note, M can never be larger than $2WR/C$. Using (4.22) in (2.38) one gets,

$$R_s(\tau) = \alpha^2 k^2 \sum_j \sum_\ell \text{sinc}\,[(c/aW)(j-\ell)] \Big\{ \text{sinc}\,[2W(\tau-(j-\ell)/2W)] + \text{sinc}\,[2W(\tau+(j-\ell)/2W)] + \text{sinc}\,[2W(\tau-(j+\ell)/2W)] + \text{sinc}\,[2W(\tau+(j+\ell)/2W)] \Big\} . \tag{4.23}$$

In Chapter V, we point out that $a = V_m/2\pi W$ ($W = W_r$ here) in the solar wind where V_m is the solar wind velocity. Thus, $c/aW = 2\pi c/V_m$ is very large such that,

$$\text{sinc } [(c/aW)(j-\ell)] \cong \delta_{j\ell} \quad . \tag{4.24}$$

Using (4.24) in (4.23) gives,

$$R_s(\tau) = \alpha^2 k^2 \left[2M \text{ sinc } (2W\tau) + \sum_{j=1}^{M} \left\{ \begin{matrix} \text{sinc } [2W(\tau - j/W)] \\ + \text{ sinc } [2W(\tau + j/W)] \end{matrix} \right\} \right] \tag{4.25}$$

Putting (4.25) into (4.21) and integrating with the aid of (4.18) one gets, for $|\tau| > 1/2W$,

$$\text{SNR} = T/(4M^2/2W + M/W + \text{smaller terms}) \quad . \tag{4.26}$$

For $M \gg 1$

$$\text{SNR} \cong 2TW/4M^2 = N/4M^2 \quad . \tag{4.27}$$

Although idealized, (4.27) demonstrates the fundamental relationship between the SNR and the number of sources or resolution cells M. Basically (4.27) is the crossnoise SNR. As expected, the SNR is proportional to the length of observation T or the number of independent signal samples N. Equation (4.27) is to be used as a first order crossnoise SNR estimate. Equation (4.20) is the exact expression to use when considering additive noise and general source distributions.

2. Sampled Data

The data is most likely to be processed via digital techniques. For this reason equivalent expressions to those in Section IV.B.1 are developed. The sampled data is,

$$y_i = S_i + n_i \qquad i = 0, \ldots N-1 \tag{4.28}$$

$$\langle y_i y_{i+j} \rangle = \langle S_i S_{i+j} \rangle + \langle n_i n_{i+j} \rangle = N_o W_r \delta_j + R_{sj}$$

$$j = 0, \ldots, N-1 \tag{4.29}$$

$$\delta_j = \begin{cases} 1, & j = 0 \\ 0, & j \neq 0 \end{cases} . \tag{4.30}$$

W_r enters (4.29) because we have assumed a band limited signal in order to sample $y(t)$ correctly.

The sample estimator is

$$\hat{R}_y \equiv \hat{R}_{yj} = (1/N) \sum_{i=0}^{N-1} y_i y_{i+j} \tag{4.31}$$

$$\text{Var } \hat{R}_y = \langle \hat{R}_y^2 \rangle - \langle \hat{R}_y \rangle^2 \tag{4.32}$$

$$\langle \hat{R}_y^2 \rangle = (1/N^2) \sum_{i,k}^{N-1} \langle y_i y_{i+j} y_k y_{k+j} \rangle \tag{4.33}$$

The y_i's are still Gaussian variables so that (4.14) (Sec. IV.B.1) is true. Hence

$$\text{Var } \hat{R}_y = (1/N^2) \sum_{i,k}^{N-1} [\langle y_i y_k \rangle \langle y_{i+j} y_{k+j} \rangle + \langle y_i y_{k+j} \rangle \langle y_{i+j} y_k \rangle] . \tag{4.34}$$

$$\langle y_\alpha y_\beta \rangle = N_o W_r \delta_{\beta-\alpha} + R_{(\beta-\alpha)} . \tag{4.35}$$

Use the form of (4.35) in (4.34) with the change of variables $\ell = k - i$ to get

$$\text{Var}\ \hat{R}_y = (1/N)\sum_{\ell=-N+1}^{N-1} \Lambda(\ell/N)\Big\{(N_o W_r \delta_\ell)^2 + 2N_o W_r \delta_\ell + R_{s\ell}^2$$

$$+ (N_o W_r)^2 \delta_{\ell+j}\delta_{\ell-j} + N_o W_r\Big[R_{s(\ell-j)}\delta_{\ell+j} + R_{s(\ell+j)}\delta_{\ell-j}\Big]$$

$$+ R_{s(\ell-j)}R_{s(\ell+j)}\Big\} \quad . \tag{4.36}$$

The sampling implicity assumes a bandwidth of W_r so that the evaluation of the δ^2 term is straightforward.

$$\sum_{i=0}^{N-1}\sum_{k=0}^{N-1}\delta_{k-i}^2 = N \quad . \tag{4.37}$$

Upon evaluation of the remaining terms in (4.36) we get,

$$\text{Var}\ \hat{R}_y = (1/N)\Big\{(N_o W_r)^2(1 + \delta_j) + 2W_r N_o\Big[R_{so} + \Lambda(j/N)R_{s2j}\Big]$$

$$+ \sum_{\ell=-N+1}^{N-1} \Lambda(\ell/N)\Big[R_{s\ell}^2 + R_{s(\ell-j)}R_{s(\ell+j)}\Big]\Big\}. \tag{4.38}$$

Expressions (4.29) and (4.38) when substituted into (4.10) give the discrete SNR_j in terms of N_o, R_{sj} and N. As in the continous case, we note that SNR_j is directly proportional to N, the number of observation samples $(N = 2W_r T)$. For $j \neq 0$,

$$SNR_j = \frac{NR_{sj}^2}{\left\{\begin{array}{l}(N_o W_r)^2 + 2W_r N_o\Big[R_{so} + \Lambda(j/N)R_{s2j}\Big] \\ + \displaystyle\sum_{\ell=-N+1}^{N-1} \Lambda(\ell/N)\Big[R_{s\ell}^2 + R_{s(\ell-j)}R_{s(\ell+j)}\Big]\end{array}\right\}} \quad . \tag{4.39}$$

C. Maximum Likelihood Estimator

In this section the maximum likelihood (MLH) estimator of the signal-correlation amplitude is developed for some fixed value of τ for $1/2\ W_r \leq |\tau| \leq 2R/v$. The signal correlation function must be known a priori for this approach. For our proposed application of the MLHE we do not have complete knowledge of this correlation function; in fact, that is the unknown quantity which we wish to measure. Hence, this section shows how to use some indirect a priori knowledge to measure the signal correlation function in addition to developing the MLHE form.

The two pieces of information at our disposal are: (1) the general correlation shape as shown in Fig. 20, and (2) a low signal-to-noise ratio. The first arises (see Chapters I and II) because two copies of the signal-source modulation waveform with a fixed delay are generated by the dual bistatic-radar. This substitutes for source-location and shape knowledge. A low SNR results because a long propagation path contains many sources which generate crossnoise in addition to thermal and receiver background noise. This eliminates the need for a priori source magnitude knowledge. A low SNR results as a practical matter, also. One does not wish to pay the extra cost of using a MLHE until the SNR is low.

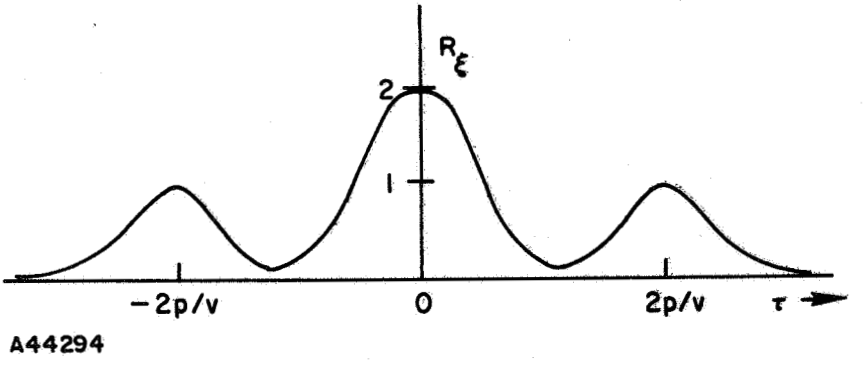

FIG. 20. SIGNAL AUTOCORRELATION FUNCTION

The received (and demodulated) signal has the form,

$$y(t) = m(t) + n(t) \tag{4.40}$$

$m(t)$ is the gaussian signal from one independent source as opposed to $s(t)$ (in Sec. IV.A) which is the accumulated signal from all sources. Correspondingly $n(t)$ now includes the remaining accumulated signal from all other sources in addition to the additive, bandlimited to W_r, white noise which is gaussian with zero mean and power spectral density $N_o/2$. Hence, $n(t)$ is a colored noise.

The signal correlation is initially assumed to be,

$$R_m(\tau) = A\, R_\xi(\tau) \quad ,$$

$$R_\xi(\tau) = 2\,\xi(\tau) + \xi(\tau - 2p/v) + \xi(\tau + 2p/v) \quad . \qquad (4.41)$$

$$\xi(0) = 1 \quad .$$

R_ξ is shown in Fig. 20 with the shape of ξ being arbitrarily chosen as gaussian.

The derivation of the MLH estimator $\hat{A}$ follows the general approach of Root [17] and Hofstetter [18]. Our primary interest is to reduce the general form of the optimal estimator by using the specific correlation shape of Fig. 20. This leads to the data scanning realization of the MLH estimator.

There are two cases of noise to be considered. In the first, the white noise N_o is assumed to dominate over the colored cross noise from other sources. One usually tries to design the receiver so as to make the detector output noise N_o negligible. Thus, in the second case, the colored cross noise with the same spectral shape as the envelope of the signal source is the dominant noise. This case is made equivalent to the first by using a whitening filter on the signal plus noise. We consider the general colored noise case first and introduce the whitening filter later.

Form the following Karhunen-Loeve expansion of the received signal correlation function, $R_y = R_m + R_n$,

$$\int_0^T dt_1 R_y(t_1,t_2)\Phi_k(t_1) = \lambda_k \Phi_k(t_2) \qquad 0 \le t_2 \le T \;\&\; k=0,1,2,\ldots \qquad (4.42)$$

where,

$$\int_0^T dt\ \Phi_i(t)\Phi_j(t) = \delta_{ij} \quad .$$

We define eigenvalues μ_k and ν_k to correspond to the signal and the noise.

$$\begin{aligned} \int_0^T dt_1 R_\xi(t_1,t_2)\Phi_k(t_1) &= \mu_k\Phi_k(t_2) \quad , \\ \int_0^T dt_1 R_n(t_1,t_2)\Phi_k(t_1) &= \nu_k\Phi_k(t_2) \quad . \end{aligned} \tag{4.43}$$

Using (4.41) to (4.43) we conclude,

$$\lambda_k = A\mu_k + \nu_k \quad . \tag{4.44}$$

With Φ_k as defined in (4.42) we have the signal expansion,

$$y_k = \int_0^T dt\ y(t)\Phi_k(t) \quad , \qquad k=0,1,2,\ldots \quad , \tag{4.45}$$

and the autocorrelation contraction,

$$R_\xi(t_1,t_2) = \sum_{k=0}^{\infty} \mu_k\Phi_k(t_1)\Phi_k(t_2) \quad , \tag{4.46}$$

which is proved by substituting (4.46) into (4.43).

The likelihood ratio L is formed by taking the ratio of the joint probability density functions of "signal plus noise" over "noise alone." Since we are assuming zero mean gaussian random signals and noise, only the variance is needed for these two cases.

$$\langle y_i y_k \rangle = \lambda_k \delta_{ik} \quad .$$

For noise alone,

$$\langle y_i y_k \rangle = \nu_k \delta_{ik} \quad .$$

Then,

$$L = P_{m+n}\left[y_i, y_2, \cdots\right] \Big/ P_n\left[y_1, y_2, \cdots\right] \quad ,$$

$$L = \exp\left\{-\frac{1}{2}\sum_{k=0}^{\infty}\left[y_k^2(1/\lambda_k - 1/\nu_k) + \ln(\lambda_k/\nu_k)\right]\right\} \quad . \tag{4.47}$$

A necessary and sufficient condition [17] for the estimation problem to be nonsingular is,

$$\sum_0^{\infty} u_k^2/\nu_k^2 < \infty \quad .$$

The strong equivalence condition of the signal plus noise probability measure [17] is,

$$\sum_0^{\infty} u_k/\nu_k < \infty \quad . \tag{4.48}$$

The eigenvalues μ_k and ν_k are positive and real because R_ξ and R_n are real and even functions. Since we are considering the noise ν_k to be larger than the signal μ_k, one expects (4.48) to hold. Assuming (4.48) is true we note that maximizing L is equivalent to maximizing,

$$\ell = \sum_{k=0}^{\infty}\left[y_k^2\, A\mu_k/\nu_k(\nu_k + A\mu_k) - \ln(1 + A\mu_k/\nu_k)\right] \quad .$$

Setting $\partial \ell / \partial A = 0$ yields an equation for $\hat{A}$,

$$\sum_{k=0}^{\infty} y_k^2 \mu_k / (\nu_k + \hat{A}\mu_k)^2 = \sum_{k=0}^{\infty} \mu_k / (\nu_k + \hat{A}\mu_k) \quad . \tag{4.49}$$

One solution for $\hat{A}$ may be expressed in terms of $\hat{A}$. Equation (4.50) is easily shown by manipulating (4.49).

$$\hat{A} = \frac{\sum (y_k^2 - \nu_k)\mu_k / (\nu_k + \hat{A}\mu_k)^2}{\sum \mu_k^2 / (\nu_k + \hat{A}\mu_k)^2} \tag{4.50}$$

Hofstetter has shown that (4.50) is the Cramer-Rao minimum variance estimator of A, provided that $\hat{A}$ on the RHS is close to the true A. He also pointed out the iteration version of (4.50) whereby one uses the present estimate $\hat{A}_n$ in the RHS to get the next estimate $\hat{A}_{n-1}$. For our application of (4.50), the signal-to-noise ratio per observable (SNR_0) is less than one,

$$SNR_0 \overset{df}{=} \hat{A}\mu_k / \nu_k \ll 1 \quad .$$

For small SNR_0 (4.50) becomes,

$$\hat{A} = \frac{\sum_0^{\infty} (y_k^2 - \nu_k)\mu_k / \nu_k^2}{\sum_0^{\infty} \mu_k^2 / \nu_k^2} \tag{4.51}$$

The estimator efficiency of (4.51) is nearly unity in this case [18].

The whitening filter appears in (4.51) through the ν_k. Later in this section we show that the μ_k and ν_k for $k=0,1,\ldots,\infty$ are basically Fourier transforms of their respective autocorrelation functions. That is, the k values are proportional to frequency and the ν_k are

the magnitude of the noise power spectral density. Restrict k to the band where significant signal exists and such that $\nu_k \neq 0$; say $k=0,1,\ldots,K$. Define $N_w/2 = \max[\nu_k,\ k=0,\ldots,K]$. From the Fourier transform of (4.25), we see that $N_w \approx M$ times larger than the maximum of μ_k. The normalized whitening filter is now given by $(N_w/2\nu_k)^{1/2}$; $k=0,\ldots,K$. The whitened data and signal correlation are,

$$x_k = y_k(N_w/2\nu_k)^{1/2} \quad ;$$
$$\mu_{wk} = \mu_k\ N_w/2\nu_k \quad . \tag{4.52}$$

Substitute for y_k and μ_k in (4.51) to get,

$$\hat{A} = \frac{\sum_0^K (x_k^2 - N_w/2)\mu_{wk}}{\sum_0^K \mu_{wk}^2} \tag{4.53}$$

When white noise N_o dominates, $\nu_k \cong N_o/2$ such that,

$$\hat{A} = \frac{\sum_0^K (y_k^2 - N_o/2)\mu_k}{\sum_0^K \mu_k^2} \tag{4.54}$$

It is no surprise that the estimators for the two noise cases are of the same form; but, it is of interest to see their equivalence as shown by (4.51) through (4.54). From this point on we use (4.54) to represent both (4.53) and (4.54).

The mean value of (4.51) is easily shown to be,

$$\langle \hat{A} \rangle = A \quad ,$$

so that the estimator is unbiased. The variance for the $SNR_0 \ll 1$ is found to be,

$$\text{Var } \hat{A} = N_o^2/2 \sum_0^K \mu_k^2 \quad . \tag{4.55}$$

Hence,

$$SNR_A = \langle \hat{A} \rangle^2 / \text{Var } \hat{A} = 2(A/N_o)^2 \sum_0^K \mu_k^2 \quad . \tag{4.56}$$

The continuous version of (4.56) is found by squaring and integrating (4.46).

$$SNR_A = 2T(A/N_o)^2 \int_{-T}^{T} dt\ \Lambda(t/T) R_\xi^2(t) \quad . \tag{4.57}$$

Similar to the time average case, SNR_A is proportional the observation length T.

Using the Fourier transform fact and (4.41),

$$\sum_0^K \mu_k = R_\xi(0) = 2 \quad .$$

The continuous version of the (4.54) is found using (4.45) and (4.46) with the above $\sum$ to get,

$$\hat{A} = \frac{\int_0^T \int dt_1\ dt_2\ y(t_1) y(t_2) R_\xi(t_1, t_2) - N_o}{T \int_{-T}^{T} dt\ \Lambda(t/T) R_\xi^2(t)} \quad . \tag{4.58}$$

Equation (4.58) shows the matched filter nature of the MLHE. The matched filter is the known signal correlation R_ξ as shown in Fig. 20 or $R_{w\xi}$, the whitened version of R_ξ. This filter weights the data lag-products to enhance the most likely data and negate the least likely data. Since R_ξ is not actually known, the filter is usually mismatched to the data. Starting with a mismatched R'_ξ, we study the sensitivity of the estimator to the source location and shape parameters. From (4.54), the mismatched estimator is,

$$\hat{A}_m = \frac{\sum (y_k^2 - N_o/2)\mu_k'}{\sum (\mu_k')^2} \quad . \tag{4.59}$$

The signal-to-noise ratio for $\hat{A}_m$ is

$$SNR_m = 2(A/N_o)^2 \left(\sum \mu_k \mu_k'\right)^2 \Big/ \sum (\mu_k')^2 \quad . \tag{4.60}$$

Using SNR_A in (4.56) and SNR_m above, we compare the mismatched filter performance.

$$\gamma \overset{df}{=} SNR_m/SNR_A = \frac{\left(\sum \mu_k \mu_k'\right)^2}{\sum \mu_k^2 \sum (\mu_k')^2} \quad . \tag{4.61}$$

Applying the Schwartz inequality to (4.61) we get,

$$\gamma \leq \frac{\sum \mu_k^2 \sum (\mu_k')^2}{\sum \mu_k^2 \sum (\mu_k')^2} = 1 \quad .$$

$\gamma = 1$ only when $\mu_k' = \mu_k$ for all k in (4.61). Thus, the properly matched signal correlation truly gives the best performance.

In order to study γ versus source position p and scale size a, we must express the eigenvalues μ_k in terms of p and a.

The problem of solving (4.43) for the eigenfunctions and eigenvalues is a complicated one because of the finite integral limits. For example Helstrom [19] works out the detailed solution for $R_\xi(\tau) = \Phi_o e^{-\alpha|\tau|}$. The eigenfunctions turn out to be the sine and cosine functions. However, by assuming large values of T, the effect of the finite limits is small.

For the stationary statistics case the eigenfunctions are

$$\Phi_k = \sqrt{2/T} \cos(\pi k t/T) \quad ; \quad k = 0,1,2,\ldots \quad .$$

Hence, for large T,

$$\sqrt{2/T}\int_0^T dt_1\, R_\xi(t_1 - t_2)\cos(\pi k t_1/T)$$

$$\cong \sqrt{2/T}\cos(\pi k t_2/T)\int_{-T}^{T} d\tau\, R_\xi(\tau)\cos(\pi k\tau/T) \quad . \tag{4.62}$$

Recall the R_ξ is also an even function in (4.62). Thus, the eigenvalues are,

$$\mu_k \cong \int_{-T}^{T} d\tau\, R_\xi(\tau)\cos(\pi k\tau/T) \quad , \quad k=0,1,2,\ldots \tag{4.63}$$

Since $R_\xi(\tau)$ is zero for $|\tau| > 2p/v$, μ_k is basically the Fourier transform of $R_\xi(\tau)$. Since $R_\xi(\tau)$ is a real, even function it is clear that μ_k are always positive and real.

Substituting for R_ξ from (4.41) we get

$$\mu_k \cong 2\left[1 + \cos\left(\frac{\pi k}{T}\,\frac{2p}{v}\right)\right] G_k \quad . \tag{4.64}$$

G_k is just the Fourier transform of the shape function $\xi(\tau)$.

$$G_k = \int_{-T}^{T} d\tau\, \xi(\tau)\cos(\pi k\tau/T) \quad , \quad k=0,1,2,\ldots \quad . \tag{4.65}$$

G_k is unity over $k=0,1,\ldots,K$ when the data $y(t)$ are whitened.

For our application the bandwidths are narrow and we expect the dominant noise to be the colored crossnoise arising from other source regions. In this case the noise and signal are whitened. The performance is found by putting (4.64) into (4.61) with G_k = unity.

$$\gamma = \frac{\left(\sum_{0}^{K}[1 + \cos(\pi k2p/vT)][1 + \cos(\pi k2p'/vT)]\right)^2}{\sum_{0}^{K}[1 + \cos(\pi k2p/vT)]^2 \sum_{0}^{K}[1 + \cos(\pi j2p'/vT)]^2} \quad . \qquad (4.66)$$

A plot of γ versus the position mismatch p'/p is shown in Fig. 21. It is clear from the figure and (4.66) that the cosine nature of the eigenvalues or the power spectral envelope (see Fig. 9a) makes the estimator sensitive to position. The scale and shape of the $\xi(\tau)$ do not enter into (4.66) at all. The parameter K is shown to have some importance. Physically K is the bandwidth of the processor. As K/p becomes large, more cosine cycles enter into the calculation of γ. Thus the ambiguity is reduced and the sensitivity to p is increased as shown in Fig. 21.

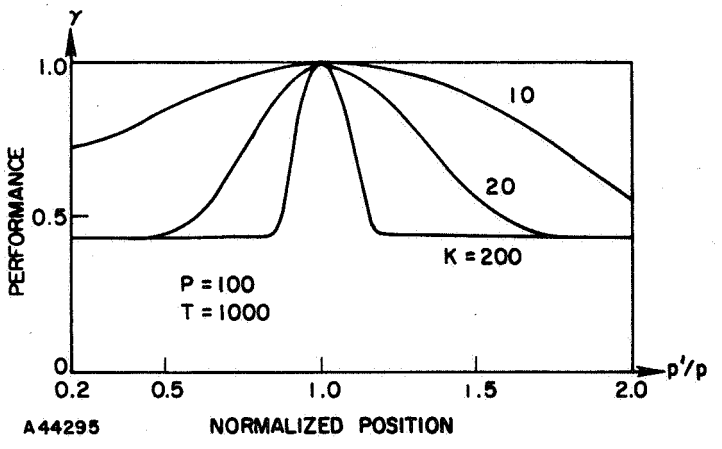

FIG. 21. MISMATCHED FILTER PERFORMANCE.

This positional sensitivity suggests a scanning technique for processing the data. From a preliminary study of the large central correlation peak in the data or the power spectrum envelope, one can determine the whitening filter and K. Then, using a whitened version of R_ξ, all values of $p, 0 \leq p \leq R$ are scanned through the data with the estimator formula (4.58).

Using $\tau = t_1 - t_2$ and the whitened data notation, an equivalent form for the numerator of (4.58) is,

$$\hat{A}_n(p) = \int_{-2R/v}^{2R/v} d\tau\, R_{w\xi}(\tau,p) \int_0^T dt\, x(t)x(t+\tau) - N_w \quad . \tag{4.67}$$

Figure 22 is a processor block diagram of (4.67).

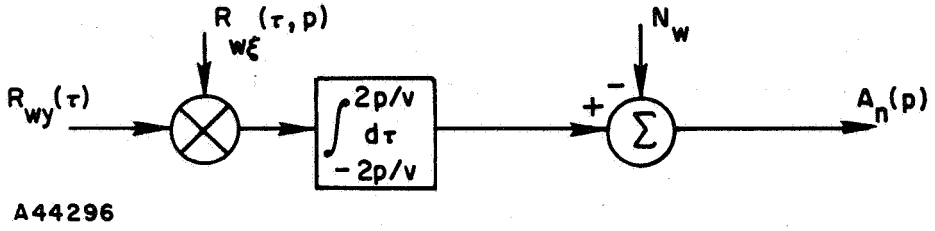

FIG. 22. MAXIMUM LIKELIHOOD ESTIMATOR.

For each change of the value p, the time average data $R_{wy}(\tau)$ is recycled through Fig. 22. It is clear that the MLHE $\hat{A}$ is a better estimator of the signal correlation than $\hat{R}_y$ of Section IV.A. This is because the MLHE uses the time averaged $\hat{R}_y(\tau)$ data in a post-averaging and weighting process. It is better by the factor,

$$SNR_A/SNR_{TA} = W_r \int_{-T}^{T} d\tau\, \Lambda(\tau/T)\, R_{w\xi}^2(\tau) \quad . \tag{4.68}$$

In summary, Chapter IV has pointed out the best way to estimate the signal correlation function from the noisy received data signal. The general data processing is done in three steps. First, the data y(t) are filtered to eliminate noise, interference, and very low frequency signal. Second, the lag-products of the filtered signal are time averaged. Third, the time averaged correlation function is matched filter processed as shown in Fig. 22. The SNR for the time averaged data is given in Section IV.B; and, the SNR for the MLHE is given by (4.56).

V SOLAR WIND EXPERIMENTAL APPLICATION

The dual bistatic radar system provides a way to simultaneously study a sizable section of the solar wind. This application is the primary motivation for the development of the dual bistatic radar technique. However, the technique is general and applications are not limited to a solar wind type of medium nor to electromagnetic propagation situations. The solar wind experiment is discussed in detail in this chapter while other potential areas of application are suggested in Chapter VI.

A. General Model of the Solar Wind

The solar wind is basically an electron-proton plasma moving radially outward from the sun. Its electromagnetic propagation characteristics are primarily determined by the electron number density. The refractive index for a static, homogeneous plasma is

$$n^2 = 1 - 80.6\bar{N}/f^2 \tag{5.1}$$

$\bar{N}$ is the mean electron density; f is the RF carrier frequencey. For a slowly varying medium $n(\bar{r},t)$ will not depart too much from the form of (5.1). Therefore we assume

$$n^2(\bar{r},t) = 1 - (80.6/f^2)[\bar{N} + N(\bar{r},t)] \tag{5.2}$$

and investigate (5.2) in terms of the two assumptions (1) weakly inhomogeneous and (2) slowly varying.

By choosing

$$f^2 \gg 80.6\bar{N}\ , \tag{5.3}$$

we may write

$$n(\bar{r},t) \cong 1 - 40.3\ N(\bar{r},t)/f^2 \tag{5.4}$$

Thus we identify n_0 and u in $n = n_0 + u$ as

$$n_0 = 1 - 40.3\ \bar{N}/f^2$$

$$u(\bar{r},t) = -40.3\ N(\bar{r},t)/f^2 \ . \qquad (5.5)$$

The "weakly inhomogeneous" assumption, $|u| \ll |n_o|$, is immediately true from (5.5).

The slowly varying assumption is rewritten in terms of $N(\bar{r},t)$.

$$|\nabla n/n| = (40.3/f^2)|\overline{\nabla N}| \ll k^2$$

$$|\dot{n}/n| = (40.3/f^2)|\dot{N}| \ll \omega \qquad (5.6)$$

Rewriting (5.6) we get the slowly varying criteria in terms of f,

$$|\overline{\nabla N}| \ll (f/\lambda)^2 = f^4/c^2$$

$$|\dot{N}| \ll f^3 \qquad (5.7)$$

The mean electron density has been well measured [20] and appears to vary with solar activity. The mean density is approximately 10 elec cm^{-3} at ranges just under 1 AU from the sun. Theoretical models [21] of the solar wind which take into account the latest measurements give the mean electron density profile vs distance from the sun. Ref. [21] also points out a profile of the solar wind velocity vs distance. At 1 AU the velocity is about 400 km/sec.

Very little data are available concerning the fluctuations of the electron density about the mean value. Scintillation of radio stars by the solar wind plasma provides some information, however. Cohen, Gundermann, Hardebeck and Sharp [22]; through scintillation measurements, have concluded that the rms fluctuation in electron density is about 2 percent of the mean; and it remains constant for $0.2 < r < 0.9$ AU: r is the distance from the sun center. This number is probably low because it is

obtained near the sunspot minimum. More important for our purposes, Ref. [22] concludes that the spatial scale size $a = 110$ km in the range $0.2 < r < 0.9$ AU.

"a" is calculated both from diffraction theory and from dividing the solar wind velocity V_m by the second moment of the fluctuation spectral width, W. The latter method ($a = V_m/2\pi W$) implies that the drift velocity is the dominant cause of the intensity fluctuations. Ref. [22] estimates the proton gyro radius to be 40 km at $80R_\odot$; and, it suggests that the irregularity size "a" is limited by the proton gyro radius. The fluctuation spectrum [22] for the weak scattering case extends up to 2 or 3 Hz. For this case the rms phase deviation is less than unity. The spectra are fairly close to gaussian with a second moment W of approximately 0.5 to 0.8 Hz. Figures 23a, b, c, and d are examples of the fluctuation spectra for radio star sources 3C-286 and 3C-287. Eighty percent confidence intervals are shown; these are applicable only to the left of the arrow.

We conclude that the parameters for the velocity dominated solar wind model are $a \cong 100$ km, the solar wind velocity is $V_m \cong 400$ km/sec, and the equivalent bandwidth is $W = V_m/2\pi a \cong 0.6$ Hz.

The interplanetary magnetic field appears to take the form of a co-rotating Archimedian spiral in the ecliptic plane. Measurements from the IMP-1 satellite [23] indicate that the field is directed outward over two opposite 100° angular sectors of the spiral and inward over two opposite 60°-100° sectors. The inward sectors alternate with the outward sectors. Within the total ecliptic plane, more field is directed outward than in toward the Sun. The transition between the inward and outward field lines is fairly abrupt and also rotates with the field sectors in a 27-day period around the Sun. Thus, one expects a very large scale distribution of similar fluctuations on the order of a 100° sector of the ecliptic plane. Also, the slowly rotating transition regions should be more active relative to the interior of a large sector; therefore, they will be more visible.

Other small scale spectral features may appear in the received signal modulation under certain conditions. For a mean electron density of

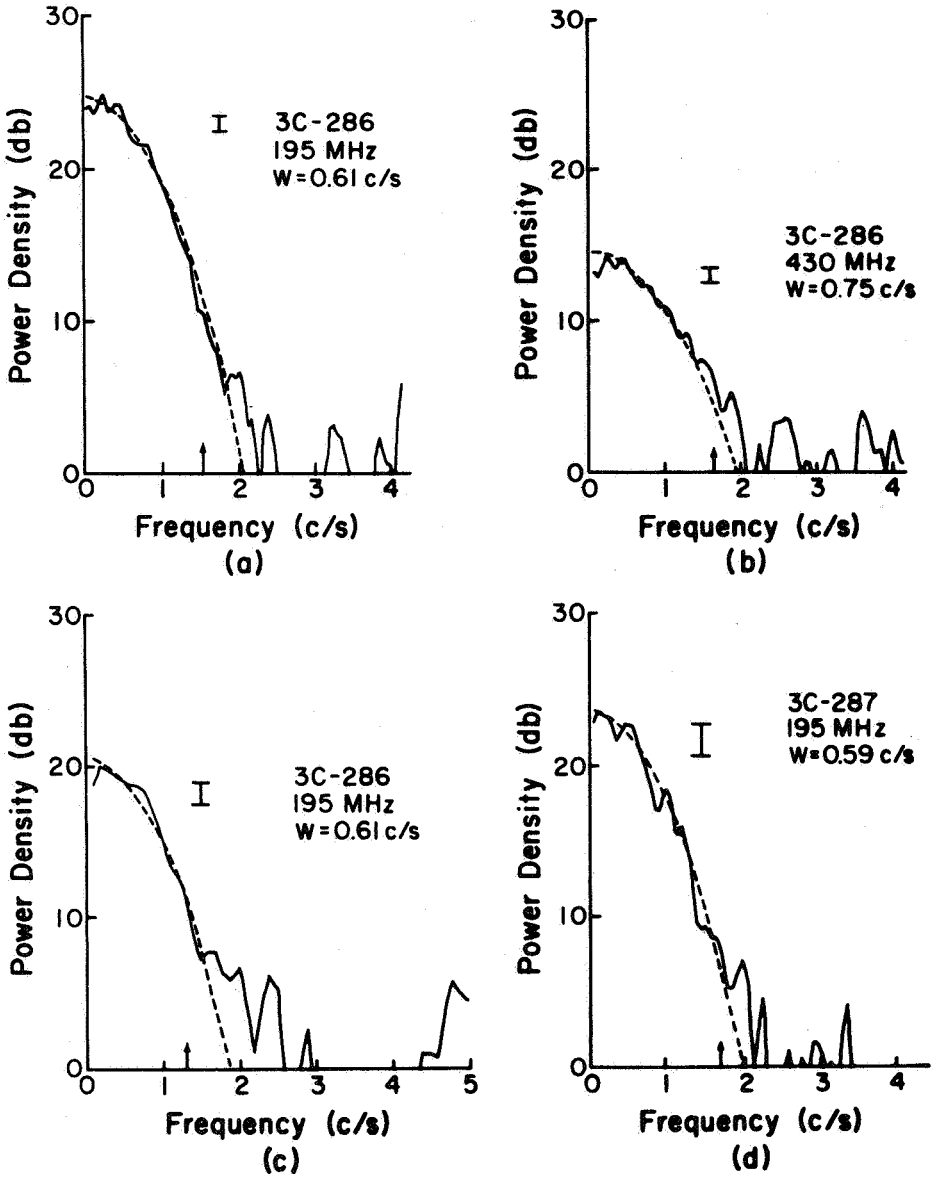

Fig. 23. RADIO STAR SCINTILLATION SPECTRA AFTER COHEN ET AL.

10 elec cm^{-3}, a narrow peak may occur at the plasma critical frequency $f_{cr} = 9N^{1/2} = 30$ kHz. Thermal energy is the energy source for these oscillations; however, they are very difficult to detect because of the very small spread of the critical frequency peak. Thermal motions may also give rise to proton or electron gyro resonance [24]. When the carrier wavelength is less than the Debye length λ_D($\lambda_D = 2m$ in the solar wind) one may possibly see the electron gyro resonance around $f_{eg} = eB/m_e \cong 280$ Hz where $B = 10^{-8}$ Weber/m^2. If $\lambda > \lambda_D$ one may possibly see the proton gyro resonance around $f_{pg} \cong 1/6$ Hz; actually, this is so low that it would be completely masked by the drift velocity fluctuations. In order see the gyro resonance phenomena, one must be propagating nearly perpendicular to the magnetic field lines and the collision frequency must be small.

Near the Earth the region between the magnetopause and the outer shock boundary is shown to be a turbulent medium [25]. The data presented in Ref. [25] are averaged to give one sample every 5.46 minutes. In the shock wave region these data are very random, clearly undersampled, which suggests a smaller time scale than 5.46 minutes. Because of the higher fluctuation rate, the shock region should be more visible than the surrounding medium in our dual-bistatic radar experiment. A similar shock region exists around the moon [25],[26]; and, it should be more visible than the surrounding medium, too.

Our experimental setup for observing the solar wind first of all requires a satellite out in the wind with a coherent transponder or a phase repeater transponder. Assuming the transponder is on board the satellite, the range R and the frequency f are the two parameters which describe the satellite and ground equipment.

Several satellites exist in the solar wind which carry the required transponder. They are the Pioneer, Mariner, and Lunar Orbiter series at S band; and, the Interplanetary Monitoring Platforms (IMP) at VHF band. In addition to those satellites in orbit, it is expected that future satellites will carry similar transponders.

B. S-band Experiment

We consider the deep space S-band satellites, Pioneer and Mariner, which orbit the Sun in this section. The results apply to the S-band Lunar Orbiter corrected to the shorter moon range; however, one wishes to use the VHF IMP satellite at this range because of its increased frequency sensitivity.

The orbits pass as close to the Sun as Venus and as far away as Mars. Figure 24 shows the orbital band and a possible 1 AU path length. In the ecliptic plane this order of range looks at a 60° cross section of the solar wind. Figure 25 is a block diagram of the coherent S-band transponder. A 2.1 GHz uplink signal is coherently translated by a ratio of 240 to 221 yielding a downlink, phase modulated, carrier frequency of approximately 2.29 GHz.

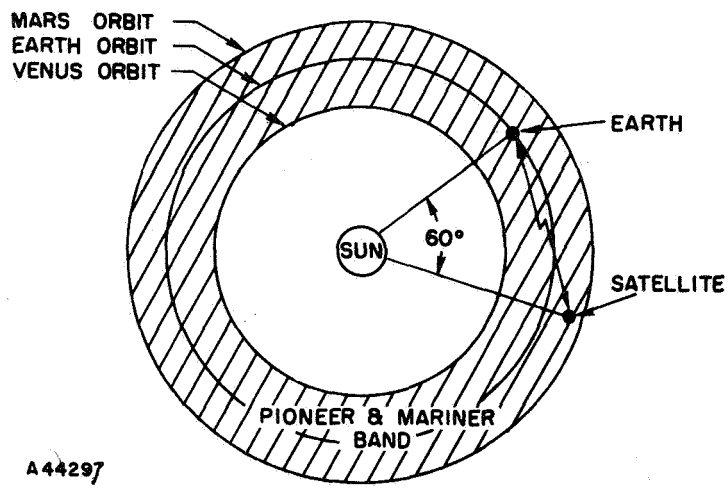

Fig. 24. S-BAND SATELLITE GEOMETRY IN THE ECLIPTIC PLANE.

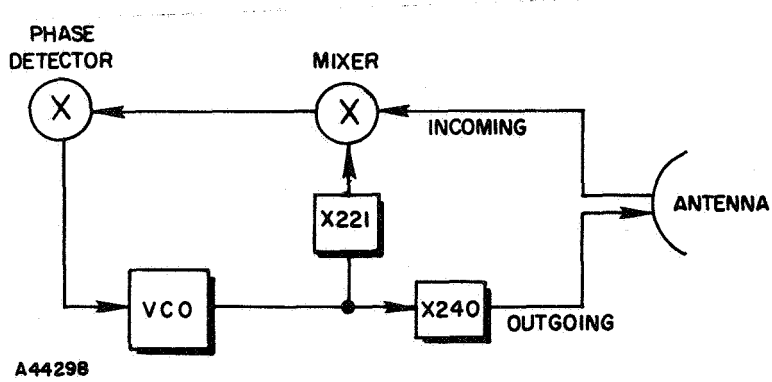

Fig. 25. S-BAND PHASE COHERENT TRANSPONDER.

From Section V.A, the effective bandwidth is $W = 0.6$ Hz. Using (3.28) the minimum resolution cell length is,

$$d_r = 0.63c/W = 1 \text{ light second} . \tag{5.8}$$

In a 1 AU path length the maximum number of resolution cells is,

$$M = R/d_r \cong 500 .$$

The sensitivity of the autocorrelation function magnitude to the refractive index variations is calculated using (3.13). We consider only one source of blobs of scale size "a" located at range p. Using $b = a < 1/W$ in (3.13) we get the mean square magnitude of the phase fluctuation.

$$R_s(\tau = 2p/v) \equiv A_1 = \pi\alpha^2 k^2 a^2 \tag{5.9}$$

$\sqrt{A_1}/\alpha$ is basically the phase deviation per effective blob variation.

$$\sqrt{A_1}/\alpha = \sqrt{\pi}\, ka \text{ radians} . \tag{5.10}$$

α is the rms magnitude of the refractive index variations. Hence, the phase deviation is directly proportional to $f(k = 2\pi f/c)$ and to the scale size or correlation length of the blobs. The sensitivity to the electron density variations may be computed from (5.5) and (5.10). In this case $\alpha = (40.3/f^2)\alpha_N$ where α_N is the rms magnitude of the electron density variations. Using this in (5.9),

$$\sqrt{A_1}/\alpha_N = 2\pi^{3/2}\, 40.3\, a/cf \text{ radians} . \tag{5.11}$$

Now the phase deviation is inversely proportional to the carrier frequency. Equation (5.11) tells us to choose f as low as possible. Hence, the sensitivity requirement is in direct conflict with (5.3)

and (5.7) which require high frequencies. At S band the phase deviation per effective blob density variation is ($a = 10^2$ km)

$$\sqrt{A_1}/\alpha_N = 7.1 \times 10^{-11} \text{ rad/(rms elec/m}^3) \qquad (5.12)$$

The experiment SNR for the time averaged data is found through (4.20). To use (4.20) we need a form for $R_s(\tau)$. Over the solar wind path one expects a fairly uniform distribution in the rms fluctuation magnitude. Consequently, we assume,

$$\sigma(z_1) = \alpha \text{ rect}[(z_1 - R/2)/R]$$

$$F(z,\tau) = \exp(-z^2/a^2 - W^2\tau^2) \ . \qquad (5.13)$$

Use (5.13) in (3.2) and the fact that $\left[1/W^2 + (a/c)^2\right]^{1/2} \cong 1/W$ to get,

$$R_s(\tau) = (\alpha^2 k^2 ac/W)\left[(2\sqrt{\pi}\, RW/c)\ e^{-W^2\tau^2} + (\pi/2)\ \text{rect}(c\tau/4R)\right]. \qquad (5.14)$$

Equation (5.14) is approximately the form given by (3.13) if $b = p = R/2$. The difference is in the choice of a uniform distribution for (5.14). The number of resolution cells in a length R is [from (3.28)],

$$M = R/d_r \cong 3WR/2c = 3WR_c/2 \ , \qquad (5.15)$$

where, $R_c \equiv R/c$. Substitute for W from (5.15),

$$R_s(\tau) = A\left[(4\sqrt{\pi}\, M/3)\ e^{-W^2\tau^2} + (\pi/2)\ \text{rect}(c\tau/4R)\right] \ , \qquad (5.16)$$

where

$$A = \alpha^2 k^2 ac/W = (40.3/f^2)^2\ \alpha_N^2 k^2 ac/W \ . \qquad (5.17)$$

The following integral is computed for (4.20) using (5.16) .

$$\int_{-T}^{T} dt\,[R_s^2(t) + R_s(t+\tau)\,R_s(t-\tau)] = (2\pi^2A^2M/3W)\left\{(8M/3\sqrt{2\pi})\,[1 + e^{-2W^2\tau^2}]\right.$$

$$\left. + 2[1 + \mathrm{rect}(c\tau/2R)] + [1 + \Lambda(c\tau/2R)]\right\} . \qquad (5.18)$$

Using (5.16) and (5.18) in (4.20) we get the average SNR for $\tau > 1/W$,

$$\mathrm{SNR} \cong \frac{W_r T\pi^2/2}{(W_r N_o/A)^2 + (8\sqrt{\pi}\,M/3)(W_r N_o/A) + \frac{4\pi^2 M}{3}\left(\frac{W_r}{W}\right)(M+3)} \qquad (5.19)$$

We have neglected the rect ( ) and Λ( ) functions from (5.18) since these terms are zero for the last half of the path and for $M > 6$ these terms have little effect on the SNR. The denominator is nearly of the form $(N_o W_r/A + 2\pi M)^2$. In order to make the SNR independent of the phase detector output noise we require a detector such that

$$W_r N_o \ll 2\pi AM \qquad (5.20)$$

As discussed in Section V.A, the rms density variations are approximately two percent of the mean density. Using $\alpha_N = 0.02$ $N = 2 \times 10^5$ elec/m^3 and the S-band frequency $f = 2.1 \times 10^9$ Hz in (5.17), $A \cong 2 \times 10^{-7}/W$ rad^2. Let E_c^2 = carrier power and E_n^2 = mean square noise power/cycle. Thus, the mean square phase deviation due to noise is,

$$N_o = E_n^2/E_c^2 \text{ rad}^2/\text{Hz} . \qquad (5.21)$$

W_r is the effective noise bandwidth. Hence,

$$W_r N_o = W_r E_n^2/E_c^2 < 2\pi AM .$$

Putting in the value for A gives,

$$E_c^2 > W_r E_n^2/2\pi AM \ . \tag{5.22}$$

Note in Fig. 23 that the effective noise power bandwidth is $W_r \cong 3W$. Thus (5.23) is,

$$E_c^2 > 3WE_n^2/2\pi AM \cong 2.4 \times 10^6 E_n^2 W^2/M \ . \tag{5.23}$$

Before calculating the necessary carrier power needed to make (5.20) valid, we assume (5.20) is true. This will enable us to find the best possible combinations for W and M. Using these values, the required carrier power capability can be computed.

Removing the $W_r N_o/A$ terms in (5.19) gives,

$$SNR \cong 3WT/8M(M + 3) \ . \tag{5.24}$$

Substitute for W from (5.15) and rearrange to get,

$$M = [T/4R_c(SNR)] - 3 \ . \tag{5.25}$$

A plot of (5.25) is shown in Fig. 26 for unity SNR. The corresponding resolution cell length d_r is also shown. Averaging 10 hours of data from a 1 AU path length gives a unity SNR for 15 resolution cells; and, for 5 hours it gives approximately 6 resolution cells. The resolution cell length is 10^7 km in the 10 hour case and 2.5×10^7 km in the 5 hour case. Figure 26 implicitly includes the bandwidth reduction associated with the decrease in M and the increase in R_c. This is seen in (5.15), also. From the data processing point of view the bandwidth is reduced by averaging groups of resolution cells together, and, this implies fewer resolution cells of longer length as shown in the figure. Hence, the performance deteriorates as the range increases.

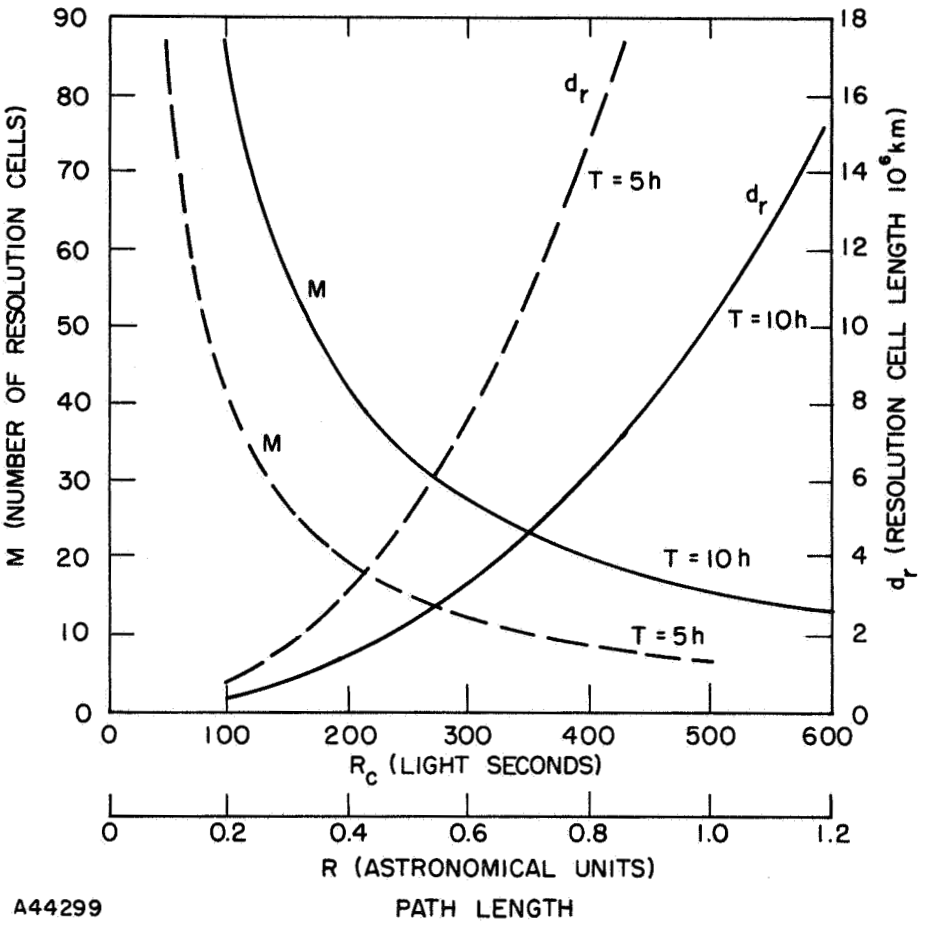

Fig. 26. UNITY SNR PLOT.

The noise power is calculated for the Goldstone 85-ft dish receiving antenna. The noise temperature is approximately 30°K. Thus,

$$E_n^2 = (\text{Boltzmann}) \times 30^\circ = 1.38 \times 10^{-23} \times 30^\circ$$

$$= 4.14 \times 10^{-22} \text{ watt sec.}$$

From (5.23) the minimum carrier power above where the thermal noise power is negligible is,

$$\min E_c^2 \cong 10^{-15} \, W^2/M \text{ watts} . \qquad (5.26)$$

The satellite antenna gain is 20 dB and the receiving area of the 85-ft dish is (efficiency = 0.7) 370 m^2. The satellite transmitter power is approximately 5 W. Thus the received power is,

$$E_r^2 = G_T P_T A_r / 4\pi R^2 \cong 1.5 \times 10^4 / R^2 \text{ watts} . \qquad (5.27)$$

Using (5.26), (5.27) and Fig. 26 some typical values are computed and listed in Table 1.

Table 1

S-BAND PERFORMANCE

Range (AU)	T (hr)	M (cells)	W (Hz)	min E_c^2 (dbm)	85 ft E_r^2 Goldstone (dbm)
0.4	5	19.5	0.065	-156.6	-143.8
0.4	10	42	0.14	-153.3	-143.8
1.0	5	6	0.008	-169.7	-151.7
1.0	10	15	0.02	-165.8	-151.7

From Table 1 it is clear that the $W_r N_o / A$ term can be neglected. That is, the received carrier power is always larger than the lower bound "min E_c^2" needed to make this approximation. Hence, the S-band experiment for ranges on the order of 1 AU with 10 hours observation time is limited by the cross noise from other sources. The overriding feature of the deep space S-band experiment is the long range involved. In order to get the SNR within a reasonable value one must narrow the effective bandwidth. This helps to reduce the noise power but hurts the resolution.

The values used for the above calculations are based on numbers for quiet Sun conditions. During the active Sun or solar storm periods, fluctuation amplitudes should be larger. The fluctuation spectrum should be wider also because the solar wind velocity is higher. This does not

improve our resolution since we have plenty of spectrum; however, it does provide a wider spectral frequency range in which to look at the medium.

We conclude that a dual bistatic-radar experiment is feasible in the solar wind. Path lengths up to and larger than 1 AU give approximately 10 resolution cells. This is an order of magnitude more resolution than currently exists in similar solar wind studies.

C. VHF-band Experiment

This section considers the potential of the IMP satellites for a dual bistatic radar experiment. These satellites are in orbit around the Earth and the Moon. We consider the Moon orbiters because their maximum ranges from Earth are usually largest. For our purposes we shall assume 500,000 km is a typical peak range.

The IMP satellites carry a phase repeater type of transponder as shown in Fig. 27. This transponder uses a crystal controlled local oscillator to generate the downlink carrier frequency. It is not as stable as the S-band PLL; however, the phase jitter occurs mostly at very low frequencies and is not a limiting factor.

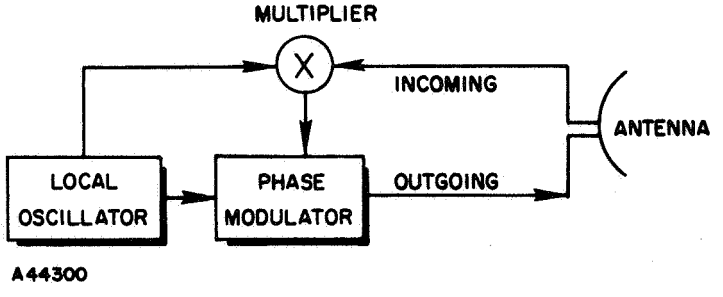

Fig. 27. VHF BAND PHASE REPEATER TRANSPONDER.

The phase is not actually demodulated in this transponder. The 136 MHz frequency and phase are translated to a 900 kHz signal which is phase modulated onto the 148 MHz downlink carrier. Because the modulation phase deviation is one radian, the downlink spectrum looks like three carrier waves. The higher frequency of the three carries the uplink phase modulation down to the ground station. The lower frequency

also carries it in an inverted form and with more phase jitter from the local oscillator.

The sensitivity per effective blob density variation is found from (5.11). It is 15 times better than at S band ($a = 10^2$ km).

$$\sqrt{A}/\alpha_N = 1.07 \times 10^{-10} \text{ rad/(rms elec/m}^3) \ . \tag{5.28}$$

The minimum resolution cell length is still one light second as given by (5.8). For this shorter range, the maximum number of resolution cells is,

$$M = R/d_r \cong 2 \ . \tag{5.29}$$

There are several reasons why M is probably lower than actual. First, it may be possible to widen the effective bandwidth W by filtering out the very low frequencies as demonstrated in Section III.C. Figure 23, for a quiet Sun, shows that energy exists up to 3 Hz. Second, during an active Sun or during solar storm periods, the solar wind velocity increases which should widen the spectrum and W. Third, the solar wind and Earth interaction region has higher fluctuation rates. The shock wave is a particularly turbulent region and should have a larger W associated with it. Also, the Earth's ionosphere is fairly turbulent and may be resolvable, also. Hence, we assume $W = 3$ Hz in some regions along the VHF path. This makes $M = WR/0.63c = 8$ cells.

The value of A increases by a factor of 15^2 because of the lower frequency; but, it also decreases due to the wider bandwidths. Thus,

$$A = (40.3/f)\ \alpha_N^2\ k^2\ ac/W \cong 4.5 \times 10^{-5}/W \text{ rad}^2 \ . \tag{5.30}$$

Use (5.30) and $W_r = 3W$ in (5.22) to get the carrier power requirement for neglecting the thermal noise

$$E_c^2 > 10^4\ E_n^2\ W^2/M \ . \tag{5.31}$$

The noise temperature for the VHF receiver is around 700°K. Then,

$$E_n^2 = 1.38 \times 10^{-23} \times 700 = 9.6 \times 10^{-21} \text{ watt sec} .$$

Using $W = 3$ Hz, $M = 8$, and E_n^2 above in (5.31) gives,

$$E_c^2 > -130 \text{ dBm} . \tag{5.32}$$

The received power at the ground station is based on (5.27) where $P_T = 38$ dBm, $G_T = -3$dB, $A_r \cong 30$ m^2, and $R = 500{,}000$ km. This gives

$$E_r^2 = G_T P_T A_r / 4\pi R^2 = -125 \text{ dBm} . \tag{5.33}$$

Since (5.33) is 5 dBm larger than (5.32), the thermal noise can be neglected in (5.19) for first order calculations. One could easily use a larger antenna to make the noise power completely negligible. From (5.24) the time T needed get a unity SNR is,

$$T = 8M(M + 3)/3W \cong 80 \text{ sec} . \tag{5.34}$$

We see that the VHF band experiment is also feasible provided the fluctuation phenomena have a wider spectrum. It is reasonable to expect a wider spectrum during solar storms, in the solar wind shock wave, and in the Earth's ionosphere.

VI. CONCLUSIONS

A method for observing and studying a tenuous medium by means of two well separated radar systems is introduced by this research. Figure 1 summarizes the basic concept very well. The unique feature of the dual bistatic-radar system is the employment of a repeater satellite to return a delayed copy of the cumulative phase modulation waveform from the tenuous medium back to the ground station. Another undelayed copy of the modulation waveform comes from the direct modulation of the downlink carrier by the tenuous medium.

The random time variations of the medium are shown to provide a window via the received signal autocorrelation function through which one may measure the spatial distribution of the variations. Hence, the autocorrelation processing of the ground receiver phase demodulated waveform yields a one dimensional mapping of the fluctuations along the propagation path.

The minimum resolution length is shown to depend upon the fluctuation rate or the spectral width of the fluctuations. Resolution length is inversely proportional to this width. During data processing resolution length may be traded for signal-to-noise ratio in the usual manner. The data processing is basically a time averaging of the signal lag-product. This may be followed by an optimal matched filter processing when one needs additional signal-to-noise ratio.

The proposed experiment to observe the tenuous solar wind variations may be expected to yield an order of magnitude improvement in locating these variations along a 1 AU path.

The general dual bistatic-radar concept can obviously be applied to any random time varying medium subject to the restrictions pointed out in previous chapters. One would expect that it could be used in the ocean in the form of a dual bistatic-sonar. For example, one might drop a coherent sonar transponder to the ocean bottom and use a surface transmitter and receiver on a ship to continuously monitor temperature changes at all depths simultaneously.

The phase fluctuation case is emphasized in this research because the experimental equipment already exists in other scientific uses.

However, the technique may be applied to the amplitude fluctuations of a medium, also.

In principle the satellite station can be replaced by a reflector surface which coherently returns the phase and/or amplitude variations and provides an effective downlink carrier. An alternate transmit and receive period are required to avoid receiver saturation; or, the reflector must be moving so that the doppler shift moves the receiver carrier frequency away from the transmitter carrier frequency.

The coherent transponder requirement may be removed. One then records data at both ends of the path and subsequently cross-correlates it. This approach is more difficult if not impossible to mechanize. Recording provisions must be available at both ends of the path and some means for keeping track of the time reference must be used so as not to lose the source location information. The advantage of this approach is a reduction in the noise by 3 dB; and, the elimination of the large self correlation peak which masks information near the origin of the auto-correlation function.

REFERENCES

1. Eshleman, V. R., "Radar Astronomy of Solar System Plasmas," SR No. 4, Stanford University, Stanford, Calif. (1964).

2. Lusignan, B. B., "Detection of Solar Particle Streams Using High Frequency Radio Waves," J. Geophys. Res. 68, 5617 (1963).

3. Fjeldbo, G., "Bistatic-Radar Methods for Studying Planetary Ionospheres and Surfaces," SR No. 2, Stanford University, Stanford, Calif. (1964).

4. Fjeldbo, G., W. Fjeldbo, and V. R. Eshleman, "Models for the Atmosphere of Mars Based on the Mariner IV Occultation Experiment," SR No. 15, Stanford University, Stanford, Calif. (1966).

5. Gee, S., "Bistatic-Radar Measurements of Interplanetary Collisionless Shock Waves," SR No. 9, Stanford University, Stanford, Calif. (1965).

6. Tyler, G. L., "Bistatic-Radar Imaging and Measurement Techniques for the Study of Planetary Surfaces," SR No. 19, Stanford University, Stanford, Calif. (1967).

7. Chernov, L. A., Wave Propagation in a Random Medium, McGraw-Hill, New York, 1960 (translated from Russian by R. A. Silverman).

8. Tatarski, V. I., Wave Propagation in a Turbulent Medium, McGraw-Hill, New York, 1961 (translated from Russian by R. A. Silverman).

9. Chernov, L. A., Wave Propagation in a Random Medium, McGraw-Hill, New York, 61 (1960).

10. Stratton, J. A., Electromagnetic Theory, McGraw-Hill, New York, 343 (1941).

11. Papoulis, A., Probability, Random Variables and Stochastic Processes, McGraw-Hill, New York, 317 (1965).

12. Mathews, J. and R. L. Walker, Mathematical Methods of Physics, Benjamin, Inc., New York, 268 (1965).

13. Chernov, L. A., Wave Propagation in a Random Medium, McGraw-Hill, New York, 64 (1960).

14. Tatarski, V. I., Wave Propagation in a Turbulent Medium, McGraw-Hill, New York, 185 (1961).

15. Woodward, P. M., Probability and Information Theory with Applications to Radar, Pergamon Press, New York, 117 (1953).

16. Parzen, E., Modern Probability Theory and Its Applications, John Wiley and Sons, Inc., New York, 379 (1960).

17. Balakrishnan, A. V., Communication Theory (chapter contributed by W. L. Root) McGraw-Hill, New York, 183-188 (1968).

18. Hofstetter, E. M., "Some Results on the Stochastic Signal Parameter Estimation Problem," IEEE PGIT IT-11, 422-429 (1965).

19. Helstrom, C. W., Statistical Theory of Signal Detection, Pergamon Press, New York, 114 (1960).

20. Koehler, R. L., "Interplanetary Electron Content Measured between Earth and Pioneer VI and VII Spacecraft Using Radio Propagation Effects," SR No. 20, Stanford University, Stanford, Calif. (1967).

21. Sturrock, P. A. and R. E. Hartle, "Two Fluid Model of the Solar Wind," Phys. Rev. Letters 16, 628-631 (1966).

22. Cohen, M. H., E. J. Gundermann, H. E. Hardebeck, and L. E. Sharp, "Interplanetary Scintillations. II: Observations," J. Astrophys. 147, 433-449 (1967).

23. Ness, N. F. and J. M. Wilcox, "A Quasi-Stationary Co-Rotating Structure in the Interplanetary," J. Geophys. Res. 70, 5793-5805 (1965).

24. Dougherty, J. P. and D. T. Farley, "A Theory of Incoherent Scattering of Radio Waves by a Plasma," J. Geophys. Res. 68, 5473-5486 (1963).

25. Ness, N. F., C. S. Scearce, and J. B. Seek, "Initial Results of the Imp 1 Magnetic Field Experiment," J. Geophys. Res. 69, 3531-3569 (1964).

26. Yoh, P., "Radar Studies of the Cislunar Medium," SR No. 12, Stanford University, Stanford, Calif. (1965).

Appendix A

THE SLOWLY VARYING ASSUMPTIONS

The purpose of this section is to show that the slowly varying assumptions

$$|\nabla n/n| \ll |kn|^2 , \tag{A.1}$$

$$|\dot{n}/n| \ll \omega \tag{A.2}$$

allow us to drop the terms on the right hand side of (2.4). n is the refractive index function, k is the free space wave number, and ω is the rf frequency.

We consider first the space variations of n, $n = n(x,y,z)$. The exact wave equation for this case is (letting $K(r) = n^2(r)$

$$\nabla^2\bar{E} - \nabla(\nabla \cdot \bar{E}) + k^2K\bar{E} = 0 , \tag{A.3}$$

Now $\nabla \cdot E$ is found by using

$$\bar{D} = e_o K\bar{E}$$

and

$$\nabla \cdot \bar{D} = \rho = 0 .$$

Then

$$\nabla \cdot \bar{E} = -\bar{E} \cdot \nabla K/K . \tag{A.4}$$

To show that $\nabla(\nabla \cdot E)$ in (A.3) and (2.4) is small, we will show that $\nabla \cdot \bar{E}$ is small with respect to either of the remaining terms in (A.3). With the Schwartz inequality

$$|\nabla \cdot E| = |E \cdot \nabla K/K| \leq |E|\,|\nabla K/K| . \tag{A.5}$$

$\nabla K = 2n\nabla n$, so that,

$$|\nabla K/K| = 2|\nabla n/n| \ll |kn|^2 , \tag{A.6}$$

by assumptions (A.4).

Using (A.6) in (A.5),

$$|\nabla \cdot \bar{E}| \ll k^2 |K| |\bar{E}| \qquad \text{Q.E.D.} \qquad (A.7)$$

Thus the spatial slowly varying assumption (A.1) leads to the quasi-homogeneous approximation

$$\nabla^2 \bar{E} + k^2 K \bar{E} \cong 0 \ , \qquad (A.8)$$

from (A.7) and (A.3).

The time varying condition is examined by considering n to be $n = n(t)$. We get the following exact wave equation

$$\nabla^2 \bar{E} - \mu_o \ddot{\bar{D}} = 0 \qquad (A.9)$$

where $\bar{D} = e_o K \bar{E}$ and $K(t) = n^2(t)$. Then

$$\dot{\bar{D}} = e_o K \dot{\bar{E}} + e_o \dot{K} \bar{E} \ . \qquad (A.10)$$

We desire the $\dot{K}$ term in (A.10) to be small with respect to the K term.

In Chapter II, our solution for $\bar{E}$ is shown to be of the form

$$\bar{E} = \hat{x} A_o e^{i(\omega t - v)}$$

such that $|\dot{v}| \ll \omega$. Then

$$\dot{\bar{E}} = \hat{x} \, A_o \, i \, (\omega - \dot{V}) \, e^{i(\omega t - V)} \cong i\omega \bar{E} \ . \qquad (A.11)$$

Now (A.10) is

$$\dot{\bar{D}} = e_o \bar{E} (i\omega K + \dot{K}) \cong i\omega e_o K \bar{E} \qquad (A.12)$$

if

$$|\dot{K}/K| = 2|\dot{n}/n| \ll \omega \ . \qquad (A.13)$$

Similarly,

$$\ddot{\bar{D}} \cong -\omega^2 e_o K\bar{E} = e_o K\ddot{\bar{E}} \ , \qquad \text{(A.14)}$$

so that (A.9) is approximately,

$$\nabla^2 E - \mu_o e_o K\ddot{\bar{E}} = \nabla^2 E - (n/c)^2 \ddot{\bar{E}} \cong 0 \ . \qquad \text{(A.15)}$$

Hence the slowly varying assumption of (A.2) allows us to drop the time derivative terms on the right hand side of (2.4).

Appendix B

SINUSOIDAL CONVOLUTION IDENTITIES

This appendix works out the identity used in (2.75) and a related identity needed to find (2.77). The identity is the evaluation of the following integral

$$I_1 = \iint_{-\infty}^{\infty} dx_o dy_o \sin\left\{A\left[\left(\frac{x}{2} + x_o\right)^2 + \left(\frac{y}{2} + y_o\right)^2\right]\right\} \sin\left\{B\left[\left(\frac{x}{2} - x_o\right)^2 + \left(\frac{y}{2} - y_o\right)^2\right]\right\}$$

$$\equiv G \sin[C(x^2 + y^2)] + H \sin[D(x^2 + y^2)], \qquad (B.1)$$

where $x = x_2 - x_1$, $y = y_2 - y$, $2x_o = x_2 + x_1$, and $2y_o = y_2 + y_1$. The identity is complete when C, D, G, and H are expressed in terms of A and B. First convert the sin functions to exponentials. Using a one to one correspondence with the LHS of (B.1)

$$-4\sin(\alpha_x + \beta_y) \sin(\gamma_x + \delta_y) = \exp[i(\alpha_x+\gamma_x+\beta_y+\delta_y)]$$

$$- \exp[i(\alpha_x-\gamma_x+\beta_y-\delta_y)] - \exp[-i(\alpha_x-\gamma_x+\beta_y-\delta_y)] + \exp[-i(\alpha_x+\gamma_x+\beta_y+\delta_y)] . \qquad (B.2)$$

These give four separate integrals of the following type

$$\int_{-\infty}^{\infty} dx_o \exp\left\{i\left[A\left(\frac{x}{2} + x_o\right)^2 + B\left(\frac{x}{2} - x_o\right)^2\right]\right\} \int_{-\infty}^{\infty} dy_o \exp\left\{i\left[A\left(\frac{y}{2} + y_o\right)^2 + B\left(\frac{y}{2} - y_o\right)^2\right]\right\}$$

$$= [i\pi/(A + B)] \exp\left\{i[AB/(A + B)]\rho^2\right\} \qquad (B.3)$$

where $\rho^2 = x^2 + y^2$.

The remaining three integrals in (B.2) can be done by merely changing the sign on A or B. Correctly summing the four results gives,

$$I_1 = \frac{\pi}{2(A - B)} \sin\left(\frac{AB\rho^2}{A - B}\right) + \frac{\pi}{2(A + B)} \sin\left(\frac{AB\rho^2}{A + B}\right) . \qquad (B.4)$$

Using the correspondence between (B.4) and the RHS of (B.1) gives,

$$G = \pi/2(A - B) , \qquad C = AB/(A - B) ,$$

$$H = \pi/2(A + B) , \qquad D = AB/(A + B) . \tag{B.5}$$

The second identity involves the double integral of the cosines. We quote the result because the integration procedure is the same as above.

$$I_2 = \iint_{-\infty}^{\infty} dx_o dy_o \cos\left\{A\left[\left(\frac{x}{s} + x_o\right)^2 + \left(\frac{y}{2} + y_o\right)^2\right]\right\} \cos\left\{B\left[\left(\frac{x}{2} - x_o\right)^2 + \left(\frac{y}{2} - y_o\right)^2\right]\right\}$$

$$\equiv \frac{\pi}{2(A - B)} \sin\left(\frac{AB\rho^2}{A - B}\right) - \frac{\pi}{2(A + B)} \sin\left(\frac{AB\rho^2}{A + B}\right) \tag{B.6}$$